Control of nonmetallic inclusions in continuously cast steels in view of macro-cleanliness, castability, precipitation modification and grain refinement

von der Fakultät für Werkstoffwissenschaft und Werkstofftechnologie
der Technischen Universität Bergakademie Freiberg

genehmigte

DISSERTATION

zur Erlangung des akademischen Grades

Doktor-Ingenieur (Dr.-Ing.)

vorgelegt

von M. Eng. Zhongting Ma

geboren am 04.09.1964 in Anhui, V. R. China

Gutachter: Prof. Dr.-Ing. habil. Dieter Janke, Freiberg
Prof. Dr.-Ing. habil. Heinz-Joachim Spies, Freiberg
Prof. Dr.-Ing. habil. Eberhard Steinmetz, Essen

Tag der Verleihung: 20. April 2001

Contents

Preface iii
Nomenclature iv

CHAPTER 1
Introduction and research objectives 1

1.1 Introduction 1
1.2 Steel quality and nonmetallic inclusions 2
1.3 Research objectives 3

CHAPTER 2
Research scenario and discussions 4

2.1 Solidification path of steel 4
2.2 Generation of finely dispersed oxide inclusions 4
2.3 Precipitation of MnS 10
2.4 Formation of intragranular ferrite (IGF) 13
2.5 Inclusions in view of castability and quality of continuously cast steel 16
2.6 Oxide metallurgy 17

CHAPTER 3
Deoxidation techniques used in steelmaking processes 24
3.1 Conventional deoxidation technologies 26
3.2 Clean deoxidation technologies 32
3.3 Alternative deoxidation techniques in view of utilization of oxide inclusions 36

CHAPTER 4
Experimental apparatus and procedures 39

4.1 Experimental apparatus and investigated steels 39
4.2 Experimental procedures 42
4.3 Oxygen sensing and control 43

CHAPTER 5
Size, composition, distribution and morphology of oxides in steel 46

5.1 Composition of oxide inclusions 46
5.2 Size and distribution of oxide inclusions 54
5.3 Shape of oxide inclusions 66

CHAPTER 6
Effects of oxide inclusions on castability and sulfides 70

6.1 Effect of oxide inclusions on castability 70
6.2 Oxide inclusions acting as nucleation sites for sulfides, nitrides and carbides 78

CHAPTER 7
Effects of oxide inclusions on microstructures and Mechanical properties of steel 86

7.1 Effect of oxide inclusions on microstructures 87
7.2 Inclusions serving as nucleation sites for IGF 90
7.3 Relation between microstructure and toughness 94

CHAPTER 8
Conclusions 100

APPENDIX A
Thermodynamics of concentrated metallic solutions 103

APPENDIX B
Interaction parameters of solutes in liquid iron 110

APPENDIX C
Calculation of precipitates in molten steel during solidification 113

Acknowledgements 122

Preface

The purpose of this doctorate thesis is to investigate a new technology termed **oxide metallurgy** aiming to improve steel service properties without additional secondary metallurgical processing in view of higher steel purity. It is difficult and cost inefficient to produce steel with extremely low contents of inclusions. Moreover, the elimination of inclusions and impurities can never be fully accomplished. Therefore, oxide metallurgy appears to be a promising additional method to produce future steels. Steel service properties can be improved and guaranteed through minimization of inclusion and grain size without the requirement of ultra clean. This approach can probably to a certain extent reduce the efforts to maintain steel cleanness in refining and tundish metallurgical processes leading to simplified requirements for the conventional slags and refractories. With the above concept, the controlled inclusions are no longer harmful to steel service properties in view of macro-cleanness, grain refinement and modification of inclusions. The contents of the present study are briefly introduced as follows.

Chapter 1 gives an introduction and outlines the present research objectives. The reported research work on oxide metallurgy is summarized and discussed in Chapter 2. Chapter 3 is devoted to discuss deoxidation technologies such as conventional, clean and alternative ones. Alternative deoxidation technology is essential for oxide metallurgy. The related laboratory-scale experimental equipment and procedure are covered at length in Chapter 4. Chapter 5 treats inclusions in steel with the aim to understand the fundamental effects of alternative deoxidation technology upon inclusions. Effects of inclusions on steel castability and precipitation of sulfides are considered in Chapter 6. Grain refinement is reached through the control of oxide inclusions and solidification, eventually contributing an improvement of mechanical properties. Chapter 7 gives a clear explanation on this subject. Meanwhile, industrial examples are also presented in this chapter. Several important conclusions obtained from the present study are summarized in Chapter 8. Finally, Appendices A, B and C deal with the fundamental knowledge related to oxide metallurgy which is directly used in the present study.

Nomenclature

A_V	Charpy-V-notch impact toughness (J)
C_i	Concentration of solute i during solidification from liquidus to solidus temperature (mass %)
C	Coulomb (A·s)
C_i^0	Concentration of solute i in liquid steel (mass %)
D_i	Diffusion coefficient of solute i in solid iron ($cm^2 \cdot s^{-1}$)
D_i^L	Diffusion coefficient of solute i in liquid iron ($cm^2 \cdot s^{-1}$)
E	Electromotive force (mV)
$\Delta E_{i\text{-}g}$	Energy change of forming a contact area between inclusion and gas or vacuum (J)
$\Delta E_{s\text{-}g}$	Energy change of forming a contact area between nozzle refractories and gas or vacuum (J)
ΔE_p	Energy for establishing a cavity (J)
ΔE_T	Total energy change (J)
$\Delta E_{V\text{-}\alpha}$	Volume free energy change for the formation of α phase (J)
$\Delta E_{\alpha\text{-}\gamma}$	Surface energy change for the formation of α phase (J)
$\Delta E_{strain,\alpha}$	Strain energy resulting from the formation of α phase (J)
$\Delta E_{\gamma\text{-}\gamma}$	Surface energy change for the diminution of contacted γ phase (J)
$\Delta E_{V\text{-}i}$	Volume free energy change for the formation of inclusion (J)
$\Delta E_{strain,i}$	Strain energy resulting from the formation of inclusion (J)
F	Faraday constant (96484.6 $C \cdot mol^{-1}$)
ΔG_i^0	Standard Gibbs free energy of element i dissolved in liquid iron based on 1 mass% standard ($J \cdot mol^{-1}$)
I_{ion}	Current of ions across the solid electrolyte (A)
$K_{M_xO_y}$	Equilibrium constant of formation of oxide M_xO_y in liquid iron
$K_{xM\text{-}yO}$	Equilibrium constant of oxide M_xO_y dissolved in liquid iron
M_i	Atomic mass of element i ($g \cdot mol^{-1}$)
N	Number of oxides per unit volume
P_θ	Parameter of partial electronic conductivity at t_{ion}=0.5 (bar)
P'_{O_2}	Oxygen partial pressure in steel melts (bar)
P_{O_2}	Oxygen partial pressure of reference electrode (bar)
P_a	Pressure outside cavity (bar)
P_i	Pressure inside cavity (bar)

R	Universal gas constant (8.314 $J \cdot K^{-1} \cdot mol^{-1}$)
R_{ion}	Resistance of ionic current between two electrodes (Ω)
R_C	Cooling rate ($K \cdot s^{-1}$)
T	Temperature of steel melts (K)
T_L	Liquidus temperature of steel (K)
T_S	Solidus temperature of steel (K)
T_0	Melting point of pure iron (K)
U	External voltage applied to a cell (mV)
ΔV	Volume change (cm^3)
t	Time (s)
f_S	Solid fraction
λ	Secondary dendrite arm spacing (cm)
k_i	Equilibrium distribution coefficient of solute i between liquid and solid phases
[wt% i](t)	Content of solute i in steel melts at time t during solidification (mass %)
$[wt\% i]_0$	Content of solute i in steel melts at time t=0 during solidification (mass %)
% [i]	Mass percentage of solute i in steel melts (mass %)
$\% [i]_{max}$	Solubility of solute i in steel melts (mass %)
a_i	Raoultian activity of element i in steel melts
h_i	Henrian activity of element i in steel melts
x_i	Mole fraction of element i in steel melts
ε_i^i	First-order self-interaction parameter of solute i based on mole fraction
e_i^i	First-order self-interaction parameter of solute i based on mass percentage
ε_i^j	First-order interaction parameter of solute j upon i based on mole fraction
e_i^j	First-order interaction parameter of solute j upon i based on mass percentage
γ_i^0	Raoultian activity coefficient of solute i at infinite dilute solution
γ_i	Raoultian activity coefficient of solute i
γ_l	Raoultian activity coefficient of solvent
f_i	Henrian activity coefficient of solute i
θ	Contact angle (degree)
θ_R	Observed contact angle with roughness (degree)
θ_S	Observed contact angle with perfectly smooth surface (degree)

r	Surface roughness
τ	Local solidification time (s)
δ	Misfit between two phases which is calculated for particular planar parallelisms
$\sigma_{x\text{-}y}$	Interfacial tension between x and y phases ($J \cdot cm^{-2}$)
ρ_A	Density of phase A ($g \cdot cm^{-3}$)

CHAPTER 1
Introduction and Research Objectives

1.1 Introduction

Steel is one of the massively used and most important materials in any industrialized society. It is regarded as one of the basic materials to the sustainable development of a modern industrial society due to its versatility and potential of nearly complete recycling. Its applications are most diverse and widespread in all major branches of industry. Steel industry is among the most productive, efficient and technologically sophisticated industries in the world. However, in a global economy that is becoming steadily more competitive steel industry must continuously find ways to stay at the forefront of manufacturing technology. Future steels will face problems such as quality, price, customer demands and environmental and ecological concerns. Steel industry should provide high quality products to its customers in an environmentally friendly, cost effective manner. To achieve this aim, the following three targets (summarized from references [1-2]) are continuously needed to be improved.

- Process efficiency
  - Improvement of quality, throughput and energy efficiency in cost effective manner
  - Development of new methods to shorten process chains in cost effective manner
  - Quantitative modeling of material performance
  - Process automation
- Product development
  - Development of steel grades for lightweight construction
  - Increase of steel consumption to key markets by developing new products with new properties
  - Achievement of maximum flexibility in production capabilities responding to ever-changing markets and customer demands
- Environmental and ecological concerns and recycling
  - Increase of steel recycling and recovery of iron units from plant solid wastes
  - Ultimate finding of ways to eliminate or at least minimize wastes

Therefore, steel industry is going through a technical revolution that will not only change the conventional steelmaking process but also establish a new industrial structure.

1.2 Steel Quality and Nonmetallic Inclusions

Normally, steel quality is greatly improved by removing impurities and inclusions to very low levels [3]. However, as in any other production facility, steelmaking has to find trade-offs between product performance and price. Extreme pursuance of purity is useless with respect to cost effectiveness and competitiveness on the one hand. On the other hand the elimination of nonmetallic inclusions can never be fully accomplished [4]. Moreover, it is a difficult task to produce steel with extremely low contents of inclusions. Thus, the performance of steel should be controlled by an advanced technology in view of an appropriate purity level. In fact, the inclusions remaining in steel exert remarkable effects on steel service properties. Control and utilization of nonmetallic inclusions in steel is one of the essential tasks in steelmaking process directly related to steel quality and process efficiency and even related to environments by alleviation of harmful effects of impurities and reduction of effluents.

The prominent characteristics for the forthcoming technologies of thin slab casting, hot direct rolling and near net shape casting is the reduction of casting thickness causing higher cooling rates. It is obvious that nonmetallic inclusions will exert more remarkable effects on steel service properties and its production processes with regard to advanced steelmaking technologies in comparison with the conventional ones. It is believed that castability, structure and properties of continuously cast steel are closely related to nonmetallic inclusions. In addition to the conventional concept, there exist the following four ways to guarantee the improvement of castability, structure and properties of continuously cast steel [5]:

- removal of nonmetallic inclusions to extremely low levels,
- modification of nonmetallic inclusions to alleviate or eliminate their harmful effects,
- control of nonmetallic inclusions for utilization,
- grain refining

It is the main purpose of the present study to investigate the two latter ways which are achieved by alternative deoxidation techniques.

1.3 Research Objectives

As mentioned above, the present study aims at the control of nonmetallic inclusions and grain size. Thus, the major objectives are focused on the following three aspects:

- alternative deoxidation technologies and its consequences for inclusions in steel and structures and properties of steel,
- mechanisms and fundamentals corresponding to alternative deoxidation technologies at different stages,
- knowledge related to these technologies.

References

[1] J. Szekely: ISIJ International, 36(1996), 121/132
[2] R. J. Fruehan: Metall. Trans. B, 28B(1997), 743/753
[3] Z. Ma, D. Peisker and D. Janke: steel research, 70(1999), 178/182
[4] Z. Ma and D. Janke: Acta Metallurgica Sinica, 11(1998), 79/86
[5] D. Janke, Z. Ma, P. Valentin and A. Heinen: ISIJ International, 40(2000),31/39

CHAPTER 2
Research Scenario and Discussions

Normally it is unavoidable to admit nonmetallic inclusions in steel, at least in small quantities, and steel service properties are strongly affected by them. These inclusions exert harmful effects to steel service properties according to the conventional experiences. However, Mizoguchi et al.[1-5] introduced a new concept of utilization of oxide particles. These particles spontaneously act as nucleation sites for sulfides during cooling and solidification and, moreover, refine structures after solidification by nucleation of fine intragranular ferrite (IGF). This approach is termed "oxide metallurgy" with a vital interest for direct hot rolling (DHR) processes, thin slab casting and near net shape casting (NNSC), i.e. direct strip casting. Research work on this item is catalogued, summarized and discussed as follows.

2.1 Solidification Path of Steel

The solidification path, i.e. micro-segregation of solutes during solidification, is important in oxide metallurgy. Extensive studies have been done on the assessment of micro-segregation in solidifying alloys. Some analytical micro-segregation models are classified in **Table 2.1** and their basic equations for these models are listed in **Table 2.2**. Many numerical micro-segregation models have also been proposed. However, the discussions on numerical models are out side the scope of the present study.

2.2 Generation of Finely Dispersed Oxides

Composition, size and distribution of precipitated oxides are greatly influenced by the deoxidants, conditions of the molten steel and solidification process. Al is widely accepted as a deoxidant in steelmaking process. Its addition is very convenient and it effectively reduces oxygen content in liquid steel to low levels. However, vast investigations found that most steel problems can be traced to alumina or Al-rich oxides. Solid alumina inclusions in molten steel tend to rapid clustering due to their dendritic morphology. The alumina clusters hardly float to the top of the molten steel because of their high apparent density in view of oxide clusters plus engulfed liquid steel. They are detrimental to castability and

quality of continuously cast steel. Calcium has been frequently employed to treat Al-killed steels since the 1970's to avoid the formation of solid alumina. Ca treatment effectively improves castability and quality of continuously cast steel, but is limited for all steel products that require either high fatigue resistance in service or high cold formability in very thin gauges. This is because of the presence of globular Ca-Al oxides. The Al, Ca and Ca-Al oxides are normally several to tens of micrometers in diameter. Partial and complete substitution of Ti, Zr and/or rare earth metals for Al is increasingly pursued recently. This endeavour is to improve castability and quality of continuously cast steel through generation of finely dispersed oxides which effectively serve as heterogeneous nucleation sites for transformation and precipitation. Thus, control of the amount, size, composition and distribution of nonmetallic inclusions in steel is of importance.

Table 2.1. Classification of models for solute redistribution during solidification

	Diffusion in the liquid	
Diffusion in the solid	Limited	Complete
No	Himemiya and Umeda [12]	Scheil [6]
Limited	Nastac and Stefanescu [11] Himemiya and Umeda [12]	Brody and Flemings [7] Clyne and Kurz [8] Ohnaka [9] Kobayashi [10] Himemiya and Umeda [12]
Complete	Nonsense	Lever rule

2.2.1 Experimental results

Goto et al.[13-17] experimentally investigated oxide precipitation of Ti-deoxidized low carbon steels. **Figures 2.1** and **2.2** demonstrate the relationship between cooling rates and oxide inclusions (number, size, composition and distribution). They further found from experiments that

the number of oxides increases with increasing oxygen content, but the average size of oxides only slightly increases.

Table 2.2. Equations of analytical micro-segregation models mentioned in Table 2.1

Model	Equation
Lever rule	$C_S = kC_0 / \left[(1 - f_S) + kf_S\right]$
Scheil [6]	$C_S = kC_0(1-f_S)^{k-1}$
Brody and Flemings [7]	$C_S = kC_0\left[1-(1-2\alpha k)f_S\right]^{(k-1)/(1-2\alpha k)}, \quad \alpha = 4D_S t_f / \lambda^2$
Clyne and Kurz [8]	$C_S = kC_0\left[(1-2\Omega k)f_S\right]^{(k-1)/(1-2\Omega k)}, \Omega = \alpha\left[1-\exp(-\frac{1}{\alpha})\right]-\frac{1}{2}\exp(-\frac{1}{2\alpha})$
Ohnaka [9]	$C_S = kC_0\left[1-(1-\beta k)f_S\right]^{(k-1)/(1-2\beta k)}, \quad \beta = \frac{2\gamma}{1+2\gamma}, \quad \gamma = \frac{8D_S t_f}{\lambda^2}$
Kobayashi [10]	$C_S = kC_0\xi^{(k-1)/(1-\beta k)}\left\{1+\Gamma\left[0.5\left(\xi^{-2}-1\right)-2\left(\xi^{-1}-1\right)-\ln\xi\right]\right\}$, $\xi = 1-(1-\beta k)f_S$, $\Gamma = \beta^3 k(k-1)\left[(1+\beta)k-2\right](4\gamma)^{-1}(1-\beta k)^{-3}$
Nastac & Stefanescu[11]	$C_S = k_{ef}C_0\left[1-\frac{(1-k_{ef})f_S}{1-(m+1)\left[k_{ef}I_S^{(m+1)}+I_L^{(m+1)}\right]}\right]^{-1}, \quad f_S = (R^*/R_f)^{m+1}$ $I_S^{(3)} = \frac{2f_S}{\pi^2}\sum_{n=1}^{\infty}\frac{1}{n^2}\exp\left[-\left(\frac{n\pi}{f_S^{1/3}}\right)^2\frac{D_S t}{R_f^2}\right]$, $m=0$, *for plate*; $m=1$, *for columnar*; $m=2$, *for equiaxed* $I_L^{(3)} = 2f_S^{2/3}(1-f_S^{1/3})\sum_{n=1}^{\infty}\frac{1}{\alpha_n^2}\exp\left[-\left(\frac{\alpha_n}{1-f_S^{1/3}}\right)^2\frac{D_L t}{R_f^2}\right]$, $\alpha_n / \tan(\alpha_n) = 1 - f_S^{1/3}$.
Himemiya & Umeda[12]	see Ref. [12]

Sawai et al.[18] reported that the oxide inclusions observed in Ti-deoxidized low carbon steel are nearly spherical and evenly distributed in the matrix with small size, and composed of Mn-silicate and (Ti,Mn)O. The element Ti remarkably facilitates grain refinement shown in **Figure 2.3** which plots

the data of austenite grain size measured in ingots quenched from several temperatures after solidification. **Figure 2.4** [20] gives the effect of Ti on MnS inclusions. Ti effectively reduces inclusion size through increasing the number of inclusions. **Figure 2.5** further demonstrates that Ti addition is much more effective to produce smaller inclusions than increased cooling rates.

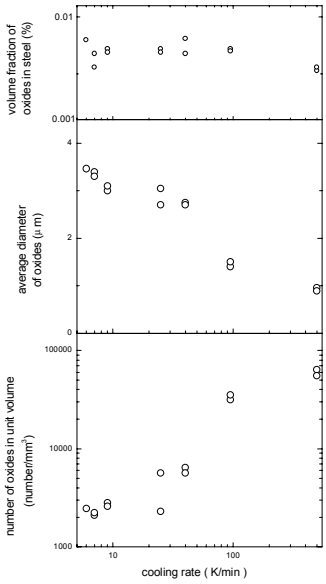

Figure 2.1. Effect of the cooling rate on oxide inclusions in Ti-deoxidized steel [13]

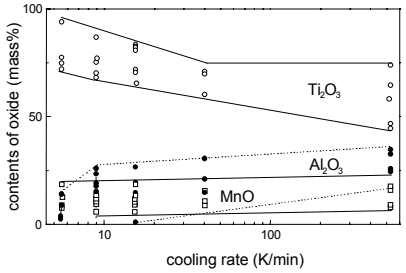

o Ti_2O_3 • Al_2O_3 MnO

Figure 2.2. Effect of the cooling rate on chemical composition of oxides in Ti-deoxidized steel [14]

Steel composition (mass%):

C	Si	Mn	Al	Ti	O
0.06	0.05	1.20	0.001	0.014	0.0027

Zr is a rather strong deoxidizing element, even stronger than Al. Therefore, the oxide inclusions in Zr deoxidized steels are mostly primary ones. Sawai et al.[18] experimentally found that the oxides distribute more evenly in Zr-deoxidized steel than in Ti-deoxidized steel. However, ZrO_2 represents an anion vacancy oxide like Al_2O_3, thus not in favour of nucleation of various foreign phases on it. In practice, Zr is not selected to treat molten steel. Zr treatment after Mn, Si and/or Ti deoxidation is experimentally proven as a useful alternative deoxidation method to generate fine complex oxides which serve as nucleation sites for MnS and IGF [23, 24]. Sawai et al. [23] found that the addition of Zr after Mn-Si deoxidation for low carbon steels leads to smaller diameter and higher

particle density of oxides. These oxides composed of MnO, SiO_2 and ZrO_2 are effective nucleation sites for MnS. Wakoh et al. [24] investigated the effect of Zr on Ti-deoxidized low carbon steels. Their experimental results suggest that Zr treatment after Ti deoxidation for low carbon steels favours uniformly distributed oxide inclusions (MnS precipitation on their surfaces) and notably weakens the dependence of oxide distribution on cooling rates in comparison with Ti-deoxidized low carbon steels.

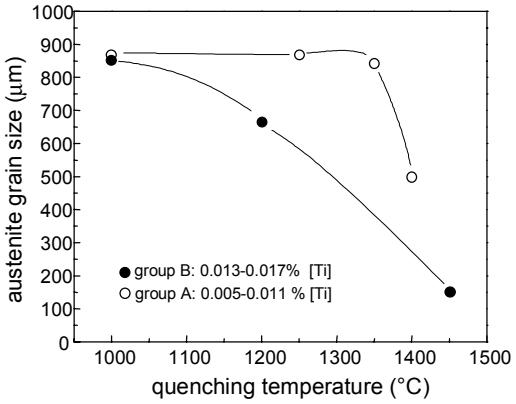

Figure 2.3. Effect of Ti content on grain growth of as-cast austenite after solidification [19]

Steel composition (mass%, * in ppm):

	C	Si	Mn	P*	S*	Nb	N*
A:	0.05/8	0.24/26	1.32/1.40	50/80	50/80	0.027/28	50
B:	0.06/8	0.25/30	1.36/1.41	50/80	40/80	0.027/30	50

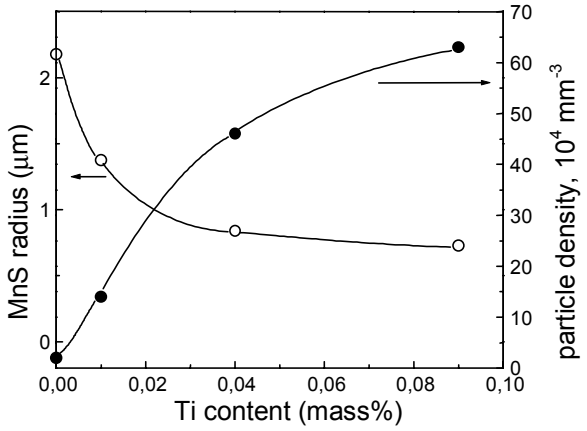

Figure 2.4. Effect of Ti content on the size and number density of MnS inclusions in the Fe-0.1C-1Mn-0.02S steel [20]

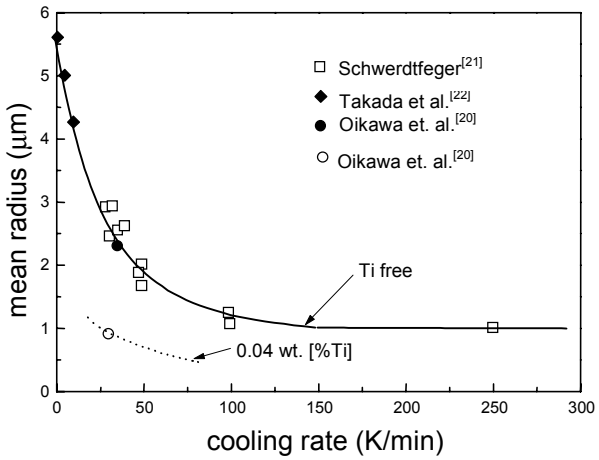

Figure 2.5. Effects of cooling rate and Ti on the size of MnS inclusions in the Fe-0.1C-1Mn-0.02S steel [20]

The People's Republic of China is rich in resources of rare earth metals (REMs). Therefore, REMs have been widely used in steelmaking since three decades for grain refining and inclusion modifying. Extensive and intensive researches were done on their behavior in molten steel and their effects on steel service properties [25, 26].

2.2.2 Modeling

Many researchers investigated the precipitation behavior of oxides during solidification and some of them attempted to simulate this phenomenon. The modeling of inclusion precipitation during solidification is summarized in the paper of Wintz et al [27]. So far, three different models have been developed to describe the precipitation and growth of nonmetallic inclusions during solidification [13, 14, 27-30]. They are NSC's (Japan) [29], IRSID's (France) [27,28] and the present models [30]. These models are experienced in the same or similar calculation algorithm, i.e. the description of inclusion precipitation is achieved through the combination of microsegregation models and multiphase equilibrium ones. The calculation tools developed by NSC are based on the juxtaposition of two calculation programs, one solving the microsegregation equations or models, the other calculating the distribution of elements between liquid metal and inclusions using a commercial multiphase equilibrium software

such as SOLGASMIX, THERMOCALC or CHEMSAGE. The IRSID model is based on the classical hypothesis of the Clyne-Kurz microsegregation model [8] and a multiphase equilibrium program. In this model, the equilibrium between liquid, solid metal and oxide, sulphide and carbide inclusions and the kinetics of solidification are combined in a general multiphase equilibrium code [27]. The present model is based on microsegregation equations and a slag model combined with mass balance equations. It is the simplest model and the details are described in Appendix C.

2.3 Precipitation of MnS

MnS is well known as sulfide inclusion in steel and it exerts harmful effects on mechanical properties. MnS precipitates either in liquid steel during cooling and solidification or in solid steel during or after solidification. Several excellent studies on precipitation and morphology of MnS have been reported [21,31-35]. However, steels with evenly dispersed MnS inclusions feature a good machinability. Moreover, finely dispersed MnS refines grain size during mechanical forming and heat treatment [1, 36, 37]. It is experimentally confirmed that the precipitation of MnS is greatly influenced by oxide inclusions and cooling rate. [1-5, 20, 23, 24, 38-43]. Ti oxides and Ti complex oxides are experimentally observed to act as nucleation sites for sulfides. **Figures 2.6** and **2.7** clearly show that Ti oxides or Ti complex oxides effectively serve as heterogeneous nuclei for MnS. Figure 2.7 further demonstrates that oxides also serve as heterogeneous nucleation sites for nitrides and carbides. It is also found from Figure 2.7 that carbon is effectively scavenged from the matrix becomes it becomes enriched at surfaces of oxide inclusions, but no micro-segregation of C exists around the oxides. The scavenging of carbon from the matrix favors improved steel service properties such as ductility, forgeability, weldability and machinability.

Steel composition (mass%)

C	Si	Mn	Ti*	N*
0.1	<0.1	1.0	270-290	20-25

* in ppm

Contents of O and S (ppm)

1-a	[%O]=98	[%S]=64
1-b	[%O]=68	[%S]=371

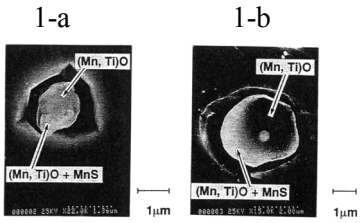

Figure 2.6. SEM images of oxides and MnS particles [42]

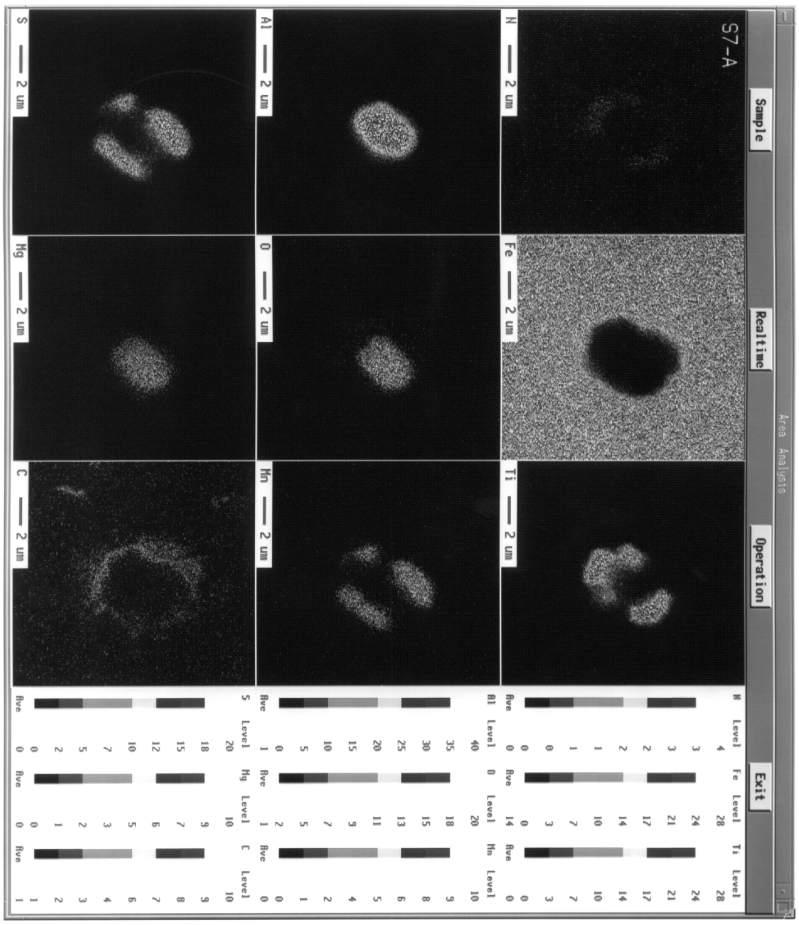

Steel composition (mass %)

C	Si	Mn	P	S	Al*	Ti*	N*	O*
0.080	0.50	1.47	0.018	0.008	360	43	34	20

* in ppm

The specimen was cut from a continuously cast slab with a thickness of 250 mm and a width of 1200 mm at the position of 1/4 width and 125 mm distance from the lower slab surface in the thickness direction.

Figure 2. 7. Characteristic X-ray images of oxides with sulfide and nitride precipitates [44]

MnS is significant in oxide metallurgy. The secondary MnS phase which precipitates during solidification in the molten steel is much more important than the primary MnS phase because MnS likely precipitates during solidification for most produced steels. The contents of Mn and S contained in these steels hardly reach the solubility product of MnS before solidification. It is evident from experiments that most MnS precipitates on the surfaces of oxides during solidification for the steels deoxidized by Ti and/or Zr[1-5, 20, 23, 24, 36-43]. A small number of globular or near globular MnS precipitates was found, resulting from homogeneous nucleation based on the metastable monotectic reaction $L_1 \rightarrow$ Fe(s) + L_2, where L_1 and L_2 present the molten steel and liquid MnS, respectively. The required supersaturation for MnS precipitation is small in the range of 1.0-1.7 [45]. As aforementioned, the precipitation and morphology of pure MnS have been extensively investigated [21, 31-35]. However, the present interest is focused on its precipitation on the surfaces of oxides.

Wakoh et al.[42] proposed a mechanism of sulfide precipitation on Mn-silicate inclusions. Oikawa et al.[20] also suggested a mechanism of MnS precipitation in Ti-killed steels. Wakoh et al.'s mechanism suggests that MnS crystallization on the surfaces of Mn-silicate is caused by the decrease of solubility of MnS for Mn-silicate with decreasing temperature during solidification. These initial MnS crystals become embryos, contributing to the further growth of MnS precipitates towards the outside and controlled by the diffusion of Mn and S in the molten steel. Oikawa et al. attributed the nucleation of MnS on the surfaces of oxides in Ti-killed steels during solidification to the monotectic reactions $L_1 \rightarrow$ Fe(s) + L_3 and $L_1 \rightarrow$ Fe(s) + L_2 + L_3, where L_1, L_2 and L_3 represent the molten steel, liquid MnS and liquid (Ti, Mn)O, respectively. Liquid nuclei of (Ti, Mn)O are primarily generated at the Fe(s)/Fe(l) interface. After the generation of the liquid (Ti, Mn)O nucleus, liquid MnS droplets (L_2) precipitate on the surfaces of these nuclei. Then, these liquid (Ti, Mn)O nuclei covered with liquid MnS are engulfed by the Fe(s)/Fe(l) interface resulting in fine dispersions of MnS and oxides. However, both proposed mechanisms cannot completely explain the experimental results and cannot generally deal with MnS precipitation in industrially produced steels. Further investigations on MnS precipitation will be discussed in Chapter 6 where a new mechanism is proposed to generally explain MnS precipitation in industrially produced steels.

2.4 Formation of Intragranular Ferrite (IGF)

Proeutectoid ferrite can nucleate at inclusions within austenite grains. This makes it possible to obtain a fine ferrite-pearlite microstructure through coarse austenite grains. The generation of IGF at inclusions to refine grain structures effectively improves the toughness of steel to a sufficient level without heat treatment in addition to the conventional austenite grain refinement techniques. This technology is called IGF technology and is of great interest to welding and structural steels and components of automobiles. Obviously, it is the crux of this technology to generate finely dispersed inclusions within austenite grains which effectively act as nucleation sites for IGF. Extensive and intensive researches have been done on IGF technology [37, 39, 46-69]. However, most of the reported results are focused on weld metals and steels at welding thermal cycles. Only in a few cases IGF technology was directly applied to steelmaking processes such as solidification[37,39] and rolling processes[52]. IGF technology in welding is quite different from that in steelmaking because of utter different thermal cycles between welding and steelmaking processes. However, the philosophy behind them is similar or consistent no matter how different the thermal cycles are.

Reported results show that intragranular ferrite can nucleate on precipitates such as oxides, sulfides and nitrides[37,39,43,46-69]. **Figure 2.8** gives an example of oxides in a low carbon steel serving as heterogeneous nucleation sites for IGF in the heat affected zone during cooling from austenite region after welding. The principles of IGF nucleation on fine oxide inclusions have been extended to sulfides, nitrides and carbides for low carbon steels at welding thermal cycles [54, 58-60]. An example is shown in **Figure 2.9**. The nucleation potential for IGF strongly depends on inclusions [49]. Up to now, there exists no uniform theory to clearly explain IGF transformation. **Table 2.3** collects various proposed theories to consider IGF transformation. It is worth mentioning that IGF transformation may be caused by a combined operation of these mechanisms. The increase of the driving force for nucleation is also an important factor.

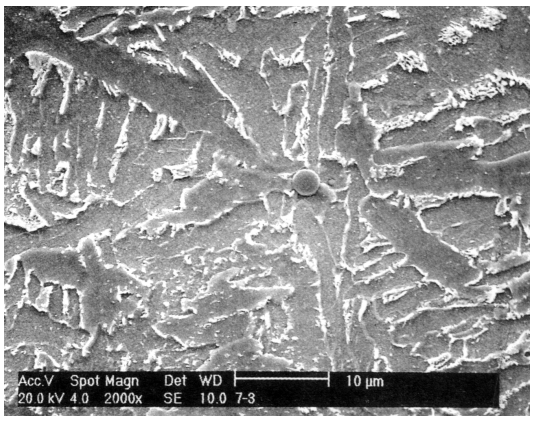

Steel composition (mass %):

C	Si	Mn	S	Ti	O (ppm)	N (ppm)
0.15	0.24	1.50	<0.007	0.011-0.014	80-120	4-10

Figure 2.8. IGF nucleated on the surface of Ti oxide in the heat effected zone after a welding thermal cycle (peak temperature of 1400 °C and cooling time of 20 seconds from 800 to 500 °C)[44]
(Note: normally sulfides precipitated on Ti-oxides)

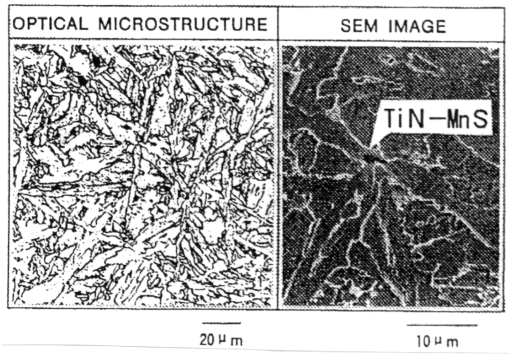

Steel composition (mass %):

C	Si	Mn	S	Ti	Al	N (ppm)
0.06	0.14	1.48	0.003	0.0011	0.033	40

Figure 2.9. TiN-MnS serving as nucleation sites for IGF in the heat affected zone after a welding thermal cycle (peak temperature of 1400 °C, heat input of 20 $kJ \cdot mm^{-1}$ and cooling time of 160 seconds from 800 to 500 °C) [60]

Table 2.3. Summary of IGF formation mechanism

Precipitates, inclusions	transformation theory	Ref.
	Epitaxitial growth theory	[50]
TiO	$\delta = 3.0\%$	[46, 48]
TiN	$\delta = 3.8\%$	[46]
VN	$\delta = 0.7\%$	[58, 60]
Fcc galaxite ($Al_2O_3 \cdot MnO$)	$\delta = 1.8\%$	[46]
γAl_2O_3	$\delta = 3.2\%$	[46]
CuS	$\delta = 2.8\%$	[46]
	Thermal expansion theory	[62]
$(MnO)_2(Al_2O_3)_2(SiO_2)$	•Thermal strain	
Al containing inclusions	• Plastic strain	
	Inclusion size theory	[67]
Inclusion size	≥ 1 μm: GBF	[67]
	≥0.6 μm: IGF	
Oxide inclusion	≥ 0.4 μm pining γ grain boundary	[69]
	Fine inclusions: ineffective	
	Composition variation	[62, 65]
	such as Mn around inclusions	
	Reducing interfacial energy	[68]
(Al·Si-S-Ti-Mn)O		[68]
TiN-MnS		[60]
TiN		[65]

where misfit between two phases, δ, is calculated for particular planar parallelisms using the following equatio

$$\delta = \delta_{(hkl)_{phase2}}^{(hkl)_{phase1}} = \sum_{i=1}^{3} \frac{| d_{[uvw]_{phase1}} \cos\theta - d_{[uvw]_{phase2}} |}{\frac{d_{[uvw]_{phase2}}}{3}} \cdot 100$$

$(hkl)_{phaseK}$: low index plane of phase K (K=1 and 2)

$[uvw]_{phaseK}$: low index direction in $(hkl)_{phaseK}$

$d_{[uvw]_{phaseK}}$: interatomic spacing along $[uvw]_{phaseK}$

θ : angle between $[uvw]_{phase1}$ $[uvw]_{phase2}$

2.5 Inclusions in view of Castability and Quality of Continuously Cast Steel

As aforementioned, alumina in steel is easily to form cluster. These cluster inclusions such as Al_2O_3, $Al_2O_3 \cdot MgO$ and $Al_2O_3 \cdot SiO_2$ are difficult to be removed from liquid steel and tend to cause nozzle clogging resulting in a breakdown of the whole casting process. They also exert detrimental effects on steel service properties. Ca is introduced to treat Al-killed steels to avoid the formation of solid alumina. Ca addition transforms solid alumina to liquid Ca-aluminates, reducing nozzle clogging and improving steel service properties. **Figure 2.10** [70] gives the effect of O content and composition of top slag on castability of continuously cast steel. Ca addition effectively modifies alumina inclusions not only in composition but also in morphology contributing to improvement of steel service properties. Steel service properties can be guaranteed without the requirement of ultra clean if the maximum particle size is controlled below a critical level [71]. Of course, finely dispersed inclusions do not tend to cause nozzle clogging. Al deoxidation as well as Ca treated Al deoxidation hardly produce fine inclusions because their corresponding inclusions are normally several to tens of micrometers in diameter. However, Ti, Zr and/or REMs provide a promising way to generate fine oxide inclusions with a diameter below 1-2 μm. After adjustment and control, the corresponding fine oxide inclusions can be evenly dispersed both in the molten steel during cooling and solidification, and in the solid steel matrix after solidification. These fine oxide inclusions guarantee macro-cleanness and serve as nucleation sites for precipitation and transformation to attain grain refinement and modification of inclusions. Finally, castability and quality of continuously cast steel are improved by the generation of these finely dispersed oxide inclusions. The present investigations show that high impact toughness for as-cast stainless, low carbon and low alloyed steels is obtained through the control and utilization of inclusions. Unfortunately, the author did not find the report on impact toughness of as-cast deoxidized steels.

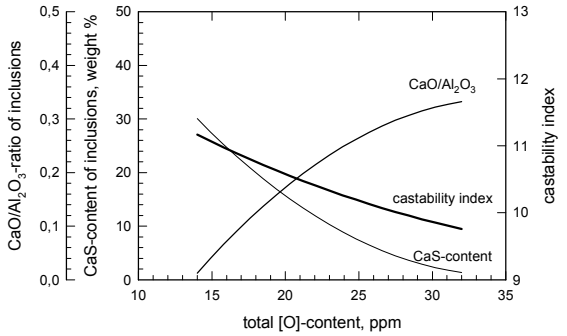

Figure 2.10. Influence of oxygen content and composition of top slag on castability [70]

2.6 Oxide Metallurgy

It is a major objective of research and development to control steel properties from either upstream or downstream processing. With the forthcoming technologies of thin slab casting, hot direct rolling and near net shape casting, important metallurgical changes from melt to sheet have taken place. **Figure 2.11** [72] predicts the tendency of using new technologies. **Figure 2.12** shows important metallurgical changes from melt to sheet with parameters of time and temperature. The changes are gradually renewing our traditional concepts and views, and transform steel production to a high-tech industry. From figure 2.12, it is obvious that inclusion precipitation starts at the very beginning of deoxidation, particularly oxide precipitation. It is also confirmed that phase transformation has close relations to inclusion precipitation. Therefore, it is possible to control steel properties pronouncedly via control of inclusion precipitation. That is why inclusion precipitation occurring during and after solidification has received great attention as to the utilization of these inclusions instead of removing them to extremely low levels. With the concept of oxide metallurgy, nonmetallic inclusions need not necessarily be harmful to steel service properties. They can effectively be used as

nucleation sites for precipitation and transformation to improve steel service properties.

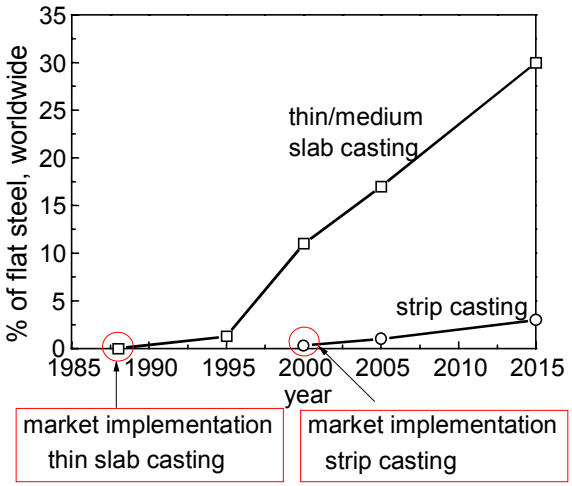

Figure 2.11. Tendencies of producing thin slab and strip casting flat steels [72, 37]

The chart shown in **Figure 2.13** clearly indicates that nonmetallic inclusions meeting the requirements are beneficial to steel service properties. This type of nonmetallic inclusion is called "designed inclusion". Its formation represents the key to oxide metallurgy. The designed inclusions (their composition, size and distribution) should be decided by the requirements (which can be generally laid down according to the demands for steel service properties) and are produced via alternative deoxidation technology during oxidizing, cooling and solidification. They will refine grains by generation of intragranular ferrite (IGF) during solidification and rolling processes. Thus, both the accessibility of determining designed inclusions by demands for steel service properties and the reliability of producing designed inclusions via alternative deoxidation technology become the central tasks of oxide metallurgy.

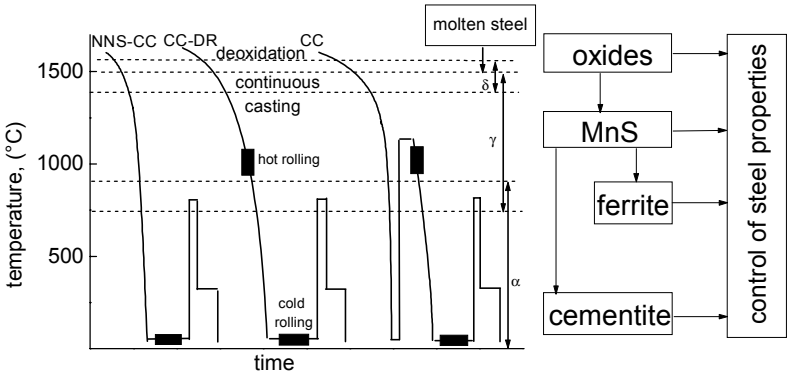

CC: Continuous casting, NNS: near net shape casting, DR: direct rolling

Figure 2.12. Temperature-time profile of various steelmaking process [2]

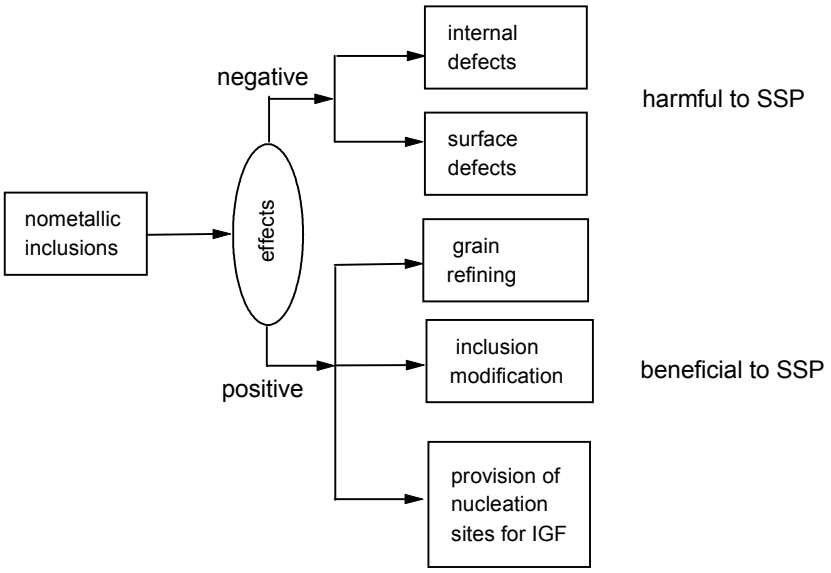

SSP: steel service properties

Figure 2.13. Effect of nonmetallic inclusions on steel service properties[73]

References

[1] T. Takamura and S. Mizoguchi: 6th Int. Iron and Steel Congress, Vol.3, Steelmaking I, Oct. 1990, Nagoya, ISIJ, 591/597

[2] S. Mizoguchi and T. Tamamura: 6th Int. Iron and Steel Congress, Vol.3, Steelmaking I, Oct. 1990, Nagoya, ISIJ, 598/604

[3] T. Sawai, M. Wakoh, Y. Ueshima and S. Mizoguchi: 6th Int. Iron and Steel Congress, Vol.3, Steelmaking I, Oct. 1990, Nagoya, ISIJ, 605/611

[4] S. Ogibayashi, K. Yamaguchi, M. Hirai and H. Goto: 6th Int. Iron and Steel Congress, Vol.3, Steelmaking I, Oct. 1990, Nagoya, ISIJ, 612/17

[5] S. Mizoguchi: "A study on segregation and oxide inclusions for the control of steel properties", Ph. D. thesis, The University of Tokyo, 1996

[6] E. Scheil: Z. Metallkd., 34(1942), 70

[7] H. D. Brody, M. C. Flemins: Trans. Metall. Soc. AIME, 236(1966), 615

[8] T. W. Clyne and W. Kurz: Metall. Trans. A, 12A(1981), 965

[9] I. Ohnaka: Tetsu-to-Hagane, 70(1984), S913 and Trans. Iron Steel Inst. Jpn., 26(1986), 1045

[10] S. Kobayashi: J. Cryst. Growth, 88(1988), 87 and Trans. Iron Steel Inst. Jpn., 28(1988), 728

[11] L. Nastac and D. M. Stefanecu: Metall. Trans. A, 24A(1993), 2107

[12] T. Himemiya and T. Umeda: ISIJ International, 38(1998), 730/738

[13] H. Goto, K. Miyazawa, K. Yamaguchi, S. Ogibayashi and K. Tanaka: ISIJ Intern., 34(1994), 414/419

[14] H. Goto, K. Miyazawa, W. Yamada and K. Tanaka: ISIJ Intern., 35(1995), 708/714

[15] H. Goto, K. Miyazawa and T. Kadoya: ISIJ Intern., 35(1995), 1477/1482

[16] H. Goto, K. Miyazawa and T. Tanaka: ISIJ Intern., 35(1995), 286/291

[17] H. Goto, K. Miyazawa and H. Honma: ISIJ Intern., 36(1996), 537/542

[18] T. Sawai, M. Wakoh, Y. Ueshima and S. Mizoguchi: ISIJ Intern., 32(1992), 169/173

[19] C. Zhou and R. Priestner: ISIJ Intern., 36(1996), 1397/405

[20] K. Oikawa, K. Ishida and T. Nishizawa: ISIJ Intern., 37(1997), 332/338
[21] K. Schwerdtfeger: Arch. Eisenhüttenwes., 41(1970), 923
[22] H. Takada, I. Bessho and T. Ito: Tetsu-to-Hagane, 62(1976), 1319
[23] T. Sawai, M. Wakoh and S. Mizoguchi: Tetsu-to-Hagane, 82(1996), 587/592
[24] M. Wakoh, T. Sawai and S. Mizoguchi: Tetsu-to-Hagane, 82(1996), 593/598
[25] T. Du, Q. Han and C. Wang: Physical Chemistry of Rare Earth, Alkaline Earth and Other Elements and Their Applications in Materials, Academic Press, Beijing, 1995
[26] L. Jia, L. Tang, Q. Lin, G. Shong and L. Liu: private communication, Project "Comprehensive Purification of the Molten Steel by Using Rare Earth and Alkaline Earth Metals" won the fourth class prize of "Development of National Science and Technology of China" 1998
[27] M. Wintz, M. Bobadilla, J. Lehmann and H. Gaye: ISIJ intern., 35(1995), 715/722 or H.Gaye, P. Rocabois, J. Lehmann and M. Bobadilla: steel research, 70(1999), 356/61 or P. Rocabois, J. Lehmann, H.Gaye and M. Wintz: Journal of Crystal Growth, 198/199(1999), 838/43
[28] C. Gatellier, H. Gaye, J. Lehmann, J. Bellot and M. Moncel: CIT-Rev. Metall., 4(1992), 361
[29] T. Matsumiya: Metall. Trans. B, 33B(1992), 783
[30] Z. Ma and D. Janke: ISIJ Intern., 38(1998), 46/52
[31] C. E. Sims and F. B. Dahle: Trans. Am. Foundarymens's Ass., 46(1938)
[32] W. Dahl, H. Hengstenberg and G. Düren: Stahl und Eisen, 86(1966), 782
[33] E. T. Turkdogan and R. A. Grange: J. Iron and Steel Inst., 208(1970), 482
[34] Y. Itoh, J. Yonezawa and Y. Matsubara: Tetsu-to-Hagane, 68(1982), 1569
[35] K. Oikawa, H. Ohtani, K. Ishida and T. Nishizawa: ISIJ International, 35(1995), 402/408
[36] F. Ishikawa, T. Takahashi and T. Ochi: Metall. Trans. A, 25A(1994), 929
[37] Z. Ma, D. Peisker and D. Janke: steel research, 70(1999), 178/182

[38] Z. Ma and D. Janke: The 3rd CAST (China Association of Science and Technology) Conference of Young Scientists, Vol. Materials Science and Industrial Technology, August, 1998, Beijing, 46/50

[39] Z. Ma and D. Janke: Technical Report "Improvement of fine grain structures of 27MnSiVS steel", Institute of Iron and Steel Technology, TU Freiberg, November, 1998

[40] K. Yamamoto, T. Hasegawa and J. Takamura: ISIJ International, 36(1996), 80/86

[41] see ref. [5]

[42] M. Wakoh, T. Sawai and S. Mizoguchi: ISIJ International, 36(1996), 1014/1021

[43] Z. Ma and D. Janke: Annual Technical Report of ECSC Sponsored Project under Grant No. ECSC-95-C2.03c, Institute of Iron and Steel Technology, TU Freiberg, 1998

[44] The picture obtained from Dr. K. S. Oh (POSCO, South Korea): Private Communication, October, 1998

[45] K. Suzuki, A. Ejima and K. Nakanishi: Trans. ISIJ, 15(1985), 433/442

[46] R. Mills, G. Thewlis and J. A. Whiteman: Materials Science and Technology, 3(1987), 1051/1061

[47] R. A. Ricks, P. R. Howell and G. S. Barrotte: J. Mater. Sci., 17(1982), 731/740

[48] J. L. Lee and Y. T. Pan: Mater. Sci. Eng., 136A(1991), 109/19, Metall. Trans. A, 22A(1991), 2818/22, 24A(1993), 1399/1408

[49] D. J. Abson: Weld. World, 27(1989), 76/101

[50] B. L. Bramfitt: Metall. Trans., 1(1970), 1987/1995

[51] F. J. Barbaro, P. Krauklis and K. E. Easterling: Materials Sci. and Tech., 5(1989), 1057/77

[52] T. Funakoshi, T. Tanaka, S. Ueda, M. Ishikawa, N. Koshizuka and K. Kobayashi: Trans. ISIJ, 17(1997), 419/424

[53] D. Yu, F. J. Barbaro, T. Chandra and D. P. Dunne: ISIJ International, 36(1996), 1055/1062

[54] H. Homma, S. Ohkita, S. Matsuda and K. Yamamoto: 67th AWS Convention, Atlanta, USA, 1986

[55] Y. Zhu, S. Guo, J. Xu, G. Jiang, D. Yu, L. Pan and Y. Wang: Acta Metallurgica Sinica, 32(1996), 891/896

[56] N. Mori, H. Honma, M. Wakabayashi and S. Ohkita: J. Jpn. Weld. Soc., 50(1981), 786
[57] I. Watanada and K. Kojima: J. Jpn. Weld. Soc., 50(1981), 703
[58] F. Ishikawa, T. Takahasi and T. Ochi: Metall. Materials Trans. A, 25A(1994), 929/936
[59] T. Ochi, T. Takahashi and H. Takada: Iron & Steelmaker, 16(1989), 21/28
[60] Y. Tomita and N. Saito: ISIJ International, 34(1994), 829/835
[61] G. M. Evans: Met. Constr., 44(1986), 631/636
[62] L. Devillers, D. Kaplan, B. Marandet, A. Ribes and P. V. Riboud: in Conf. on the effects of residual, impurities and micro-alloying elements on the weldability and weld properties, The Welding Institute, Abington, UK, 1983, 1/12
[63] S. St-Laurent and G. L'Esperance: Mater. Sci. Eng. A, 149A(1992), 203/216
[64] Y. Ueshima, H. Yuyama, S. Mizoguchi and H. Kajioka: Tetsu-to-Hagane, 75(1989), 501/08
[65] K. Yamamoto, T. Hasegawa and J. Takamura: ISIJ International, 36(1996), 80/86
[66] S. Kanazawa, A. Nakashima, K. Okamoto and K. Kanaya: Trans. ISIJ, 16(1976), 486/495
[67] J. Jang and J. E. Indacochea: J. Mater. Sci., 22(1987), 689/700
[68] M. Enomoto and H. I. Aaronson: Metall. Trans. A, 17A(1986), 1381/1384
[69] M.Ferrante, K. Akune and M. Odaina: J. Mater. Sci., 22(1987), 351
[70] D. Janke, Z. Ma, P. Valentin, A. Heinen: "Improvement of castability, structure and properties of continuously cast steel", 10th Japan-Germany Seminar on the Fundamentals of Iron- and Steelmaking, Tokyo, 18-19 May, 1999
[71] H. Kobayashi, T. Kurokawa, T. Shimomura, K. Matsudo and S. Miyahara: Trans. ISIJ, 23(1983), 410/416
[72] K. Schwaha: 1996, cited from the report "Strangiessen und Brammeneinsatz bei der Stahlerzeugung" by M. Wolf, Institute of Iron and Steel Technology, TU Freiberg, July 17, 1997, 44
[73] Z. Ma and D. Janke: Annual Technical Report of ECSC Sponsored Project under Grant No. ECSC-95-C2.03c, Institute of Iron and Steel Technology, TU Freiberg, 1997

CHAPTER 3
Deoxidation Techniques Used in Steelmaking Processes

The temperature dependence of oxygen solubility in pure liquid iron is expressed by Eq. (3-1).

$$\log\%[O]_{\max} = -\frac{6380}{T} + 2.765 \quad [1] \qquad (3\text{-}1)$$

At normal steelmaking temperatures, oxygen solubility is above 0.2 mass% and it is 0.168 mass% at the monotectic temperature (1527 °C) in the Fe-O binary system. However, oxygen solubility is negligibly small in solid iron shown in **Figure 3.1**.

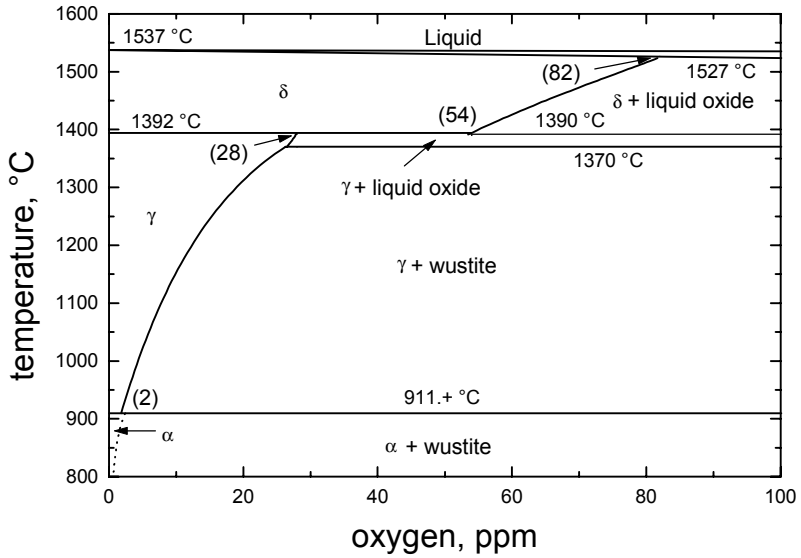

Figure 3.1. Iron side of the Fe-O phase diagram [1]

Thus, the dissolved oxygen in liquid steel may react with alloying elements during cooling and solidification to form oxides. These reactions will consume alloying elements and carbon resulting in different defects. Moreover, the reaction products may greatly deteriorate steel service properties such as ductility, fracture toughness, machinability, wear

resistance and susceptibility to hydrogen induced cracking. Therefore, the oxygen content in steel melts must be reduced to a desired low level. This basic need for steelmaking leads to deoxidation technology. However, it is unavoidable to admit nonmetallic inclusions in steel, at least in small quantities. These residual inclusions exert strong effects on steel service properties. Attention has been increasingly devoted to control these residual inclusions. It is the aim to produce finely dispersed inclusions and to use them to alleviate or diminish their harmful effects and even to exert beneficial effects on steel service properties.

According to the conventional steel deoxidation, there exist the following three categories:

- resulphurised and rimming steel deoxidized with ferromanganese to 100-200 ppm oxygen,
- semi-killed steel deoxidized with Si-Mn to 50-70 ppm, with Si-Mn-Al to 40-20 ppm and with Si-Mn-Ca to 20-15 ppm oxygen,
- killed steel fully deoxidized with a strong deoxidizer such as Al or Al-Ca, preventing any reaction between carbon and oxygen during solidification.

However, most of the presently produced steels are killed steels. Normally, deoxidation is performed during tapping and refining. With a wide application of various types of steel refining processes in recent years, it is now a common practice to produce steel grades with low levels of impurities and inclusions.

As mentioned above, Al is widely used as deoxidant in steelmaking. However, most steel problems can be traced to alumina or Al-rich oxides. To alleviate or eliminate their harmful effects on steel service properties, Ca has been frequently employed to treat Al-killed steels to avoid the formation of solid alumina. However, Ca treatment cannot meet the requirements of either high fatigue resistance in service or high cold formability in very thin gauges. The residual inclusions in steel are of importance to steel service properties. Therefore, **clean deoxidation technology** is becoming a topic for discussion which is to prevent steel from contamination with deoxidation products through special means to avoid their formation in steel melt. As a matter of fact, the elimination of impurities and inclusions from steel can never be fully achieved. Therefore, the composition, size, distribution and number of residual inclusions are the main objectives to the subject of attaining higher steel

purity. Partial and/or complete substitution of Ti, Zr and/or rare earth metals for Al is increasingly pursued aiming at the generation of finely dispersed oxides which can effectively act as nucleation sites for sulfide, nitride and carbide precipitates and intragranular ferrite. In this chapter, the following three deoxidation techniques are discussed and analyzed:

- conventional deoxidation technologies,
- clean deoxidation technologies,
- alternative deoxidation technologies in view of utilization of inclusions.

3.1 Conventional Deoxidation Technologies

3.1.1 Conventional and Innovative Al Deoxidation Practice

Depending on the particular process route followed at a plant, the deoxidation process is carried out by the addition of solid lump Al into the molten steel during tapping. The added Al, Al_{add}, is generally consumed by the following reactions [2,3]:

- Al oxidized by furnace slag, Al_{slag},
- Al oxidized due to air entrainment, Al_{air},
- Al dissolved in steel, Al_{diss},
- Al reacted with dissolved oxygen, $Al_{react\text{-}O}$.

$Al_{react\text{-}O}$ is simply composed of two parts. One is the reaction product Al_2O_3 retained in steel as inclusions and the other floated up as a part of the slag. According to material balance, the following Eq. (3-2) is obtained

$$Al_{add} = Al_{slag} + Al_{air} + Al_{diss} + Al_{react\text{-}O} \qquad (3\text{-}2)$$

The loss of aluminum due to reaction with oxygen picked up by the metal through the entrainment of air is usually less than 20 ppm. Thus, this loss is negligible compared with the other terms mentioned above. Normally, this deoxidation process is easy to complete, but the products hardly float up and become inclusions entrained in the molten steel. To improve steel cleanliness, exchange treatments with non-oxidizing synthetic slag and with conditioned slag normally enhanced by stirring and degassing are proposed. Exchange treatment with non-oxidizing synthetic slag aims to achieve deoxidation, desulphurization and inclusion modification. Exchange treatment with conditioned slag can be reached by adding pure CaO or a mixture of limestone ($CaCO_3$) and aluminum to the top slag in

order to lower the activity of FeO in the slag. Stirring and degassing are used to improve the kinetics of reactions.

Besides the methods mentioned above, innovative Al deoxidation techniques are pursued to more effectively reach higher purity of steel. Treatments such as injection of powered agents like Al, Ca-Al, rare earth metals and Al + CaO-Al_2O_3 into the molten steel with the help of an inert carrier gas or by submerged cored-wire injection are practically adopted[3]. Most recently, the addition of aluminum in liquid state with or without other co-additives is proposed and a higher cleanliness is obtained. However, this technique is just in primary stage and further investigations are necessary [4].

3.1.2 Ca Treatment of Al-Deoxidized Steel

Al effectively reduces the dissolved oxygen of the molten steel by the formation of solid alumina. However, the solid alumina particles in the molten steel are easily clustering due to their dendritic morphology. They hardly float to the top of the molten steel becoming inclusions detrimental to steel service properties. Ca treatment has been employed to treat Al-killed steels to avoid the formation of solid alumina mainly for long products, i.e. bloom/billet casting, but also in standard practice for slab casting, and is 100% in use for thin slab casting.

The benefits from Ca addition are briefly summarized as follows:

(1) Ca addition conventionally aims to transfer solid alumina inclusions into liquid Ca-aluminates. These liquid particles, in contrast to solid alumina, can grow in size and float up from the liquid steel to be absorbed by the top slag and resulting in cleaner steel with low oxide contents. The results are solidly confirmed by the fact that the total oxygen content in the molten steel is greatly decreased by Ca treatment after Al deoxidation compared to the molten steel deoxidized by Al. Finally, both castability and quality of continuously cast steel are improved by Ca treatment.

(2) In addition to the formation of liquid Ca aluminates, another important aspect of Ca treatment is to modify inclusion morphology, schematically shown in **Figures 3.2** and **3.3**.

Low S (S≤50 ppm):

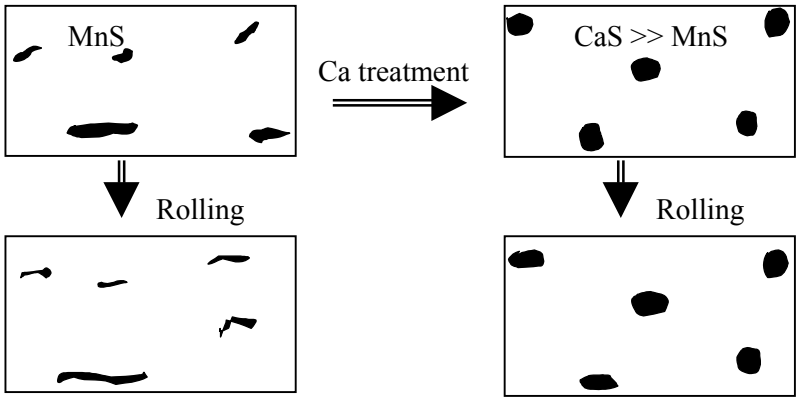

(**Figure 3.2a**)

High S (S≥300 ppm):

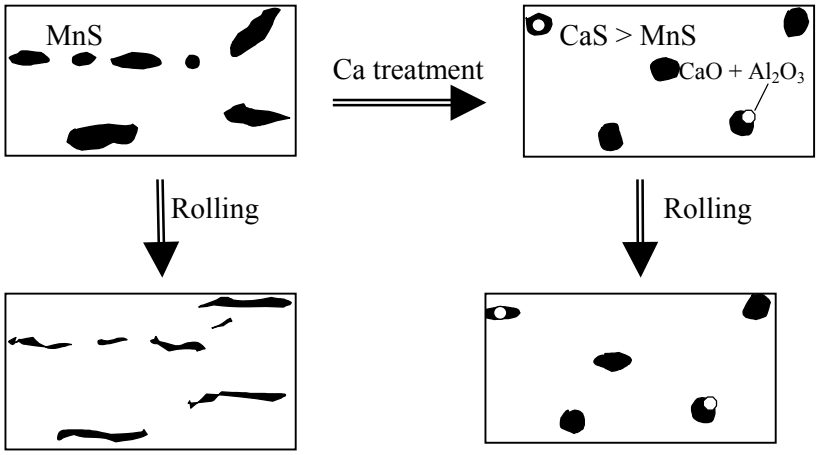

(Figure 3.2b)

Figure 3.2. Schematic images of sulfides in steel after casting and rolling
Note: Dimensions of inclusions are not in scale

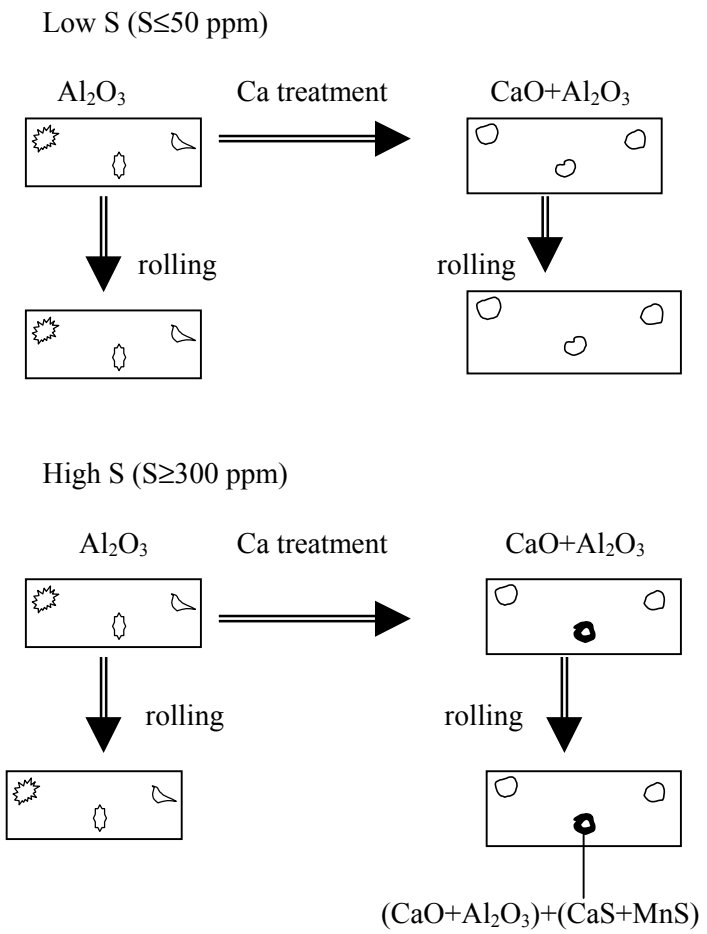

Figure 3.3. Schematic images of oxides in steel after casting and rolling
Note: Dimensions of inclusions are not in scale

When the small globular inclusions are unable to float out, they are found to have less or even no detrimental effects to both castability and service properties. In conventional steels, some sulfur exists as type II MnS which is deformed during the rolling process resulting in elongated platelets or stringers. These elongated platelets or stringers greatly deteriorate steel service properties. With Ca treatment, the type II MnS is modified to globular or near globular sulfides such as CaS and (Ca,Mn)S which are much less deformable than pure MnS. In low sulfur steels (S≤50 ppm),

most of sulfur combines Ca as Ca rich sulfides and only a small amount of sulfur exists as MnS in complex sulfides. However, Ca hardly combines all sulfur as CaS rich sulfides in high sulfur steels (S≥300 ppm). In fact, a larger amount of MnS rich sulfides is formed during and/or after casting. Therefore, increasing attention has been drawn to develop new methods to nucleate sulfides on the surfaces of oxides. The formation of these less deformed sulfides makes a great contribution to the improvement of steel service properties.

The added Ca gradually converts solid dendritic alumina inclusions to globular or near globular C-A inclusions (C: CaO and A: Al_2O_3). This kind of modification is greatly beneficial to steel castability and service properties. It is worth mentioning that the reaction between Ca and oxides continuously occurs from tapping to casting. The continuous change of inclusion composition clearly confirms this result shown in **Figures 3.4** and **3.5** [5].

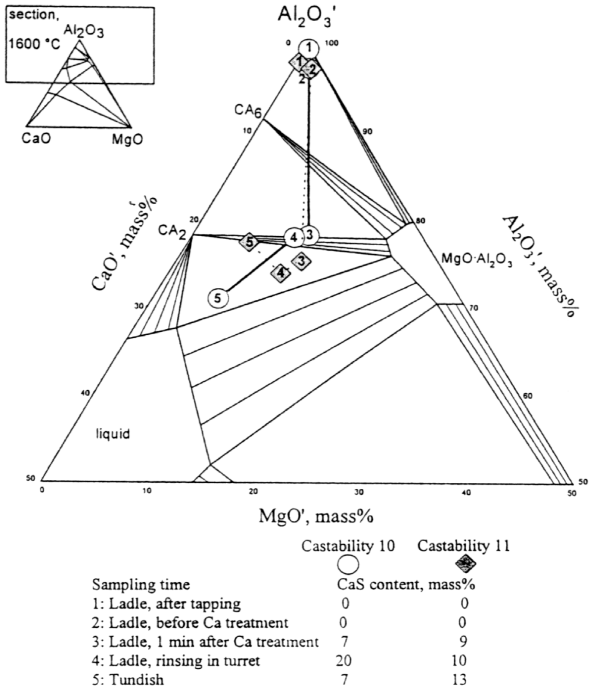

Figure 3.4. Inclusion path of the heats without RH treatment in the pseudo-ternary system CaO´-MgO´-Al_2O_3´ [5]

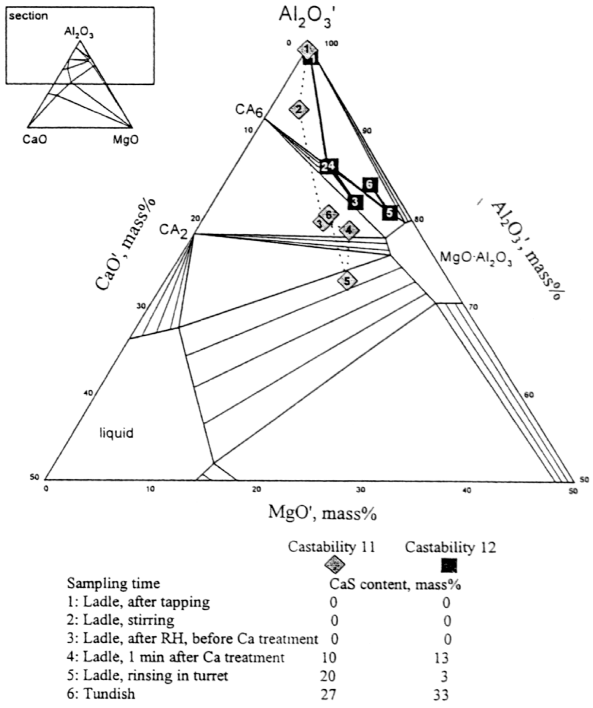

Figure 3.5. Inclusion path of the heats with RH treatment in the pseudo-ternary CaO´-MgO´-Al_2O_3´ [5]

Normally, Ca is added to molten steel through the following five methods [6].

- Conventional Method: Ca containing agents are thrown into the melt stream during teeming or into the ladle or tundish. A second popular method is to place the Ca containing agents into the ladle and tundish before pouring the steel melt.
- Injection Method: Ca containing agents are injected into the molten steel with the help of an inert carrier gas.
- Cored-Wire Injection: This is similar to the technology of introducing Al wire into steel melts, but the wire consists of a steel sheath which is tightly wrapped around a core of Ca containing agents.
- Bullet Shooting Method: Ca containing bullets, as an Al shell in which compressed Ca-Si powder is enclosed, are shot into the molten steel by a shooter powered by gas pressure.

- Wire Lance Injection: This method combines features of the Injection Method and the Cored-Wire Injection. The calcium wire is fed into the molten steel through a ceramic lance, which is submerged into the molten steel. Before feeding, the lance is purged with an inert gas and the gas flow continues during the whole wire feeding operation.

The injection of Ca and its alloys into the molten steel is important for control of sulfur, oxygen and inclusions and the production of quality steels with improved service properties. After the injection of Ca into the molten steel, Ca melts, vaporizes and then partially dissolves into the liquid steel, Ca (s) $\rightarrow$ Ca (l) $\rightarrow$ Ca (g) $\rightarrow$ [Ca] (in liquid steel). The dissolved Ca reacts not only with the dissolved oxygen and oxide inclusions such as Al_2O_3, but also with the dissolved sulfur or sulfide inclusions such as MnS in the light of the following reactions

$$[Ca] + [O] = (CaO)\ , \qquad (3\text{-}3)$$

$$[Ca] + (x+1/3)\ (Al_2O_3) = (CaO{\cdot}xAl_2O_3) + 2/3\ [Al], \qquad (3\text{-}4)$$

$$[Ca] + [S] = (CaS), \qquad (3\text{-}5)$$

$$[Ca] + (MnS) = [Mn] + (CaS). \qquad (3\text{-}6)$$

Calcium aluminates may form in the following sequence depending on the contents of Ca, Al, O in the molten steel and Al_2O_3, CaO in inclusions:

$$A \rightarrow CA_6 \rightarrow CA_2 \rightarrow CA \rightarrow C_{12}A_7$$

Thermodynamic considerations on Ca treatment are discussed in detail in Ref. [5, 7-9]. Detailed studies of the effect of inclusions on the physical and mechanical properties of steel are available in Ref. [10-12].

3.2 Clean Deoxidation Technologies

In view of the fact that several steel problems can be traced back to nonmetallic inclusions, a deoxidation technology is wanted that can effectively remove oxygen from steel melts with prevention of contamination by deoxidation products. **Clean deoxidation technology** has increasingly received attention from both metallurgists and

metallurgical engineers. It is time to deeply and systematically investigate the new technology. The available research work related to this technology is summarized and discussed as follows.

3.2.1. Electrolytic Deoxidation

Electrochemical cells based on oxygen ion-conducting ceramics electrolytes have been used to determine the dissolved oxygen in metal melts since the 1960's. In such a cell, the measured EMF, E, is closely related to the oxygen partial pressure in the melt, $p_{O_2}(M)$, and that of the reference electrode, $p_{O_2}(R)$ as shown in Eq. (3-7). The used symbols are listed and explained in the "nomenclature".

$$E = \frac{RT}{F} \ln \frac{p_{e'}^{1/4} + p_{O_2}^{1/4}(R)}{p_{e'}^{1/4} + p_{O_2}^{1/4}(M)} \tag{3-7}$$

It is obvious from Eq. (3-7) that the oxygen partial pressure in the melt, $p_{O_2}(M)$, is obtained from the measurement of E when $p_{O_2}(R)$ and T are known. The Henrian activity of oxygen, h_O, is deduced from the following equation

$$h_O = \exp\left(-\frac{\Delta G_O^0}{RT}\right) p_{O_2}^{1/2}(M) \tag{3-8}$$

where ΔG_O^0 represents the Gibbs free energy change of the dissolution reaction of oxygen in pure liquid iron.

When an external voltage, U, is applied to the cell, the solid electrolyte cell mentioned above can be used to adjust the dissolved oxygen content in metal melts achieving deoxidation or oxidation. The following equation is considering this process [13]:

$$U = E + I_{ion} \cdot R_{ion} = \frac{RT}{F} \ln \frac{p_{e'}^{1/4} + p_{O_2}^{1/4}(R)}{p_{e'}^{1/4} + p_{O_2}^{1/4}(M)} + I_{ion} \cdot R_{ion} \tag{3-9}$$

where I_{ion} and R_{ion} represent the ion current across and the ion current resistance of the ceramic electrolyte.

A continuous deoxidation can be achieved when a negative polarity is attributed to molten metal electrode. Laboratory scale tests were performed on the applicability of this method to remove oxygen from liquid Fe, Co, Ni, Cu and Ag [13, 14]. **Figure 3.6** gives an example of electrolytic deoxidation of an iron melt [13].

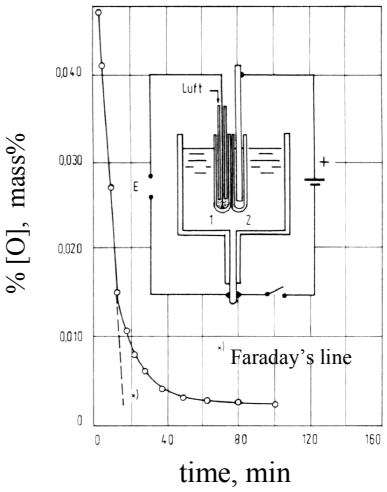

1: measuring cell ZrO_2 (CaO)
2: electrolysis cell ZrO_2 (CaO) (anodic current density 0.37 $A \cdot h^{-1}$; melt weight 460 g; melt continuously stirred; Al_2O_3 crucible; argon stream 100 $l \cdot cm^{-3}$)

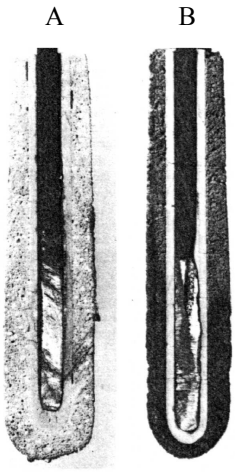

Electrolysis immersion cells with copper/gra-phite anode in longitu-dinal section after ele-ctrolytic deoxidation of iron melts

A: porous ZrO_2 (CaO)
B: porous ThO_2 (Y_2O_3)

Figure 3.6. Change of oxygen content during electrolytic deoxidation of an iron melt at 1873 K and electrolysis cells after electrolytic deoxidation [13]

The prominent advantage of this technology is that it successfully reaches deoxidation of metal melts without generation of oxidation products in the melts. This advantage is wanted for the production of clean steel. However, this technology faces some problems for its industrialization such as efficiency, reliability and costs. Most recently, Li and his co-workers [15,16] improved and modified this technology. They successfully developed a "deoxidation unit" in which solid electrolyte ZrO_2, short-circuited materials and deoxidizer are integrated into one unit. When this deoxidation unit is immersed into a liquid metal, the dissolved oxygen is forced to pass through the solid electrolyte into the deoxidation unit. The diffused oxygen reacts with the deoxidizer contained in the deoxidation unit. Therefore, deoxidation products are present inside the deoxidation unit rather than in the liquid metal. **Figure 3.7** indicates that the oxygen content in liquid steel is reduced from hundreds to several ppm in one or two minutes after the immersion of the deoxidation unit. It is found that the experimental data are located above the theoretically calculated results after 2 minutes of deoxidation. This is caused during the change of oxygen sensors because this action allows a little air to enter the atmosphere above the melt resulting in its reoxidation.

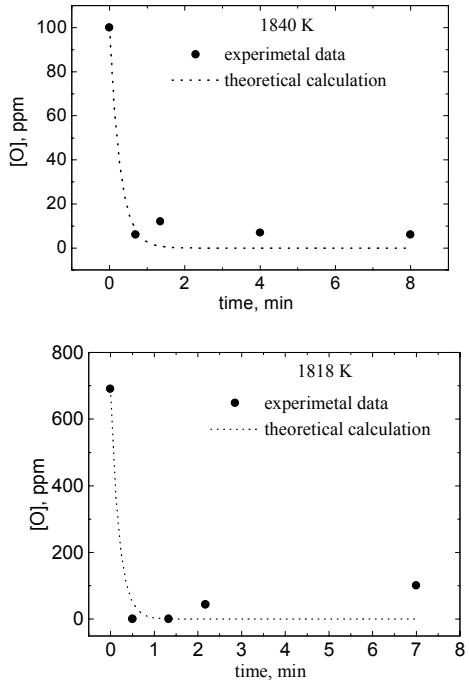

Figure 3.7. Change of oxygen content in steel melts after immersion of deoxidation units into the melts (melt weight of 200 g; the volume of the deoxidation unit represents about five percent of the melt volume)[15]

3.2.2. Deoxidation with Carbon-bearing Oxide Materials

Mixtures of oxides with graphite such as MgO+C and dolomite+C have been recently employed as refractory materials in refining of steel because these refractory materials demonstrate a superior resistance to steel melts and slags [17-20]. Janke and the present author [20] proposed a reaction mechanism between the refractory materials and steel melts revealing the fact of its superior resistance to steel melts. According to this mechanism, these refractory materials can also be employed to remove the oxygen dissolved in steel melts. Najafabadi et al. [21] experimentally confirmed that MgO+C porous tubes can be used to remove the oxygen in steel melts to low levels. Clean deoxidation (without or less deoxidation products present in steel melts) is easily reached by using this deoxidation technique. Reducing the internal pressure of the MgO+C porous tube favors the deoxidation process. Further investigations are needed for improving this new technology.

3.3 Alternative Deoxidation Techniques in view of Utilization of Inclusions

The improvement of steel cleanness is a key task in conventional steelmaking processes. Steel castability and quality have been greatly improved by adoption of advanced steelmaking technologies, particularly secondary refining metallurgy, which effectively removes impurities and inclusions to very low levels. Numerous investigators found that most steel problems can be traced to nonmetallic inclusions. It is a commonly accepted view that nonmetallic inclusions are harmful to both steelmaking processes and steel service properties. However, the potential to further improve steel cleanliness based on the addition of Al and Ca seems to be limited. Moreover, low levels of impurities and inclusions need not necessarily guarantee excellent steel service properties because these are greatly influenced by the remaining inclusions. It has to be recognized that steel service properties can be guaranteed without the requirement of ultra cleanness under the following conditions

- the maximum size of inclusions is controlled below a critical level [22],
- the inclusions possess acceptable properties for the hot-linked processes such as DHR (direct hot rolling), DSC (direct strip casting) and welding [22, 23].

Thus, generation of finely dispersed inclusions with favorable properties related to the hot- linked processes is of importance to produce quality steel. This approach provides a radical change in future cleanness assurance, i.e. inclusions have to be controlled below a critical level in diameter despite a higher total oxygen content resulting in lesser demands in view of refining and tundish metallurgical process. These simplify the requirements for conventional slags and refractories in view of the production of clean steel. Since Ti, Zr and rare earth metals are strong oxide formers, they can be used to remove oxygen from molten steel. Steels deoxidized by Ti, Zr and rare earth metals have increasingly been pursued more recently because their deoxidation products are finely dispersed in steel in globular or nearly globular shape with a low tendency to collision growth in molten steel. These finely dispersed oxides not only guarantee good castability but also further improve steel service properties through effectively acting as nucleation sites for precipitates such as MnS and for phase transformation with respect to IGF. With this approach, the controlled nonmetallic inclusions are no longer harmful to steel service properties in view of insuring macro-cleanness, grain refinement and modification of inclusions. This approach terms **Oxide Metallurgy** as a foremost tool of "Inclusion Engineering". The following chapters will discuss it in detail.

References:

[1] E. T. Turkdogan: Fundamentals of Steelmaking, The University Press, Cambridge, 1996

[2] E. T. Turkdogan: Ironmaking and Steelmaking, 15(1988), 311/17

[3] B. Deo and R. Boom: Fundamentals of Steelmaking Metallurgy, Prentice Hall International, New York, 1993, 216/253

[4] J. Whitbread, A. Cubero and L. Zampetti: Draft Final Report "Improved Deoxidation Practices for Ultra Clean Steel Production", ECSC sponsored project, Jan. 1999, British Steel plc, Sidenor I & D and Centro Sviluppo Materiali.

[5] D. Janke, Z. Ma, P. Valentin and A. Heinen: ISIJ International, 40(2000), 31/39

[6] T. Ototani: Calcium Clean Steel, Springer-Verlag, Berlin, 1986, 20/28

[7] H. Gaye, D. C. Gatellier, M. Nadif, P. V. Riboud, J. Saleil and J. Faral: Congress "Clean Steel 3", Balatonfüred, 1986, 433/439
[8] K. Larsen and R. J. Fruehan: Trans. ISS, I&SM, 1990, July, 45
[9] O. Wijk: "Inclusion Engineering", ScanJect VII. 7th International Conference on Refining Process, Ludea, June 7-8, 1995, 35/67
[10] L. E. K. Holappa: Int. Mater. Rev., 27(1982), 53/76
[11] K. W. Lange: Int. Mater. Rev., 33(1988), 53/89
[12] L. E. Holappa and R. V. Väinölä: "Inclusion Control – Key to Mastering Properties of High Performance Steels", XLVIII Berg- und Hüttenmännischer Tag, 20-21 June, 1996, Freiberg, Paper 3
[13] D. Janke: Arch. Eisenhüttenwes., 49(1978), 217/24
[14] D. Janke: Z. Metallkde., 69(1978), 302/307
[15] F. Li et al: unpublished paper
[16] K.-C. Chou and F. Li: China Patent, No. 97116954.3, 1997
[17] V. Brabie: steel research, 68(1997), 54/60
[18] S. Miglani and J. J. Uchno: Veitsch-Radex Rundschau, 1998, No. 2, 3/12
[19] W. Meyer, A. Franchi, G. Buchebner and M. Willingshofer: Veitsch-Radex Rundschau, 1998, No. 2, 32/44
[20] D. Janke and Z. Ma: Veitsch-Radex Rundschau, 1999, No.2, 61/83
[21] M. A. Najafabadi, M. Hirasawa and M. Sano: ISIJ International, 36(1996), 1366/1372
[22] H. Kobayashi, T. Kurokawa, T. Shimomura, K. Matsudo and S. Miyahara: Trans. ISIJ, 23(1983), 410/416
[23] Z. Ma, D. Peisker and D. Janke: steel research, 70(1999), 178/82

CHAPTER 4
Experimental Apparatus and Procedures

The present experiments aim to generate finely dispersed oxides serving as nucleation sites for intergranular ferrite (IGF) and sulfides, nitrides and carbides through alternative deoxidation technology and control of solidification. These aims are supposed to be reached by partial and/or complete substitution of Ti and Zr for Al and increased cooling rates. Commercial steels such as low carbon steel, Cr-Ni based austenitic stainless steel and 27MnSiVS steel are investigated objectives. In this chapter, the presently employed experimental equipment and procedure are systematically given and explained. The experimental investigations are carried out for determining the optimum conditions of generating finely dispersed oxides. Different factors to influence oxides' composition, size and distribution and their capability to act as nucleation sites for IGF and sulfides, nitrides and carbides are investigated.

4.1 Experimental Unit and Investigated Steels

A vacuum induction furnace is used in the present experiments schematically shown in **Figure 4.1**. **Figure 4.2** illustrates the interior of the furnace and **Figure 4.3** indicates the sizes of the presently used casting moulds.

The compositions of the investigated steels are given in **Table 4.1** and the purities of the metallic materials and the argon gas used in the present experiments are summarized in **Table 4.2**.

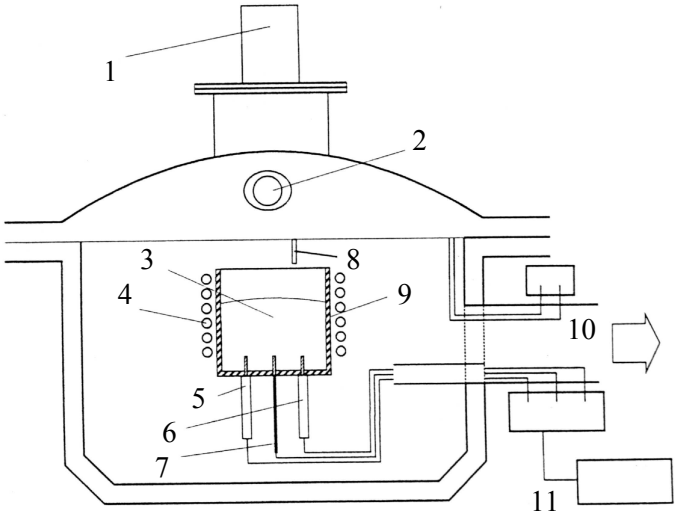

1 sampling and adding 2 viewing window 3 steel melt
4 wire 5 oxygen sensor 1 + thermocouple 6 oxygen sensor 2 + thermocouple
7 Mo rod 8 thermocouple 9 crucible
10 vacuum pumping 11 measuring equipment

Figure 4.1. Schematic vacuum induction furnace

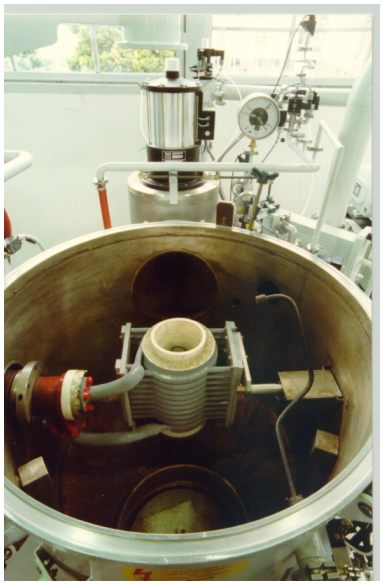

Figure 4.2. Internal view of the vacuum induction furnace

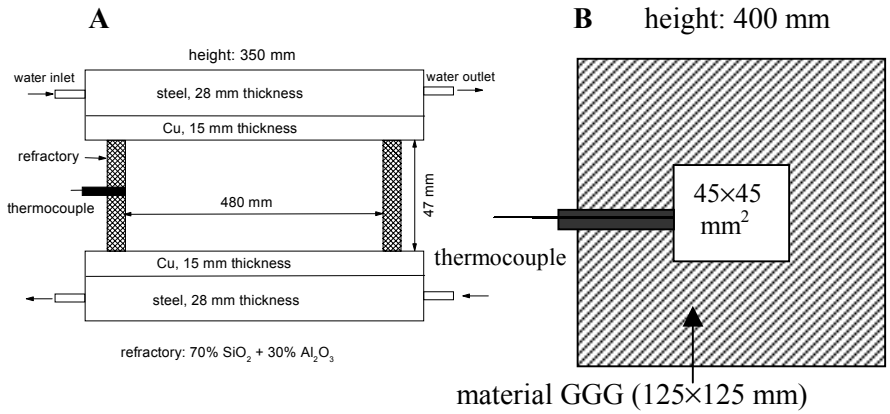

Figure 4.3. Size of casting moulds (casting mould 3-B only used for some stainless steels)

Table 4.1. Compositions of the investigated steels

Fe-Cr-Ni austenitic stainless steel

C	Si	Mn	P	S	Cr	Ni	Mo	V	Co	Cu	Nb*	N*
0.024	0.48	1.45	0.033	0.010	17.95	9.10	0.30	0.045	0.090	0.19	70	450
0.035	0.44	1.55	0.025	0.015	18.19	9.20	0.33	0.048	0.095	0.22	180	500

Low carbon steel

C	Si	Mn	P	S	Cr	Ni	Cu	Nb	N*
0.020	0.035	0.40	0.010	0.002	0.030	0.15	0.020	0.010	28
0.030	0.080	1.50	0.030	0.012	0.140	0.25	0.030	0.012	40

Ultra-low carbon steel

C*	Si	Mn	P	S	Cr	Ni	Cu	Nb
8	0.005	0.40	0.010	0.009	0.03	0.09	0.020	0.009
10	0.028	1.20	0.015	0.011	0.08	0.14	0.030	0.012

27 MnSiVS steel

C	Si	Mn	P	S	Cr	Ni	Mo	V	Cu	Nb*	N*
0.022	0.60	1.45	0.010	0.017	0.15	0.15	0	0	0	0	20
0.027	0.70	1.55	0.015	0.033	0.20	0.20	0.050	0.13	0.15	55	200

* ppm the contents of Al, Ti, Zr and O are controlled variables

Table 4.2. Purities of metallic materials and argon gas used in the experiments

Materials	Ti	Al	Zr	argon gas
Purity	99.9%	99.9%	99.9%	99.996%

4.2 Experimental Procedures

About 20 kg of the charge material (the investigated steel used to be deoxidized by designed deoxidants) were placed into an alumina crucible (90% Al_2O_3+10% SiO_2) and the size of which is shown in **Figure 4.4**. After heating the furnace under vacuum ($3\text{-}5\times10^{-1}$ mbar) until complete melting of the charge materials, argon gas was introduced into the furnace up to 200 mbar. This pressure was maintained in the furnace till the end of each experiment. The detailed experimental procedure is shown in the flow chart below which only represents three intervals of casting, but the intervals and weights were different in practice. Each casting weight is roughly the same. The temperature of the ingot was measured during cooling and solidification using a thermocouple as shown in Figure 4.3. Thus, the cooling rate of ingot could be estimated according to the measured temperatures.

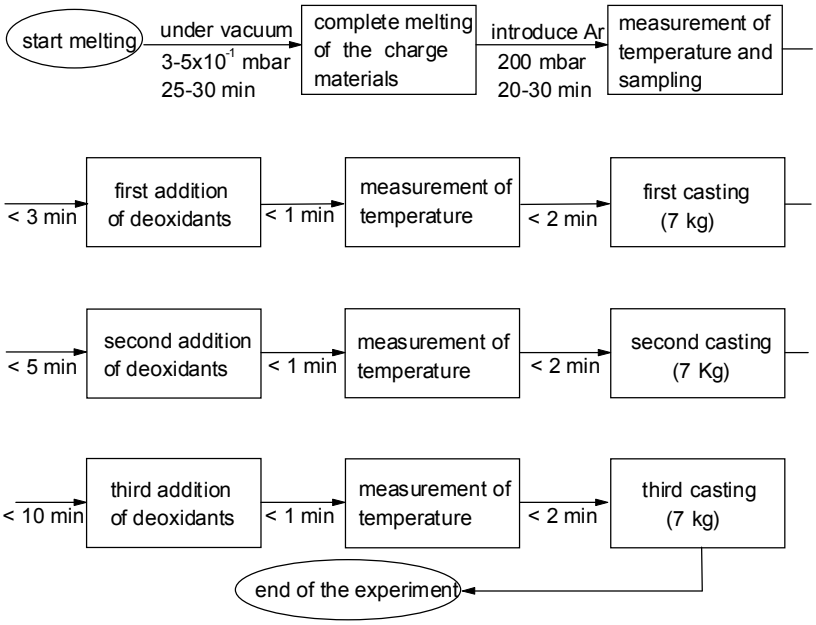

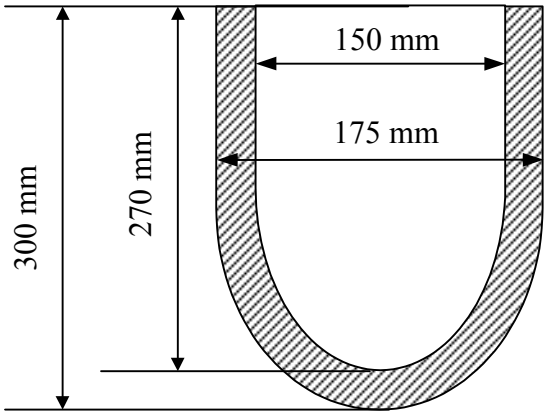

Figure 4.4. Size of the used crucible

The dissolved oxygen in the molten steel was measured using an oxygen sensor (see below) and the solid steel samples were taken from ingots for different investigations such as metallography with optical microscope and SEM micro-analysis with EPMA and SEM-EDX, microstructures and mechanical properties. Metallographic investigations were carried out by a Camera-microscope Neophot 21 with software Image C, SEM-EDX and EPMA. The surface size of the metallographic specimens was about 15×15 mm. Charpy-V-notch impact toughness of the investigated as-cast steels was also determined.

SEM: scanning electron microscope
EMPA: electron microprobe analysis
EDX: energy-dispersive X-ray micro-analysis

4.3 Oxygen Sensing and Control

Oxygen in molten steel occurs in different forms either dissolved or chemically bound in the form of oxide particles suspended in it. The total oxygen content can be determined by conventional sampling with subsequent chemical analysis while the dissolved oxygen can be directly determined by oxygen sensor measurement of the EMF generated across the sensor. One surface of the electrolyte is in contact with the molten metal and the opposite surface in contact with a reference electrode which

consists of equilibrated mixture of another metal with its oxide schematically shown in **Figure 4.5**. The electrochemical potential drop across the electrolyte is given by:

$$E = \frac{RT}{4F} \ln \frac{P_{O_2}^{'\,1/4} + P_\theta^{1/4}}{P_{O_2}^{1/4} + P_\theta^{1/4}} \qquad (4\text{-}1)$$

where R, F and T are gas constant, Faraday constant and absolute temperature, respectively; $P_{O_2}^{'}$ *and* P_{O_2} are the oxygen partial pressures in the reference electrode and the molten steel, respectively.

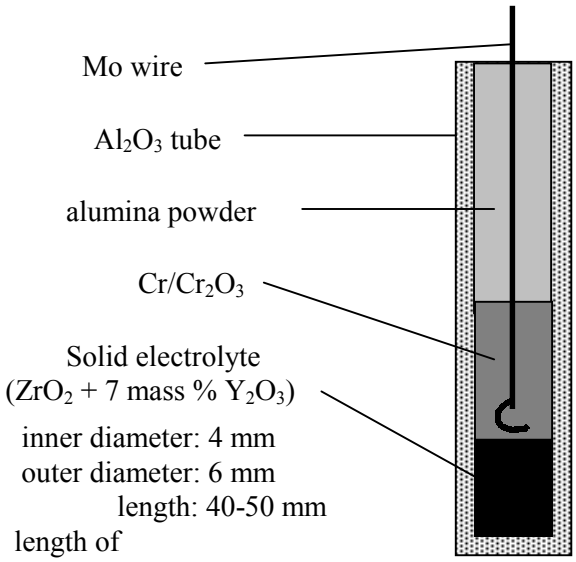

Figure 4.5. Schematic diagram of the electrochemical probe

The basic formula to determine oxygen activity in the molten melt is expressed as

$$a_O = \exp\left(-\frac{\Delta G_O^0}{RT}\right)\left[\left(P_\theta^{1/4} + P_{O_2}^{1/4}\right)\cdot \exp\left(-\frac{EF}{RT}\right) - P_\theta^{1/4}\right]^2 \qquad (4\text{-}2)$$

In the present experiments, Y_2O_3 (7 mole %) stabilized zirconia was used

as the ceramic electrolyte and a mixture of chromium and chromium oxide Cr_2O_3 (9:1 wt %) for the reference electrode. The values of the relevant parameters are given as follows:

$$P'_{O_2} = \exp\left(\frac{-747583 + 170.162T}{RT}\right) \quad \text{ref. [1]} \quad (4\text{-}3)$$

$$\log P_\theta = -\frac{58{,}600}{T} + 15.9 \quad \text{ref. [2]} \quad (4\text{-}4)$$

$$\Delta G^0_O = -115{,}750 - 4.63T \quad \text{J, at 1 mass \% O} \quad \text{ref. [3]} \quad (4\text{-}5)$$

where the units for p'_{O_2}, p_θ and ΔG^0_O are bar, bar and J·mol^{-1}, respectively.

References

[1] S. Dimitrov, H. Wenz, K. Koch and D. Janke: steel research, 66(1995), 39/43

[2] D. A. J. Swinkels: J. Electrochem. Soc., 117(1970), 1267

[3] E. T. Turkdogan: Ironmaking and Steelmaking, 29(1993), 469

CHAPTER 5
Size, Composition, Distribution and Shape of Oxides in Steel

One of the major concerns for steelmaking is to improve castability and quality of continuously cast steel in an economical and environmentally friendly way. Castability and quality standards have been greatly improved by adoption of advanced steelmaking technologies, particularly of secondary refining metallurgy which can remove impurities and inclusions to extremely low levels. It is generally accepted that the improvement of steel cleanness is an effective way to improve castability and quality of steel since conventional experiences indicate that most steel problems are in close relation to inclusion behaviour. However, the elimination of inclusions is never fully accomplished. Moreover, it is difficult and costly to produce steel with extremely low contents of inclusions. The residual inclusions exert a remarkable influence on both steelmaking processes and steel service properties. As mentioned in the first three chapters, control and utilization of these inclusions guarantee good castability and high quality of steel. Therefore, alternative deoxidation technology is meaningful to improve steel quality and castability. The generation of fine oxide inclusions is characterised by the following items:

- even distribution in globular or nearly globular shape;
- formation of nucleation sites for precipitation and phase transformation;
- modification including morphology, structure, composition, size and other properties;
- low tendency to collision growth in molten steel;
- favorable properties with respect to hot-linked processes.

Among them, morphology, size, composition and distribution are basic properties which are needed to be well controlled. Fundamentals behind them are focused on an accurate understanding of the influencing factors. However, little has been reported in this field. This chapter concentrates on Ti and/or Zr deoxidized steels which are particularly attractive in oxide metallurgy.

5.1 Composition of Oxide Inclusions

Normally, oxides start to precipitate directly after deoxidation of the molten steel and continue to precipitate and grow during cooling and

solidification. The composition of oxide precipitates is an important parameter for control and utilization of inclusions. Oxidation reactions in steel melts follow the general reaction

$$x\,[M] + y\,[O] = (M_xO_y) \qquad (5\text{-}1)$$

$$K_{M_xO_y} = \frac{a_{M_xO_y}}{h_M^x \cdot h_O^y} \qquad (5\text{-}2a)$$

$$K_{xM-yO} = 1/K_{M_xO_y} = h_M^x \cdot h_O^y \quad (a_{M_xO_y}=1) \qquad (5\text{-}2b)$$

The temperature dependence of the equilibrium constants for Al, Mn, Si, Ti and Zr has been determined and compiled by several researchers [1-7]. The selected values are listed in **Table 5.1**. These values were frequently used and recommended by experts for allowing accurate evaluations.

Table 5.1. Temperature dependence of K_{xM-yO} from different sources

Oxide	Year	Authors	$\log K_{xM-yO}$-T function	Ref.
Al_2O_3 (s)	1971	Rohde et al.	20.57-64000/T	[6,8,9]
MnO (l)	1988	Sakaoand Fujisawa	5.53-12590/T	[6]
MnO (s)	1988	Sakao and Fujisawa	6.67-14880/T	[6]
SiO_2 (s)	1988	Sakao and Fujisawa	11.40-30110/T	[6]
ZrO_2 (s)	1986	Ghosh and Murthy	11.86-41258/T	[7,10]
Ti_2O_3 (s)	1981	ISIJ	18.08-56060/T	[11]
Ti_3O_5 (s)	1986	Ghosh and Murthy	29.34-91304/T	[7,10]
TiO_2 (s)	1979	Gatellier and Olette	$K_{Ti\text{-}2O}=5.0\cdot10^{-7}$ at 1873 K	[3]

It is obvious from Eqs. (5-1) and (5-2) that $K_{xM\text{-}yO}$ and the Henrian activities of elements M and O in the molten steel determine the composition of oxide inclusions under equilibrium conditions. In other words, the **composition** and **temperature** of the molten steel determine the composition of oxide inclusions. In order to predict the composition of oxide inclusions, component activities of the molten steel and oxides are needed.

Relations between component activities and compositions of oxides have not been completely revealed. However, some valuable models have been proposed since the 1960's. Outstanding summaries on these models were given in Refs. [12-14]. Further studies on this subject are needed. More detailed discussions are beyond the scope of the present study.

The interpretation of thermodynamic properties of multicomponent systems represents a permanent matter of interest because it is significant for the fundamental understanding of metal and non-metal solutions. Quite a number of researchers have tried to develop formalisms to describe the thermodynamic properties of multicomponent systems. Unfortunately, none of them is applicable for all ranges of composition. The interaction parameter formalism which is expressed in terms of a MacLaurin series expansion of partial excess free energy was first developed by Wagner [15, 16]. It is frequently used to express the thermodynamic properties of dilute solutions particularly of metals. However, any truncated MacLaurin series expansion weakens the exactness of the expression for the activity coefficient of a solute in a multicomponent system and at higher solute concentrations the thermodynamic inconsistency may result in significant errors [17-21]. In view of this, several other approaches to overcome the thermodynamic inconsistency of Wagner's ε formalism have been developed trying to extend them to concentrated solutions. The merits and demerits of the different formalisms are summarized in **Table 5.2**. **Table 5.3** gives the mathematical expressions of the different approaches. The present author developed an useful modified ε formalism featuring thermodynamic consistency at both dilute and concentrated levels with the adoption of only the first-order interaction parameters [21]. This formalism was successful-ly applied to evaluate element activities in metallic solutions [21-28] yielding a higher accuracy in comparison with the traditionally used Wagner's ε formalism and the other available formalisms. It is composed of two equations which represent analytical expressions of the activity coefficients of solvent and solutes. Eq. (5-3) is used to calculate the activity coeffi-cient of solvent 1 and Eq. (5-4) is applied to calculate the activity coefficient of the solute i. **Appendix A** gives the details on the deduction of Eqs. (5-3) and (5-4). A computer program-me was subsequently developed on the basis of the modified ε formalism to perform thermo-dynamic calculations. The present evaluations of element activities in metallic solutions have been performed

Table 5.2. Merits and demerits of the different formalisms

Formalism	Advantages	Disadvantages	Comments
1st and 2nd order parameter interaction formalism [15, 16] (Wagner & Lupis)	●Simplicity in expression ●Extensive compilation of ε parameters available ●2nd order formalism applicable to larger concentration range than the 1st order one	●Thermodynamically inconsistent at finite levels ●Path dependent integral ●A limited number of 2nd order interaction parameters available	●An extensively used formalism with reasonable accuracy ●Applied special relations, the 2nd order formalism is identical to Darken's QF and to equation suggested by Schuhmann
MacLaurin infinite series[16] (Lupis & Elliott)	●Thermodynamically consistent and mathematically exact	●Interaction parameters beyond 2nd order not available	●Lacking practical utility
the Unified ε formalism [19] (Pelton and Bale)	●Thermodynamically consistent ●Valid for wider range of composition ●Using available ε parameters	●No rigorous definition of parameters such as ε_{ij} ●A mathematical fitting treatment	●Unification of standard ε formalism, quadratic formalism and polynomial expression of Marglues[41]
QF Formalism and its extension to multi-component Solutions[17, 29] (Darken, Srikanth & Jacob)	●Thermodynamically consistent ●Valid for wider range of composition than ε formalism in simple systems ●Values of α_{ij} can be derived from ε formalism	●Not yet very popular ●Not applicable to strongly interacting systems	●Identical to 2nd order ε formalism incorporating special relations (formalism of Pelton and Bale, and that of Schumann)
Quasi-chemicality [30] (Lupis)	●Thermodynamically consistent ●Very similar to QF	●Different relation with ε formalism than QF with it ●No rigorous definition of $\ln\gamma_j^o$	●Lacking experimental investigations ●Not applicable to strongly interacting systems
Modified MIS [31] (Hajra & Frohberg)	●Thermodynamically consistent ●depending on the experimental accuracy ●Using available ε parameters	●Not popular ●Complex in expression ●Used in binary and ternary systems	●Questioning applicability to multicomponent systems ●Lacking practical utility
Modified ε formalism (the present study)	ibid	●Not popular ●Complex in expression	●Giving more accurate results in comparison to ε formalism

QF: quadratic formalism MIS: MacLaurin infinite series

Table 5.3. Analytical expressions of the different formalisms

Formalism	Analytical expression
1st and 2nd ε formalism (Wagner and Lupis)	$\ln\gamma_i = \ln\gamma_i^0 + \sum_{j=2}^{n}\varepsilon_i^j x_j + \sum_{j=2}^{n}\rho_i^j x_j^2 + \sum_{j=2}^{n}\sum_{k>j}^{n}\rho_i^{jk} x_j x_k$
Modified ε formalism (Bale and Pelton)	$\ln\gamma_i = \ln\gamma_i^0 + \ln\gamma_1 + \sum_{j=2}^{n}\varepsilon_{ij}x_j + \sum_{j,k=2}^{n}\varepsilon_{ijk}x_j^2 + \sum_{j,k,l=2}^{n}\varepsilon_{ijkl}x_j x_k x_l + \cdots$ $\ln\gamma_1 = -\frac{1}{2}\sum_{j,k=1}^{n}\varepsilon_{jk}x_j x_k - \frac{2}{3}\sum_{j,k,l=1}^{n}\varepsilon_{jkl}x_j x_k x_l - \frac{3}{4}\sum_{j,k,l,m=1}^{n}\varepsilon_{jklm}x_j x_k x_l x_m - \cdots$
MacLaurin infinite series (Lupis and Elliott)	$\ln\gamma_i = \ln\gamma_i^0 + \sum_{j=2}^{n}\varepsilon_i^j x_j + \sum_{j=2}^{n}\rho_i^j x_j^2 + \sum_{j=2}^{n}\sum_{k>j}^{n}\rho_i^{jk} x_j x_k + \cdots$
Quadratic formalism (Darken, Srikanth and Jacob)	$\log\gamma_1 = \sum_{j=2}^{n}\sum_{k>j}^{n}(\alpha_{1j} + \alpha_{1k} - \alpha_{jk})x_j x_k + \sum_{j=2}^{n}\alpha_{1j}x_j^2$ $\log\gamma_i = \log\gamma_i^0 + \log\gamma_1 - \sum_{j=2(\neq i)}^{n}(\alpha_{1i} + \alpha_{1j} - \alpha_{ij})x_j - 2\alpha_{1i}x_i$
Quasi-chemicality (Lupis)	$\ln\gamma_1 = -5L_2x_2^2 - 5L_3x_3^2 - 10L_1x_2x_3$ $\ln\gamma_i = \ln\gamma_1 + 5\ln(1-L_i) + 10L_ix_i + 10L_1x_j$ for ternary 1-i-j system
Modified MacLaurin infinite series expansion (Hajra and Frohberg)	for ternary 1-i-j system $\ln\gamma_1 = \sum_{i=2}^{3}\left(\ln(1-x_i)\varepsilon_i^i + x_i\varepsilon_i^i - \frac{x_i^2 x_j}{1-x_i}\varepsilon_i^j - x_i x_j \varepsilon_i^j\right) + Z$ where Z represents the infinite series which includes x_2x_3 terms.

Modified ε formalism (the present study) * i is solute and 1 is solvent. The meanings of the symbols listed in this table can be found in the corresponding references.	$\ln\gamma_1 = \sum_{i=2}^{m}\varepsilon_i^i\left[x_i+\ln(1-x_i)\right]-\sum_{j=2}^{m-1}\sum_{k=j+1}^{m}\varepsilon_j^k x_j x_k\left(1+\frac{\ln(1-x_j)}{x_j}+\frac{\ln(1-x_k)}{x_k}\right)$ $+\sum_{i=2}^{m}\sum_{\substack{k=2\\(k\neq i)}}^{m}\varepsilon_i^k x_i x_k\left(1+\frac{\ln(1-x_k)}{x_k}-\frac{1}{1-x_i}\right)+\frac{1}{2}\sum_{j=2}^{m-1}\sum_{k=j+1}^{m}\varepsilon_j^k x_j{}^2 x_k{}^2\left(\frac{1}{1-x_j}+\frac{1}{1-x_k}-1\right)$ $-\sum_{i=2}^{m}\sum_{\substack{k=2\\(k\neq i)}}^{m}\varepsilon_i^k x_i^2 x_k^2\left(\frac{1}{1-x_i}+\frac{1}{1-x_k}+\frac{x_i}{2(1-x_i)^2}-1\right)$ $\ln\gamma_i = \ln\gamma_1+\ln\gamma_i^o-\varepsilon_i^i\ln(1-x_i)$ $-\sum_{\substack{k=2\\(k\neq i)}}^{m}\varepsilon_i^k x_k\left[1+\frac{\ln(1-x_k)}{x_k}-\frac{1}{1-x_i}\right]$ $+\sum_{\substack{k=2\\(k\neq i)}}^{m}\varepsilon_i^k x_k^2 x_i\left(\frac{1}{1-x_i}+\frac{1}{1-x_k}+\frac{x_i}{2(1-x_i)^2}-1\right)$

$$\ln\gamma_1 = \sum_{i=2}^{m}\varepsilon_i^i\left[x_i+\ln(1-x_i)\right]-\sum_{j=2}^{m-1}\sum_{k=j+1}^{m}\varepsilon_j^k x_j x_k\left(1+\frac{\ln(1-x_j)}{x_j}+\frac{\ln(1-x_k)}{x_k}\right)$$

$$+\sum_{i=2}^{m}\sum_{\substack{k=2\\(k\neq i)}}^{m}\varepsilon_i^k x_i x_k\left(1+\frac{\ln(1-x_k)}{x_k}-\frac{1}{1-x_i}\right)+\frac{1}{2}\sum_{j=2}^{m-1}\sum_{k=j+1}^{m}\varepsilon_j^k x_j{}^2 x_k{}^2\left(\frac{1}{1-x_j}+\frac{1}{1-x_k}-1\right)$$

$$-\sum_{i=2}^{m}\sum_{\substack{k=2\\(k\neq i)}}^{m}\varepsilon_i^k x_i^2 x_k^2\left(\frac{1}{1-x_i}+\frac{1}{1-x_k}+\frac{x_i}{2(1-x_i)^2}-1\right) \qquad (5\text{-}3)$$

$$\ln\gamma_i = \ln\gamma_1+\ln\gamma_i^o-\varepsilon_i^i\ln(1-x_i)-\sum_{\substack{k=2\\(k\neq i)}}^{m}\varepsilon_i^k x_k\left[1+\frac{\ln(1-x_k)}{x_k}-\frac{1}{1-x_i}\right]$$

$$+\sum_{\substack{k=2\\(k\neq i)}}^{m}\varepsilon_i^k x_k^2 x_i\left(\frac{1}{1-x_i}+\frac{1}{1-x_k}+\frac{x_i}{2(1-x_i)^2}-1\right) \qquad (5\text{-}4)$$

using the thermodynamic data of γ_i^0 and e_i^j which are listed in **Appendix B**. Since the temperature dependence of e_i^j is not known, all calculations are referred to a typical melt temperature of 1873 K.

In theory, it is possible to predict the required contents of deoxidants and oxygen in the molten steel to produce oxides with the expected composition. For example, relations between the activities of Al, Ti and O in the molten steel deoxidized by Ti and/or Al can be calculated as shown in **Figure 5.1**. The curves in planes such as plane A, B, C and D indicate the relations between activities of Al, Ti and O at different assumed activities of the oxides Al_2O_3 and Ti_2O_3. It is evident that the curves shift in the direction shown in figure 5.1 as the ratio of $a_{Ti_2O_3} / a_{Al_2O_3}$ increases. Ti_2O_3, TiO_2 and Ti_3O_5 are possible deoxidation products in the molten steel deoxidized by Ti. The present author and Janke canvassed this problem. Detailed information can be found in Refs. [26, 32]. Goto et al.[33, 34] experimentally found that oxide inclusions with above 50% Ti_2O_3 and less 20% Al_2O_3 favour the generation of finely dispersed oxides. The required contents of Al and O for the investigated steels can be calculated according to the mentioned conditions. The experimental and calculated results are listed in **Table 5.4**. It is obvious that the present model calculation can accurately predict the required conditions for the molten steel if the composition of the oxide inclusions are set. That is, the required conditions for the molten steel can be predicted according to the designed oxides under the assumption of reactions in the molten steel reaching equilibrium state. This assumption is reasonable for steel melts at high temperatures. However, factors such as kinetics of reactions and cooling rates influence oxide inclusions including their composition, distribution and size. Therefore, it is very useful and important in practice to predict the composition of oxide inclusions according to the existing conditions of the molten steel. The present author and Janke[32] developed a model to predict the composition of oxide inclusions. The detailed deduction is given in **Appendix C**. The predicted and experimental results are listed in **Table 5.5**. It is obvious that the presently proposed model evaluates the composition of oxides for Ti- and Zr-killed steels.

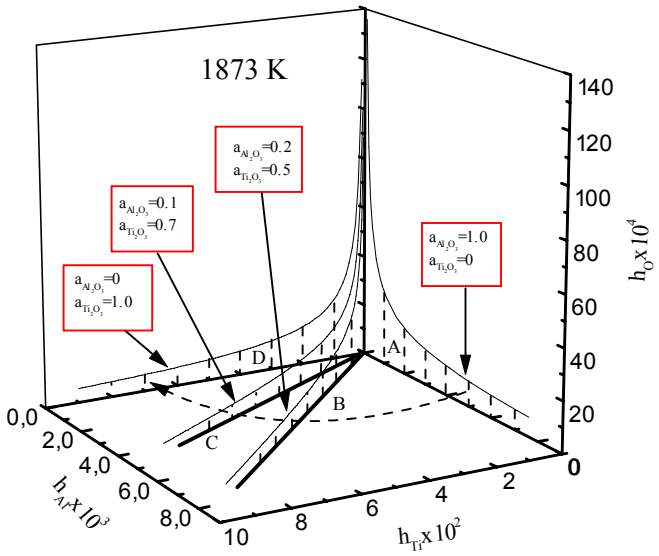

Figure 5.1. Relations between the activities of Al, Ti and O in molten steel at given activities of Al_2O_3 and Ti_2O_3 in the oxide phase (The lines in the horizontal plane are projective lines of the corresponding curves)

Table 5.4. Comparison of experimental with calculated results for steel and oxide phase

No.	Required contents Al*	O*		Composition of oxides Ti_2O_3	Al_2O_3	MnO	SiO_2	CaO	MgO
1	<10	21	Cal.	assumed $a_{Ti_2O_3}$=0.5 and $a_{Al_2O_3}$=0.2					
	10	27	Ref. [33]	61.1	19.1	10.3	0.5	3.4	1.4
2	<3-9	21-40	Cal.	assumed $a_{Ti_2O_3}$=0.6 and $a_{Al_2O_3}$=0.2					
	n.d.	17-39	Ref. [34]	78.2	12.9	4.7	1.1	0.8	0.9

* in ppm n.d.: not determined

Compositions of the molten steels (mass%):

	C	**Si**	**Mn**	**Ti**
No.1	0.06	0.05	1.2	0.014
No.2	0.06-0.11	0.05-0.26	1.20-1.54	0.006-0.016

All calculations are for 1600 °C. The experimental data are chemically analyzed results and the temperature of the molten steels is in the range from 1560 to 1600 °C. The data for oxides are referred to solidified specimens.

Table 5.5. Experimental and calculated composition of oxides

composition of molten steel (wt%)									Composition of oxides (wt%)						Remarks
C	Si	Mn	P	S	N*	O*	Ti*	Al*	Ti_2O_3	Al_2O_3	SiO_2	MnO	CaO	MgO	
0.06	0.05	1.20	0.025	0.025	60	27	140	<3	55~75	~20	~0.2	~2.5	/	/ **	Cal.
0.06	0.05	1.20	n.d.	n.d.	n.d.	27	140	n.d	61.1	19.1	0.5	10.3	3.4	1.4***	Ref. [33]
0.06	0.05	1.20	n.d.	n.d.	n.d.	17	60	n.d.	78.2	12.9	1.1	4.7	0.8	0.9***	Ref. [34]
|	|	|				|	|								
0.11	0.26	1.54	n.d.	n.d.	n.d.	39	160								
0.042	0.84	1.53	0.019	0.018	28	15	208	10	60~85	10~40	~2.5	~3.5	/	/ **	Cal.
0.042	0.84	1.53	0.019	0.018	28	15	208	10	35~86	13-60	<5	<5	1.3~5.0	1.7~5.0 ***	Exp.+
0.079	0.50	1.45	0.017	0.009	36	20	43	30	~3.5	>90	~1.5	~3.5	/	/ **	Cal.
0.079	0.50	1.45	0.017	0.009	36	20	43	30	1.0~6.0	>80	~3.0	<20	<0.5	<10 ***	Exp.+

* in ppm. n.d.: not determined

** Without considering the formation of CaO and MgO; calculations based on the temperature range from liquidus to solidus temperature.

*** Chemical analysis results from specimens which were cut from continuously cast slabs in the thickness direction.

\+ K. S. Oh: private communication, POSCO, South Korea, 1998

5.2 Size and Distribution of Oxide Inclusions

Size and distribution of inclusions play a key role in Ti and Zr deoxidized steels. It is experimentally confirmed that Ti and Zr oxides have a low tendency to collision growth and the average particle size is much smaller than that of alumina in the case of Al-killed steels [33, 35-39]. **Figure 5.2** clearly indicates that the average size of oxides in Ti- and Mn-killed steels is smaller in comparison with that in Al-killed steels. This difference becomes prominent at the surfaces of slab where have higher cooling rates. The remarkable change of the average size of alumina suggests the fact that alumina in liquid steel easily forms clusters. Recently, Sawai et al. [37, 38] experimentally found that Zr treatment of Ti-killed and Mn-Si-killed steels leads to an improvement of oxide distribution and weakens the sensitivity of oxide distribution to the cooling rate.

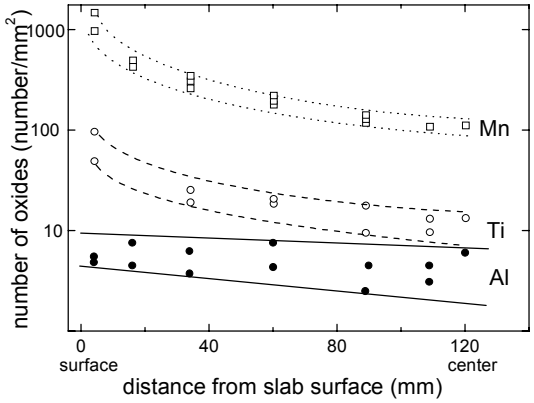

Note: the areas between dot, dash and solid lines represent the limits of scatter for Mn, Ti and Al deoxidized steels, respectively

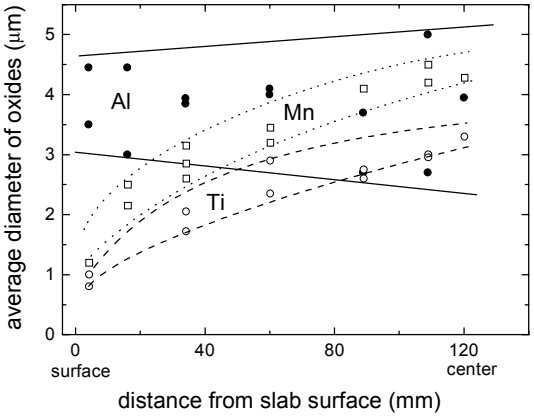

Figure 5.2. The number and size of oxides along slab thickness direction for various deoxidations [35]

(mass%)	C	Si	Mn	Al	Ti
Ti deoxidation	0.06	0.05	1.20	0.001	0.014
Mn deoxidation	0.003	0.003	0.34	0.001	
Al deodidation	0.17	0.09	0.35	0.008	

According to their investigations, deoxidants and cooling rates greatly influence the size and distribution of oxides. Systematic understanding of the effects of deoxidants and cooling rates upon size, composition and distribution of oxides is required. However, this understanding is at the very beginning. In the present investigation important results are obtained on this subject which are valuable to practice.

5.2.1. Effect of Al on Size and Distribution of Oxide Inclusions

Figure 5.3 shows the effect of Al on oxide inclusions. It is widely accepted that Al deoxidation products such as alumina easily form clusters in molten steel and the cooling rate weakly affects the formation of clusters. This tendency is also clearly demonstrated in figure 5.3. However, it is obvious that a higher addition of Al is in favour of reducing the size of oxide inclusions and improving their distribution although it advances the formation of oxide clusters. Therefore, it is hard to avoid the formation of oxide clusters for steels deoxidized only by Al. Here the index of formed oxide clusters is defined as the ratio of the number of formed oxide clusters to that of total oxide inclusions. Its value is in the range between zero and one.

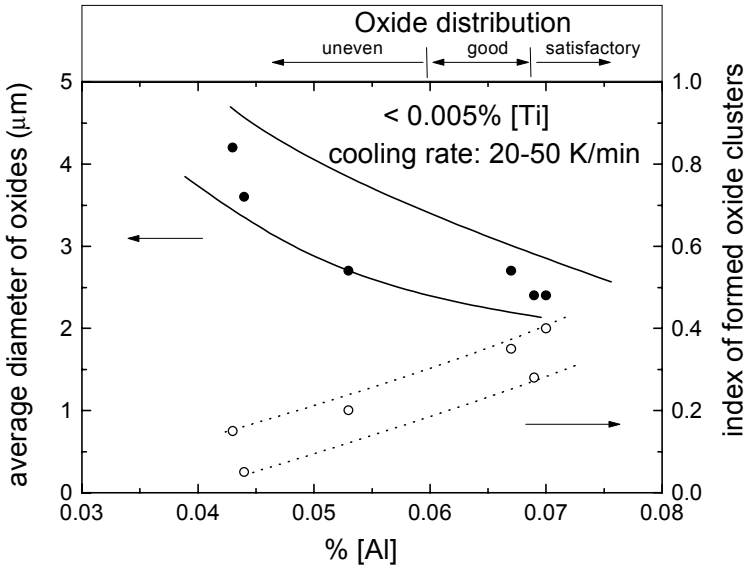

Figure 5.3. Effect of Al content on oxide inclusions in as-cast Fe-Cr-Ni stainless steel

5.2.2. Effect of Ti on Size and Distribution of Oxide Inclusions

The addition of Ti tends to improve the distribution of oxides and to reduce their size as shown in **Figure 5.4**. A further addition of Ti tends to

form clusters although the tendency of forming clusters is low at both high and low contents of Ti. However, high cooling rates effectively reduce this tendency. For example, **Figures 5.5** clearly indicates that an increasing cooling rate strongly reduces the tendency of forming oxide clusters and their size. **Figure 5.6** demonstrates the comprehensive influence of cooling rate and Ti and Al contents on oxide inclusions in as-cast low carbon steel. For low carbon steel, Al exerts a great influence on oxide inclusions when Ti content is below 50 ppm. It is more favorable to control Al content below 30 ppm for generating finely dispersed oxides in low carbon steel. Distributions of oxides in the investigated steels are demonstrated in **Figures 5.7-5.9** as a further explanation to figures 5.4-5.6.

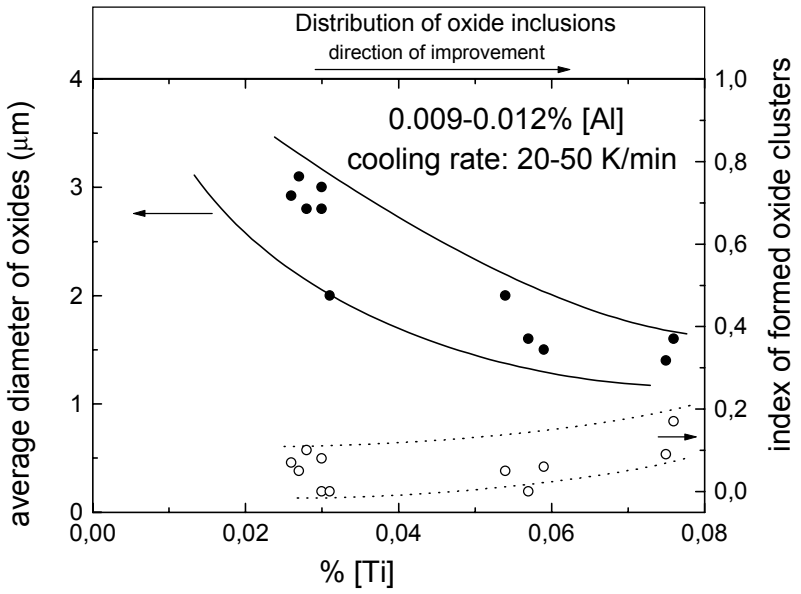

Figure 5.4. Effect of Ti content on oxide inclusions in as-cast Fe-Cr-Ni stainless steel

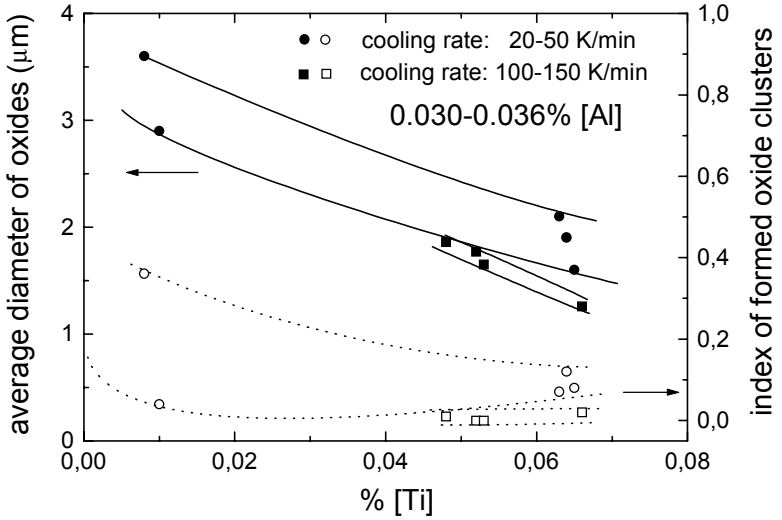

Figure 5.5. Effects of Ti content and cooling rate on oxide inclusions in as-cast Fe-Cr-Ni stainless steel

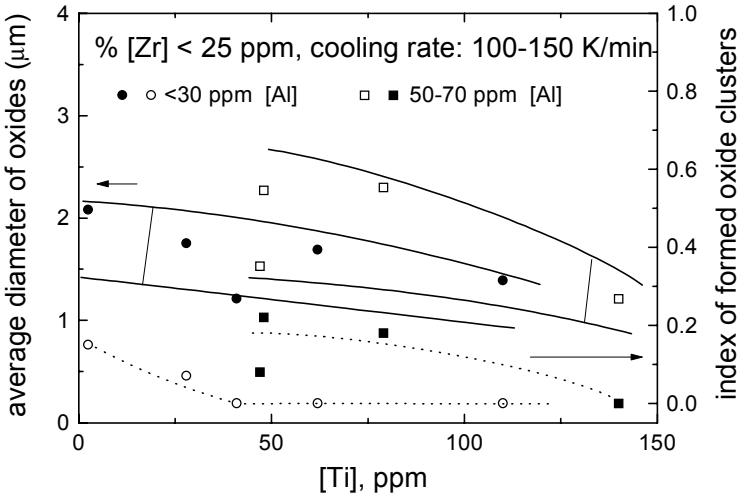

Figure 5.6. Effect of Ti content on oxide inclusions in as-cast low carbon steel

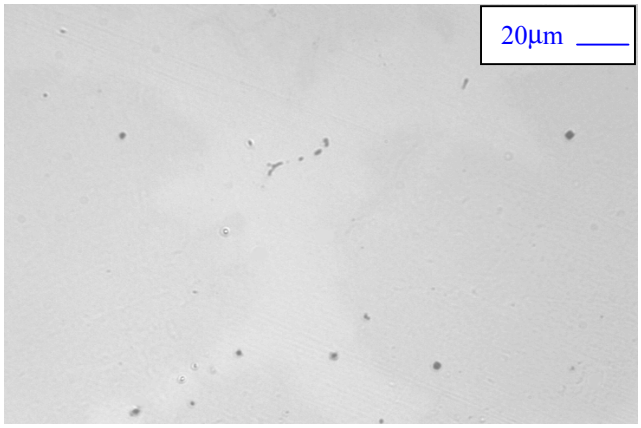

0.030% [Ti], 0.011% [Al], R_C =20-50 K/min

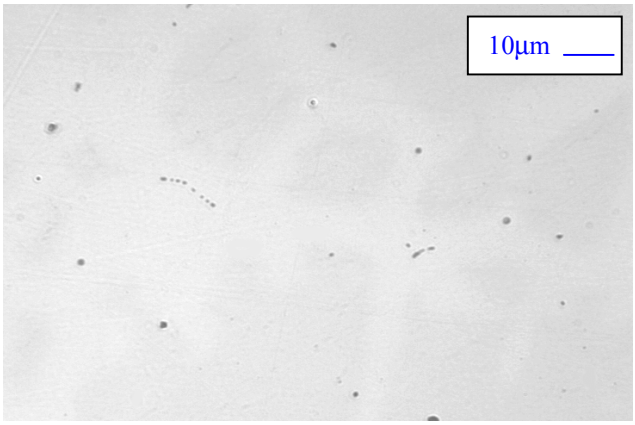

0.075% [Ti], 0.012% [Al], R_C =20-50 K/min

Figure 5.7. Effect of Ti content on oxide inclusions in as-cast Fe-Cr-Ni stainless steel

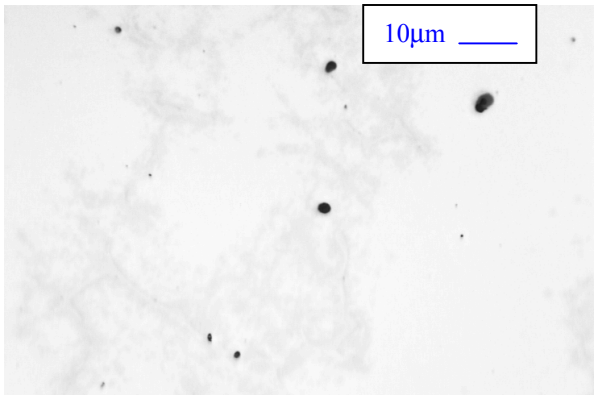

0.063% [Ti], 0.034% [Al], R_C =20-50 K/min

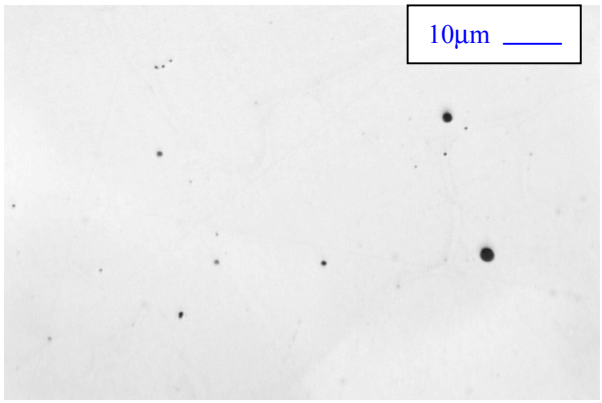

0.066% [Ti], 0.032% [Al], R_C =100-150 K/min

Figure 5.8. Effect of cooling rate on oxide inclusions in as-cast Fe-Cr-Ni stainless steel

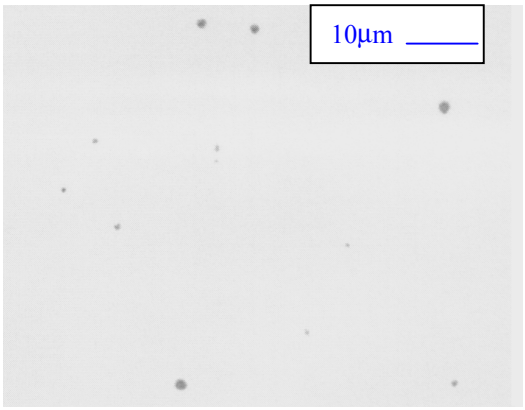

0.041% [Ti], <0.001% [Al] R_C =100-150 K/min

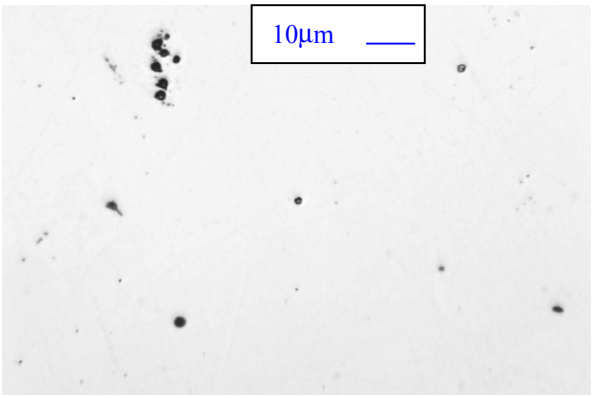

0.048% [Ti], 0.007% [Al] R_C =100-150 K/min

Figure 5.9. Effect of Al content on oxide inclusions in as-cast low carbon steel

5.2.3. Effect of Mn on Size and Distribution of Oxide Inclusions

The element Mn has a strong impact on oxide inclusions in Ti-killed carbon steels. This effect has not been brought to a great attention so far. However, the present investigation indicates that it must be taken serious for employing oxide metallurgy to low and ultra low carbon steels. **Figure 5.10** demonstrates the effect of Mn on oxide inclusions. It is obvious that

Mn favors the generation of finely dispersed oxides and alleviates the tendency of forming oxide clusters. It is possible to generate finely dispersed oxides in low and ultra low carbon steels by partial and complete substitution of Ti for Al. The allowable contents of Ti and Al for generating finely dispersed oxides are influenced by Mn. The main reason for the presence of MnO in the oxide phase perhaps is the formation of liquid oxide inclusions in the molten steel at high temperatures. MnO greatly reduces the melting point of the oxides. At higher temperatures the liquid inclusions tend to evenly disperse in the steel matrix and to become nucleation sites for sulfides, carbides and nitrides during cooling and solidification. These phenomena will be discussed in section 6.2.

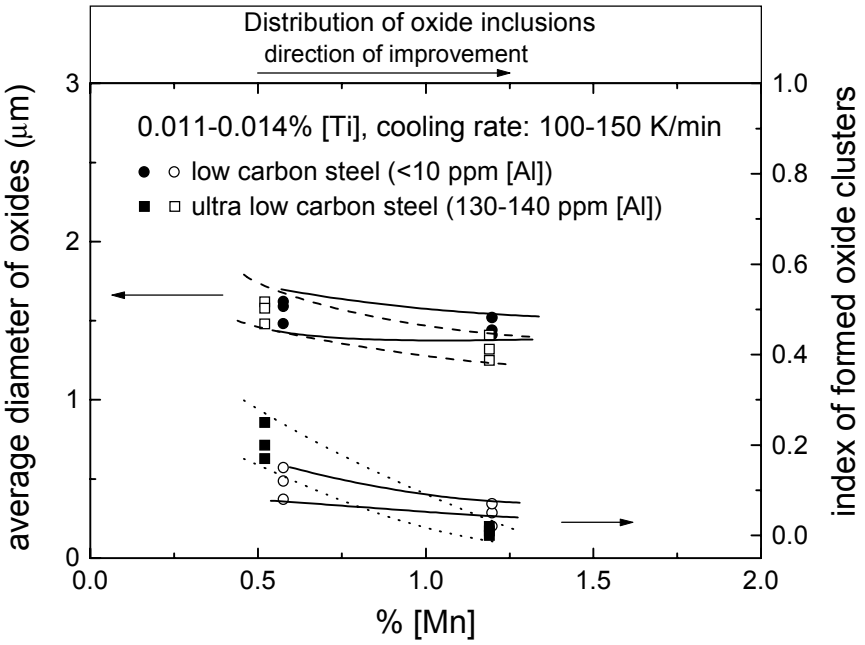

Figure 5.10. Effect of Mn content on oxide inclusions in as-cast low and ultra low carbon steels

5.2.4. Effect of Zr on Size and Distribution of Oxide Inclusions

Zr is a rather strong deoxidant and even more effective than Al. Therefore, oxide inclusions in Zr-killed steels are mostly primary ones. In addition to that ZrO_2 represents an anion vacancy type oxide like Al_2O_3 which does not promote preferential nucleation of various foreign phases on it. However, it is experimentally found that a more even distribution and smaller size of oxides in Zr-killed or Zr-treated steels were obtained in comparison to Ti-killed steels [36-38]. It is also found that distribution and size of oxide inclusions in Zr-killed and Zr-treated steels are not sensitive to the cooling rate [36-38]. Thus, in practice, Zr alone is not selected to treat the molten steel, but Zr-based deoxidants are used. In the present experiments it was found that Mn content hardly influences the oxide inclusions in Zr-base-killed steels. However, oxygen content has a strong impact on the size of oxide inclusions as shown in **Figure 5.11**. Ti+Zr-killed steels feature the same characteristics as Zr-killed steels, i.e. oxide inclusions are finely dispersed in the steel matrix and are hardly influenced by Mn content and cooling rate. For the following two reasons, the contents of Ti, Zr and O should be well controlled in view of the formation of finely dispersed oxides

- strong additions of Ti may promote the formation of oxide clusters
- high oxygen contents favour the formation of large oxides.

5.2.5. Effect of Cooling Rate on Oxide Inclusions

For Ti-killed low carbon steels, the cooling rate has a great impact on the number of oxide inclusions in a unit volume. **Figure 5.12** numerically shows this effect by plotting the experimental data of Goto et al. [33]. It is obvious that a higher number of oxides per unit volume is obtained at a higher cooling rate. Similar results were obtained as discussed above for low carbon steel and Cr-Ni-based stainless steel shown in Figures 5.2 and 5.5. It is obvious that higher cooling rates favour the generation of fine and evenly distributed oxides in Ti-killed steels. The present investigation further confirms this result as shown in **Figures 5.13** and **5.14**.

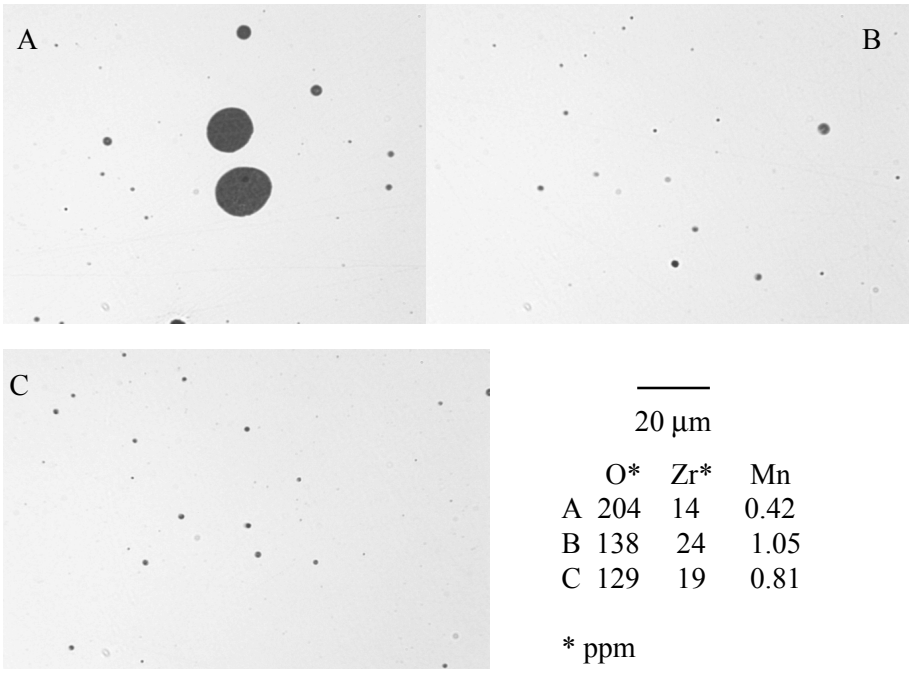

	O*	Zr*	Mn
A	204	14	0.42
B	138	24	1.05
C	129	19	0.81

* ppm

Figure 5.11. Effect of oxygen content on oxide inclusions in as-cast Zr treated low and ultra low carbon steel

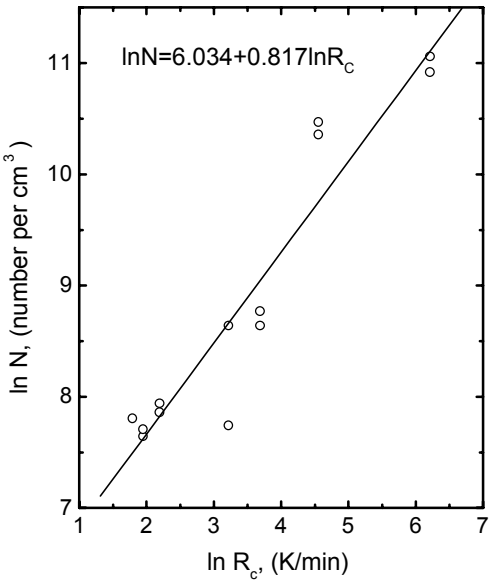

Figure 5.12. Relation between number of oxides per unit volume and cooling rate in low carbon steel [33]

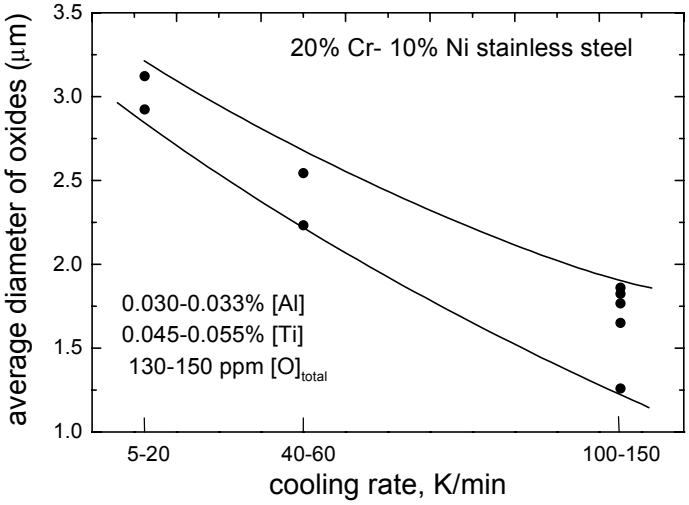

Figure 5.13. Influence of cooling rate on the average diameter of oxide inclusions in Ti-killed 20% Cr-10% Ni stainless steel

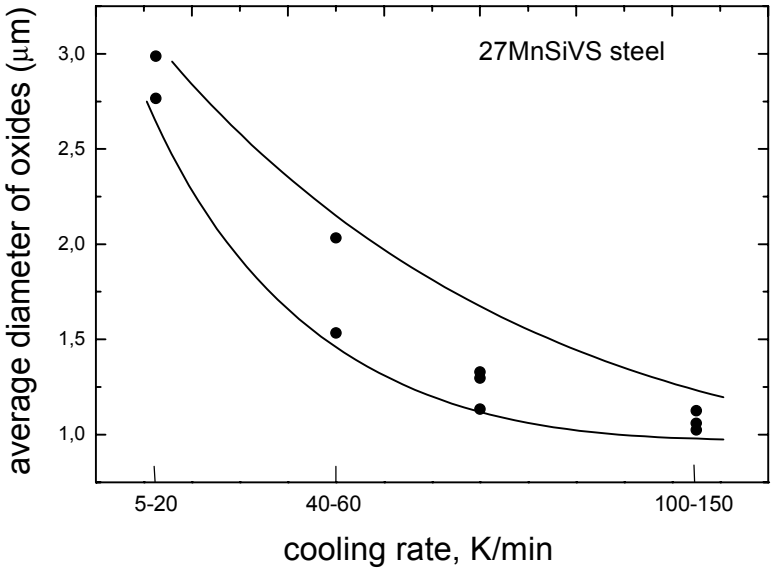

Figure 5.14. Influence of cooling rate on average diameter of oxide inclusions in Ti-killed 27MnSiVS steel

Oxide radii are also influenced by the cooling rate in Ti-killed low carbon steels. **Figure 5.15** illustrates the changes of oxide radii during solidification. The calculated results are based on the presently proposed model as aforementioned (details see Appendix A). It is obvious that the cooling rate greatly influences the radii of secondary oxides, but hardly affects the radii of primary ones, particularly in the case of larger primary oxides at higher cooling rates. This may lead to a useful method of distinguishing the secondary from primary oxides according to their size.

5.3 Shape of Oxide Inclusions

The shape of oxide inclusions is influenced by many factors such as composition of oxides and steel melts, cooling rate and type of deoxidants. For example, Ti oxides in Ti-killed steels are normally globular, but a strong addition of Ti makes Ti oxides forming clusters as discussed above. However, the composition of oxide inclusions is decisive for their morphology. In general, liquid inclusions in molten steel easily form globular ones finely dispersed in solid steel. The reported results on the shape of pure or nearly pure oxide inclusions are summarized in **Table 5.6**.

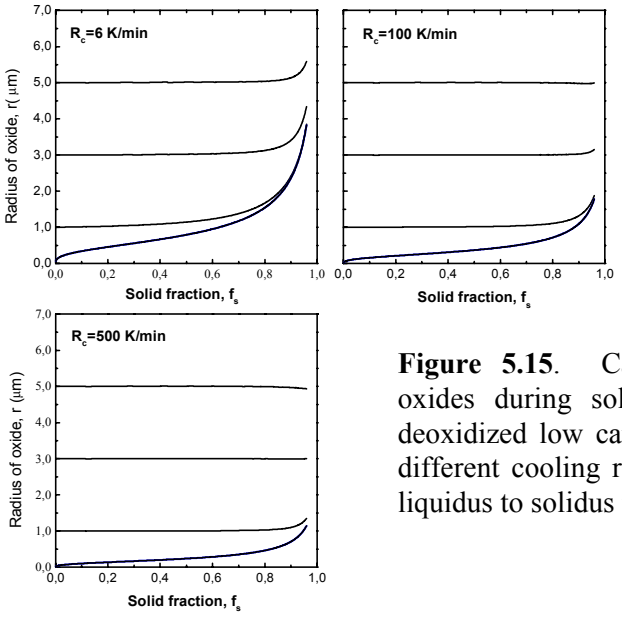

Figure 5.15. Calculated radii of oxides during solidification of Ti-deoxidized low carbon steel at three different cooling rates (cooling from liquidus to solidus temperature)

Table 5.6. Shapes of pure or near pure oxides in steel

Oxides	Shape	Collision
Al_2O_3	Irregular with tips	Loose cluster
SiO_2	Nearly globular with hard surface	Coarse cluster
Ti_2O_3	Globular or nearly globular	No collision
MgO	Polyhedron or nearly globular	Dense cluster
CaO	Globular or nearly globular	No collision
ZrO_2	Globular or nearly globular with faceted surface	No collision

Oxide inclusions in steel are normally complex oxides rather than pure ones. It is found from the reported results that a complex oxide in steel tends to take the shape of the main component and the others contribute a modifying effect to this shape. For example, Al_2O_3 is irregular with tips easily forming loose clusters. The shape of the inclusions containing Al_2O_3 gradually changes away from the shape of Al_2O_3 depending on the contents of the other components as shown in **Table 5.7** [40]. It is found that the liquid oxides in molten steel easily take globular shapes finally present in solid steel.

Table 5.7. Shapes of oxides in steel dependent on composition [40]

Oxides and composition				
Al_2O_3	SiO_2	CaO (%)	Shape	Collision
100	0	0	Irregular with tips	Loose cluster
>80	<20	0	Irregular with smooth surface	Dense cluster
75-90	10-20	<10	Irregular with smooth surface	Dense cluster
~60	<10	>30	Globular	No collision
40-60	20-30	20-30	Globular	No collision
>80	0	<20	Irregular with coarse tips	Coarse cluster
60-65	0	30-25	Irregular to globular	Dense cluster
40-60	0	40-60	Globular	No collision

Reference:

[1] D. Janke and W. A. Fischer: Arch. Eisenhüttenwes., 47(1976), 195/198; 589/594
[2] D. Janke and W. A. Fischer: Stahl u. Eisen, 96(1976), 398/401
[3] C. Gatellier and M. Olette: Rev. Met., 76(1979), 377/386
[4] E. T. Turkdogan: Arch. Eisenhüttenwes., 54(1983), 1/10
[5] F. Oeters: "Metallurgy of steelmaking", Verlag Stahleisen mbH, Düsseldorf, 1994, 3/102
[6] Steelmaking Data Sourcebook, Revised ed. The Japan Soc. For Promotion of Science, 19th Committee on Steelmaking, Gordon and Breach Science Publ., New York, 1988, 278/93.
[7] B. Deo and R. Room: Fundamentals of steelmaking metallurgy, Prentice Hall Int., New York, 1993, 53
[8] L. E. Rohde, A. Choudhury and M. Wahlster: Arch. Eisenhüttenwes., 42(1971), 165/174
[9] D. Janke, Z. Ma, P. Valentin and A. Heinen: ISIJ International, 40(2000), 31/39
[10] A. Ghosh and G. V. R. Murthy: Trans. ISIJ, 26(1986), 629/637
[11] Iron and Steel Handbook, 3rd ed., Vol.1, ed. by ISIJ, Maruzen Co. Ltd., Tokyo, 1981, 15
[12] Slag Atlas, edited by Verein Deutscher Eisenhüttenleute (VDEh), 2nd edition, Verlag Stahleisen GmbH, Düsseldorf, 1995, 25/29, 105
[13] Y. Waseda and J. M. Toguri: The structure and properties of oxide melts, Word Scientific Publishing Co. Pte. Ltd., Singapore, 67/106
[14] G. Jiang, K. Xu and S. Wei: ISIJ International, 33(1993), 20/25
[15] C. Wagner: Thermodynamics of alloys, Addison-Wesley, reading, Massachusetts, 1952
[16] C. H. P. Lupis and J. F. Elliott: Acta Met., 1(1966), 529/538
[17] L. S. Darken: TMS-AIME, 239(1967), 80/89
[18] R. Schuhmann, Jr.: Metall. Trans. B, 16B(1985), 807/813
[19] A. D. Pelton, C. W. Bale: Metall. Trans. A, 17A(1986), 1211/1215; Metall. Trans. A, 21A(1990), 1997/2002
[20] S. Srikanth and K. T. Jacob: Metall. Trans. B, 19B(1988), 269/275
[21] Z. Ma, J. Ohser and D. Janke: Acta Met. Sinica, 10(1997), 375/385
[22] Z. Ma and D. Janke: Acta Met. Sinica, 11(1998), 235/240
[23] Z. Ma and D. Janke: Acta Met. Sinica, 12(1999), 127/136
[24] Z. Ma, L. Savov and D. Janke: Metall, 53(1999), 61/67
[25] Z. Ma and D. Janke.: Metall, 53(1999), 334/338

[26] Z. Ma and D. Janke: steel research, 71(1999), 395/401
[27] Z. Ma and D. Janke: steel research, 71(1999), No.12
[28] D. Janke and Z. Ma: Veitsch-Radex Rundschau, 1999, No. 2, 61/83
[29] S. Srikanth and K. T. Jacob: Trans. ISIJ, 29(1989), 171/174
[30] C. H. P. Lupis: Chemical thermodynamics of materials, North Holland, Amsterdam, 1983
[31] J. P. Hajra and M. G. Frohberg: steel research, 60(1989), 479/484; Metall. Trans. B, 23B(1992), 23/28
[32] Z. Ma and D. Janke: ISIJ International, 38(1998), 46/52
[33] H. Goto, K. Miyazawa, K. Yamamuchi, S. Ogibayashi and T. Tanaka: ISIJ International, 34(1994), 414/419
[34] H. Goto, K. Miyazawa and T. Tanaka: ISIJ International, 35(1995), 286/291
[35] H. Goto, K. Yamamuchi, S. Ogibayashi, T. Tanaka and S. Nishimori: CAMP-ISIJ, 4(1991), 284
[36] T. Sawai, M. Wakoh, Y. Ueshima and S. Mizuguchi: ISIJ International, 32(1992), 169/173
[37] T. Sawai, M. Wakoh and S. Mizoguchi: Tetsu-to-Hagane, 82(1996), 587/592
[38] M. Wakoh, T. Sawai and S. Mizoguchi: Tetsu-to-Hagane, 82(1996), 593/598
[39] Z. Ma and D. Janke: Technical report “Improvement of nonmetallic inclusions and fine grain structures of continuously cast steel by oxide metallurgy”, European Coal and Steel Community (ECSC) sponsored project under grant No. 7210.CC/115, 1997; 1998.
[40] H. Yin, H. Shibata, T. Emi and M. Suzuki: ISIJ International, 37(1997), 946/955
[41] M. Margules: Situngsber Wiend Akad., 104(1895), 1243

CHAPTER 6
Effects of Oxide Inclusions on Castability and Precipitation of Sulfide

It is experimentally found that oxide precipitates exert a strong effect on steel castability and the precipitation of sulfides, nitrides and carbides. Steel castability directly influences production efficiency and product quality. One of the important tasks in steelmaking is to guarantee good castability of the molten steel during the continuous casting process. An important aspect of steel castability concerns nozzle clogging which should be eliminated. Therefore, the effect of oxide inclusions on steel castability is important from both practical and theoretical views, particularly regarding the application of oxide metallurgy.

It is commonly accepted that sulfides in steel strongly influence its service properties. Finely dispersed sulfide improves steel machinability and refines grain size during heat treatment and mechanical forming on the one hand. On the other hand, larger sulfides with dendritic or irregular shape exert harmful effects on service properties. A close control of sulfides in steel becomes an important measure to produce high quality steel.

6.1 Effect of Oxide Inclusions on Castability

Castability is closely related to fluidity, chilling tendency and shrinkage characteristics. Unfortunately, there exists no clear definition for castability. Thus, castability is a relative feature depending on various factors such as the kind of metal and its making process. Here our interests are focused only on the steelmaking process. In continuous casting processes, castability concerns fluidity of steel melts and nozzle clogging tendency. It is accepted that temperature determines fluidity of steel melts, and inclusions present in steel melts influence nozzle clogging. The present objective is to discuss the effect of inclusions on nozzle clogging. According to the author's knowledge, the present understanding on this effect is empirical, i.e. directly referred to the practical results. It is of significance to fundamentally understand this phenomenon from both the practical and theoretical point of view.

6.1.1 Basic Principles on Nozzle Clogging

In a continuous casting process, it is normally hard to avoid the accumulation of inclusions at the nozzle wall responsible for clogging. Nozzle clogging is conventionally regarded as a symptom of cleanliness. However, it can be avoided if the inclusions in the steel melt are well controlled. Therefore, the basic principles for the accumulation of inclusions on nozzle refractories need to be discovered. The research results on interactions between solids in molten steel supply sources to reveal the aforementioned phenomena, although little information on it is available.

The attachment of an inclusion toward the inside nozzle wall is achieved by three main steps. First, the inclusion transports to the nozzle wall and it is then adhered to the wall or rejected by the wall. After adhesion, the inclusion sinters with the nozzle refractories through physical and chemical reactions at high temperatures. **Figure 6.1** schematically illustrates the mechanism of attachment process of an inclusion to the nozzle wall. As aforementioned, the inclusion will be pushed away from or attached to the nozzle wall after it reaches the nozzle wall. Some of the steel melts between the nozzle wall and the inclusion have to withdraw if the inclusion is attached to the nozzle wall. Thus, a small vacuum or gas space is produced between the wall and the inclusion as shown in figure 6.1. At higher temperatures (>1673 K), the attached inclusions easily sinter with the nozzle refractories and with themselves and then they are firmly adhered or attached to the nozzle wall.

The present study attempts to give a quantitative description of adhesion behavior of an inclusion to the nozzle wall. The critical point for the adhesion behavior of inclusions to the nozzle wall is the determination of determining factors of adhesion and rejection. The following two basic assumptions are proposed to be the determining factors.

Assumption 1. Attachment of an inclusion occurs results from the reduction of total energy change in the local area or system, ΔE_T.

Assumption 2. If the kinetic energy of the inclusion in liquid metal flow is smaller than $|\Delta E_T|$, the attachment of the inclusion will occur.

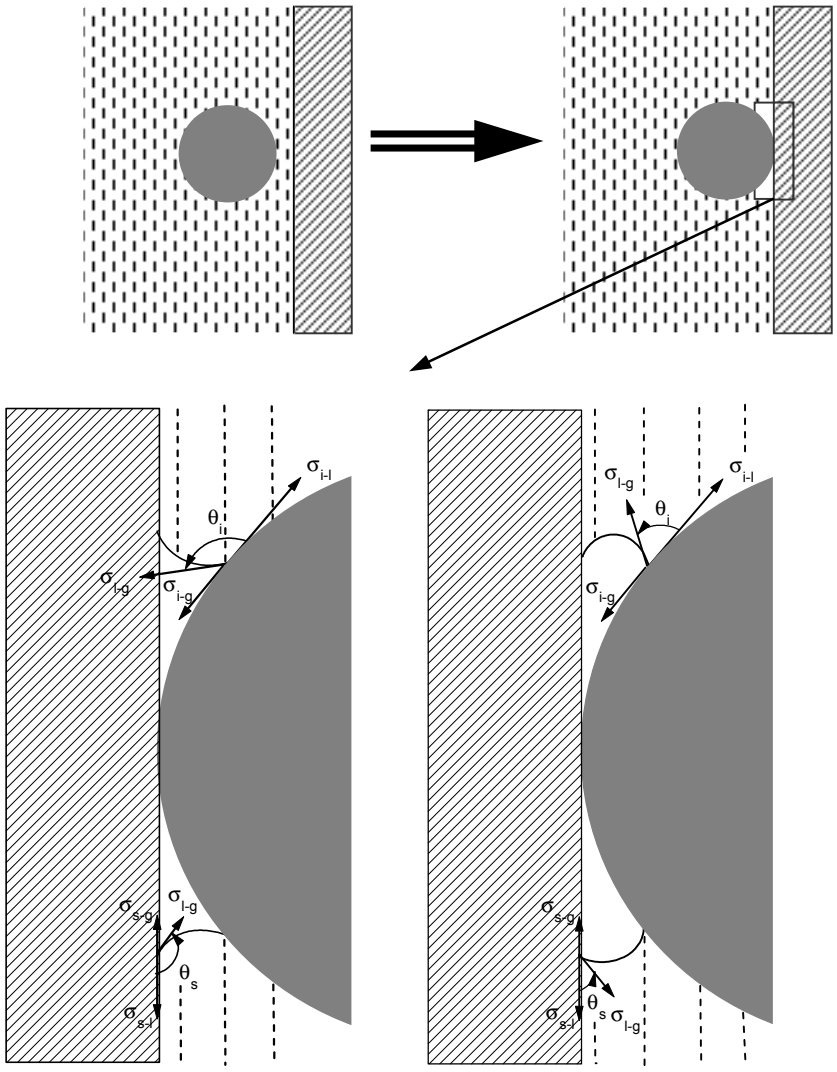

Figure 6.1. Approach and adhesion of an inclusion to the nozzle wall

Where i, l, s, g and $\sigma_{x\text{-}y}$ represent inclusion, steel melt, nozzle refractory, gas/vacuum and interfacial tension between x and y (x and y represent i, l, s or g), respectively.

The total local energy change, ΔE_T, is expressed as

$$\Delta E_T = \Delta E_{i-g} + \Delta E_{s-g} + \Delta E_p \qquad (6\text{-}1)$$

where $\Delta E_{i\text{-}g}$ and $\Delta E_{s\text{-}g}$ represent the change of energy by forming a contact area ΔA_1 between the inclusion and the gas or vacuum cavity and by forming a contact area ΔA_2 between the nozzle wall and the gas or vacuum cavity, respectively. ΔE_p is the needed energy to establish the cavity.

$\Delta E_{i\text{-}g}$, $\Delta E_{s\text{-}g}$ and ΔE_p are given as follows

$$\Delta E_{i-g} = (\sigma_{i-g} - \sigma_{i-l})\Delta A_1 = \sigma_{l-g} \cdot \cos\theta_i \cdot \Delta A_1 \qquad (6\text{-}2)$$

$$\Delta E_{s-g} = (\sigma_{s-g} - \sigma_{s-l})\Delta A_2 = \sigma_{l-g} \cdot \cos\theta_s \cdot \Delta A_2 \qquad (6\text{-}3)$$

$$\Delta E_p = \Delta V \cdot (p_a - p_i) \qquad (6\text{-}4)$$

The contact angles, θ_i and θ_s, are determined by interfacial tensions expressed by the Young equations:

$$\cos\theta_i = \frac{\sigma_{i-g} - \sigma_{i-l}}{\sigma_{l-g}} \qquad (6\text{-}5)$$

$$\cos\theta_s = \frac{\sigma_{s-g} - \sigma_{s-l}}{\sigma_{l-g}} \qquad (6\text{-}6)$$

Eq. (6-1) can be rewritten as

$$\Delta E_T = \sigma_{l-g}(\cos\theta_i \cdot \Delta A_1 + \cos\theta_s \cdot \Delta A_2) + \Delta V(p_a - p_i) \qquad (6\text{-}7)$$

If the velocity of the inclusion is taken as v_i, its kinetic energy is $\frac{1}{2} m_i v_i^2$ where m_i represents the mass of the inclusion. According to the assumptions, the following inequality represents the condition for the inclusion to be attached to the nozzle wall.

$$\frac{1}{2} m_i v_i^2 < \left| \sigma_{l-g} (\cos\theta_i \cdot \Delta A_1 + \cos\theta_s \cdot \Delta A_2) + \Delta V (p_a - p_i) \right| \qquad (6\text{-}8)$$

It is obvious that all influential factors rendering ΔE_T more negative for an inclusion favour its attachment to the nozzle wall. The following sections will discuss these influential factors in detail based on this mechanism.

6.1.2 Inclusion Morphology

Derivation of the Young equations (6-5) and (6-6), is based on the assumption that the investigated surfaces are perfectly smooth. In a practical situation, however, the surfaces are rough and consequently the surface energy differs from the apparent surface energy based on the assumption of a smooth surface. The change of surface energy due to surface roughness was considered by Wenzel [1] giving a simple relation between the observed contact angle θ_{Rough} on a rough surface and the angle θ_{Smooth} measured at a perfectly smooth surface:

$$\cos\theta_{Rough} = r \cdot \cos\theta_{Smooth} \qquad (6\text{-}9)$$

where r, the surface roughness factor, is defined as the ratio of the true surface area to the geometric area based on the assumption of a smooth surface. The Wenzel relation was proven by experimental work of Ogino [2] as shown in **Figure 6.2**. It is evident from this relation that the observed contact angle θ_{Rough} for a wetted system decreases with increasing r, and θ_{Rough} for a non-wetted system increases with increasing r. It is concluded that rough non-wetting inclusions in liquid steel tend to be easier attached to the nozzle wall, but wetting inclusions are likely to be rejected by the nozzle wall. **Table 6. 1** gives the contact angles between various oxides and liquid iron. It is obvious that TiO_2 represents wetting inclusions in liquid steel. If the assumption of Ti-oxides being fairly wetted by liquid

steel is valid, the Ti-oxides are unlikely to be attached to the nozzle wall. Therefore, the alternative deoxidation technology, suggesting partial or complete substitution of Ti for Al, is an effective method to improve castability of continuously cast steel. Al_2O_3 represent non-wetting inclusions in liquid steel. Vast experimental results indicated that alumina in liquid steel easily form clusters. **Figure 6.3** gives typical topographies of alumina in steel [4]. Therefore, alumina in molten steel is easy to cause nozzle clogging from a theoretical point of view, and this conclusion was confirmed by experimental results. In order to avoid this harmful effect of alumina, the topography of alumina should be modified. Ca treatment has convincingly proven as an effective way in practice to transform alumina clusters to individual globular $CaO\text{-}Al_2O_3$ inclusions as schematically shown in **Figure 6.4** [5]. Thus, the castability of Al-killed steels is improved by Ca treatment. It is suggested that liquid inclusions in liquid steel are easy to form globular ones fairly wetted by the liquid steel resulting in even dispersion in solid steel. This means that steel castability can be improved through generation of liquid inclusions. In the present investigation, it was found that steel castability is improved with increasing the ratio of CaO/Al_2O_3 in inclusions [4]. However, it is not the unique requirement to liquefy alumina inclusions for the improvement of castability. It is found from the present mechanism that steel castability can also be improved through generation of wetting solid inclusions or non-wetting solid inclusions with smooth surfaces and improved wettablility. It is also obvious that an increase of roughness of the nozzle wall favours the entrapment of inclusions.

Table 6.1. Contact angles between various oxides and liquid iron at 1823-1873 K [3]

Oxides	Al_2O_3	MgO	CaO	MnO	SiO_2	ZrO_2	Cr_2O_3	TiO_2
θ_{Smooth} *	126	118	116	113	112	111	95	79

* average values from different sources

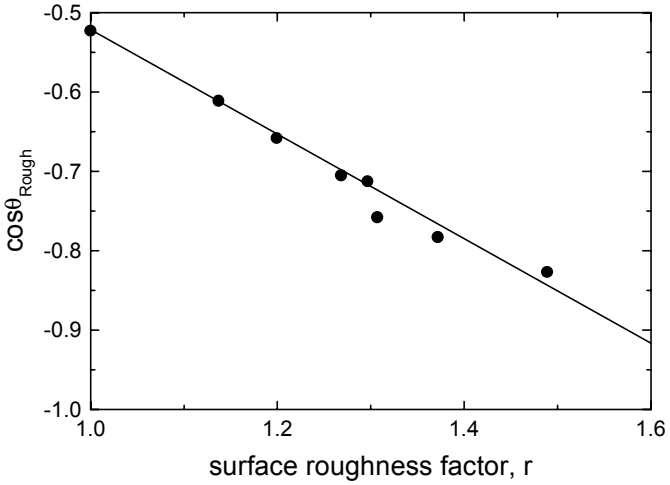

Figure 6.2. Experimental data verifying the Wenzel relation between θ_{Rough} and R for the Fe-Al_2O_3 system at 1873 K [2]

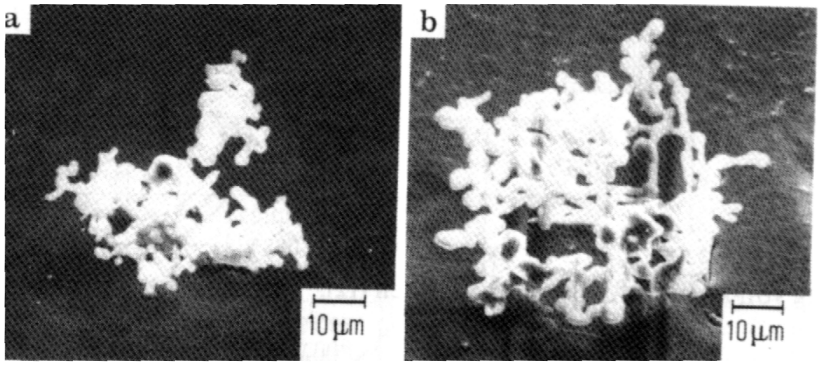

Figure 6.3. A typical topography of Al_2O_3 inclusions in steel [5]

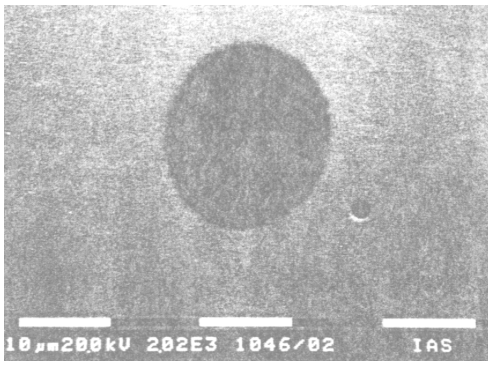

Figure 6.4. A typical partial modified Al_2O_3 inclusion in Ca treated Al-killed steels [6] (spherical calcium aluminate inclusion)

6.1.3 Size, Composition and Porosity

Inclusion size directly influences the parameters of ΔA_1, ΔA_2 and ΔV in Eq. (6-7). In general, larger inclusions lead to greater values of ΔA_1, ΔA_2 and ΔV. Thus, the value of $|\Delta E_T|$ for smaller inclusions is lower than that for larger inclusions. Therefore, larger inclusions are easier to be attached by the nozzle wall in comparison with smaller ones at the same mass. It is concluded that generation of smaller inclusions in liquid steel favours improvement of steel castability.

It is experimentally found that composition of oxides has a weak impact on the contact angles between the oxides and liquid metal [3]. Therefore, the change of size and topography caused by the change of oxides' composition is the main source to contribute to the change of ΔE_T. Ca treated Al-killed steels as discussed before are a good example.

The porosity of inclusions is another factor to influence the contact angles between liquid metal and the inclusions. It is experimentally found that porosity greatly reduces the contact angles for the wetting systems, but it has no significant effect on the contact angles for the non-wetting systems. However, high porosity leads to an increase of size which is harmful to steel castability.

6.1.4 Density, Velocity and Chemical Forces

It is a fact that density and velocity of inclusions directly influence their kinetic energy. High density and velocity increase the kinetic energy of inclusions which are beneficial to reduce nozzle clogging.

If chemical reactions occur when the contact is formed between inclusions, liquid steel and nozzle refractory, the initial system is in non-equilibrium state. This phenomenon is out of the scope of the present study. However, it is also important to continuous casting processes. Chemical reactions or sintering between inclusions and nozzle refractories are easy to occur because of high temperature and high chemical activities of inclusions. This forms a part of future work.

6.1.5 Ways to Reduce Nozzle Clogging

It is obvious that the improvement of steel cleanliness is a fundamental countermeasure to reduce nozzle clogging. Steel cleanliness has been greatly improved during the last decades through the employment of advanced metallurgical technologies such as ladle and tundish metallurgy and refining.

The occurrence of nozzle clogging is connected to the use of the SEN (**s**ubmerged **e**ntry **n**ozzle). Therefore, materials and structures of the SEN are important factors to influence nozzle clogging which were discussed in detail elsewhere [7]. It is worth mentioning that the control of steel flow pattern is significant to reduce clogging through modification of nozzle geometry and adoption of an electromagnetic force.

Two factors directly influence nozzle clogging. One is the type of SEN as mentioned above and the other is related with the nonmetallic inclusions in liquid steel. The present study suggests that the size, morphology, density and contact angle of inclusions are important factors to influence the adhesion behaviour of inclusions toward the nozzle wall. These properties are directly related to the inclusion composition. Therefore, composition control of inclusions is significant to reduce nozzle clogging. This control is closely related to deoxidation technologies and inclusion modification. Finely dispersed globular inclusions with a smooth surface, high density and small contact angle are beneficial to reduce nozzle clogging. Of course, high speed of steel flow is also beneficial to reduce nozzle clogging. Therefore, a possible maximum casting speed is expected in practice.

6.2 Oxide inclusions Acting as Nucleation Sites for Sulfides, Nitrides and Carbides

One of the aims of oxide metallurgy is to control oxide inclusions serving as nuclei for the formation of highly dispersed sulfides, nitrides and carbides. **Figure 6.5** shows that oxides with a certain solubility for sulfide effectively serve as nucleation sites for MnS. This result was confirmed by various reports [8-24]. Figure 2.7 (page 11) further shows that oxides also serve as nucleation sites for nitrides and carbides. It clearly indicates that carbon is effectively scavenged from the matrix because of precipitation of

carbides on the surface of oxide inclusions. The scavenging of carbon from the matrix provides a tool to improve steel service properties such as ductility, forgeability, weldability and machinability.

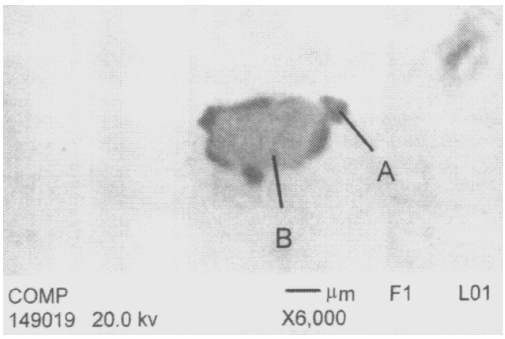

A: MnS
B: Al-Ti-Mn-Ca-O oxide with dissolved MnS

Steel composition (mass%):

C	Si	Mn	P	S	Al*	Ti*	N*	O*
0.079	0.50	1.45	0.017	0.009	30	43	36	20

* in ppm

Figure 6.5. MnS precipitated on the surfaces of oxides in low carbon steel

6.2.1 Sulfide Formation on Oxide Nuclei

The mechanism of MnS precipitated on oxide nuclei is considered an important issue for oxide metallurgy. Wakoh et al. [17, 18] and Oikawa et al. [19] proposed mechanisms of MnS precipitated on oxides. Both proposed mechanisms can be schematically described by **Figure 6. 6** and are explained as follows.

A. Mechanism of Mn precipi a ed on Mn si ica e inc sions a oh e a . [17,18]

Some of the S in steel melts is dissolved in liquid Mn-silicate inclusions at high temperatures. The decrease of temperature during solidification decreases the solubility of MnS in Mn-silicate resulting in the diffusion of MnS from the interior of Mn-silicates to their surface to form initial crystals. These initial crystals become embryos contributing to the further growth of MnS precipitates. The growth of MnS is controlled by the diffusion of Mn and S in the steel.

B. Mechanism of Mn forma ion in i i ed s ee i awa e a. [18]

Figure 6.7 is a schematic representation of the mechanism of nucleation and growth of MnS inclusions during solidification of Ti-killed steels. As solidification proceeds liquid nuclei of (Ti,Mn)O (L_3) are formed first on the solid/ liquid interface (figure 6.7-a) via the monotectic reaction: $L_1 \rightarrow Fe(S)+L_3$. Afterwards MnS droplets (L_2) precipitate on the surface of the liquid (Ti,Mn)O (figure 6.7-b) according to the metastable ternary monotectic reaction: $L_1 \rightarrow Fe(S)+L_2+L_3$ (**Figure 6.8** [18] shows a schematic phase diagram of the pseudo-binary Fe-MnS system). The nucleated MnS droplets on the surface of the liquid (Ti,Mn)O will then be engulfed by the solid/liquid interface together with the (Ti,Mn)O shown in figure 6.7-c, resulting in a fine dispersion of MnS.

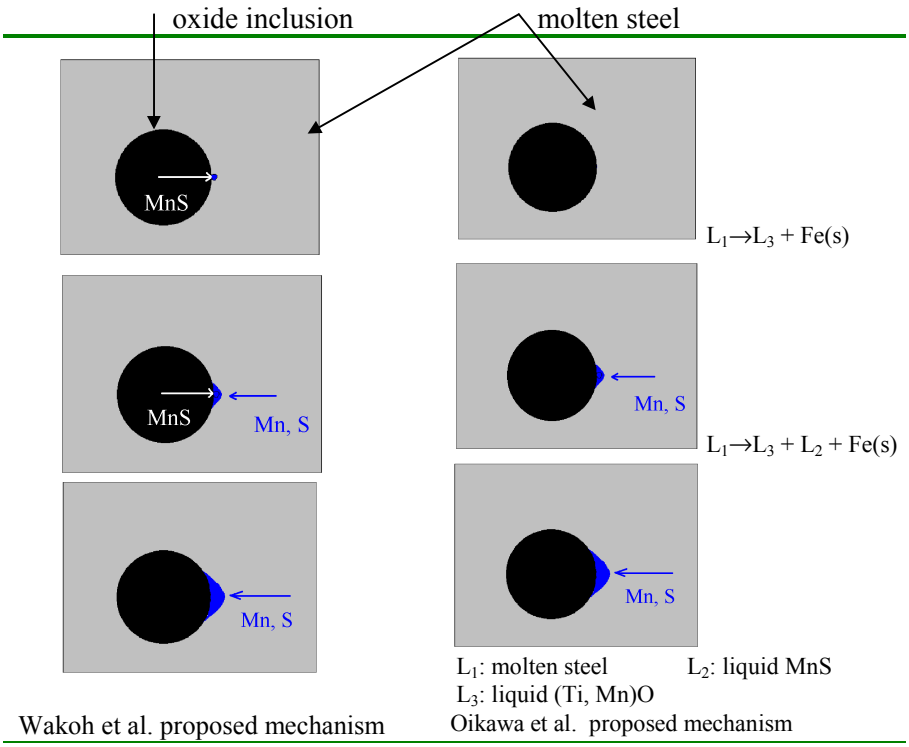

Figure 6.6. The available mechanisms of MnS precipitated on oxides in steel melts during solidification

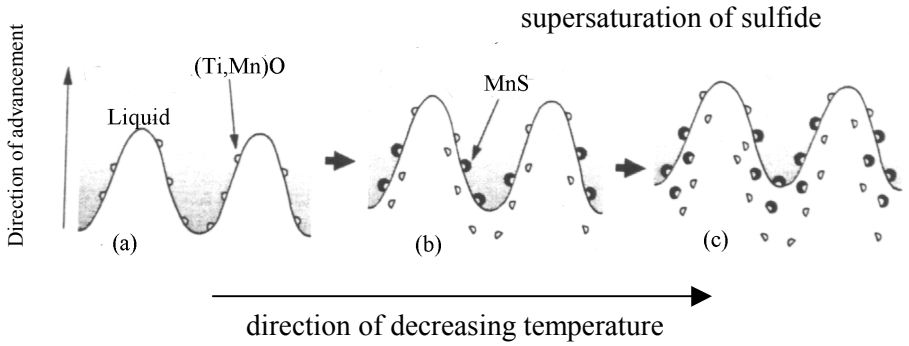

Figure 6.7. Schematic illustration of MnS formation during solidification of Ti-killed steel [18]

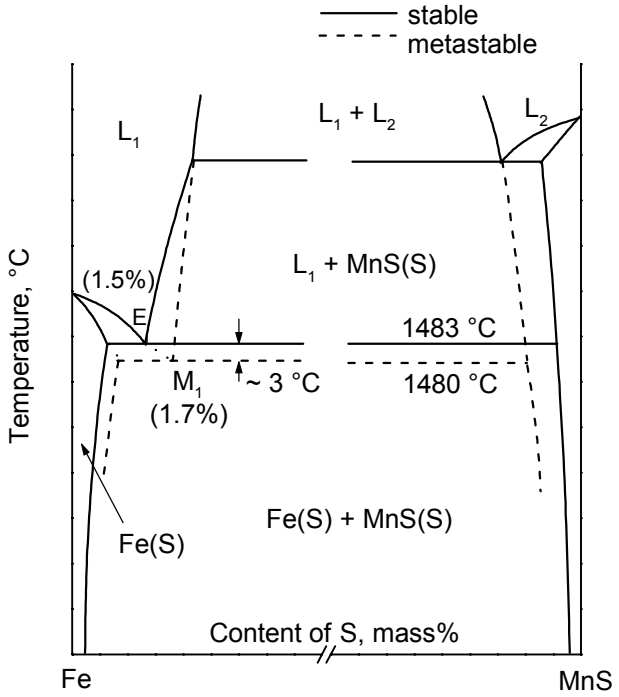

Figure 6.8. Schematic stable and metastable phase diagram of the pseudo-binary Fe-MnS system [18]

C. New proposed mechanism of Mn precipi a ed on o ides in s ee

Oikawa et al. [19] reported that the metastable liquid MnS inclusions in Ti-free steel are formed during solidification when the degree of supersaturation of MnS reaches a high level. Since the metastable liquid MnS features low wettability with respect to the advancing solid/liquid interface of iron, MnS droplets are rejected by the interface to the iron-rich liquid where they grow by collision and coalescence. This result is directly opposed to Wakoh et al.'s reported results [18] which indicate that the precipitation ratio of MnS in Mn-Si deoxidized steel is higher than that in Ti-killed steel at lower S contents. The precipitation ratio of MnS is defined as the ratio of the number of oxide particles bearing MnS precipitates to the total number of oxides. Moreover, both of the mechanisms proposed by Wakoh et al. and Oikawa et al. do not explain why high MnS precipitation ratios are obtained for all deoxidized steels at high S content independent of the deoxidants as shown in **Figure 6.9**. From figure 6.6, it is easy to find the shortcomings contained in both mechanisms. The following new mechanism is proposed to overcome the problem by effectively combining both mechanisms.

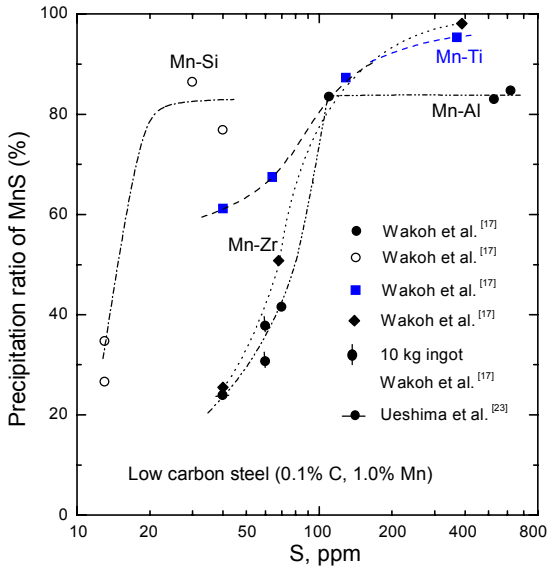

Figure 6.9. Precipitation ratio of MnS depending on S content and deoxidants [17]

In molten steel, S is distributed over oxides and the molten steel. As the temperature decreases, a small amount of MnS crystallizes on the surface of oxides acting as embryos for MnS precipitates. These small MnS crystals on the surface of oxides are produced in the following ways

- In the low S region, MnS crystallizes at lower temperatures due to the decrease of the solubility of MnS in oxides. Micro-segregation of solutes hardly allows the contents of Mn and S to reach the required supersaturation of MnS.
- In the high S region, microsegregation of solutes easily renders the contents of Mn and S to reach the required supersaturation of MnS. Thus, MnS crystallizes on the surface of oxides due to either the microsegregation of solutes or the decrease of the solubility of MnS in oxides. Moreover, the higher the content of S, the higher is the amount of crystallized MnS inclusions on the surface of oxides depending on microsegregation.

Further growth of MnS is controlled by the diffusion of Mn and S in steel. It is worth mentioning that the level of S content depends on the sulfide capacity of oxide inclusion and its sensitivity to temperature. The demarcation line between the low and the high S level varies with the oxides.

The present proposed mechanism fully explains the above experimental results [16]. At low S content, the formation of embryo MnS depends on the sulfide capacities of oxides. Therefore, there obviously exist different MnS precipitation ratios for different oxides. However, MnS precipitation ratios are small for all oxides. At high S content, the formation of embryo MnS depends on micro-segregation and oxide structure. MnS precipitation ratios are high for almost all tested oxides shown in figure 6.9. The difference of MnS precipitation ratios between different oxides is largely decided by the structures of oxides. Normally, oxides and oxide compounds such as Ti_2O_3, MnO, FeO, (Fe,Mn)O, $MnO{\cdot}SiO_2$ and $MnO{\cdot}TiO_2$ contain cation vacancies which contribute greatly to preferential nucleation of various foreign phases on them. On the other hand, oxides such as SiO_2, Al_2O_3 and ZrO_2 contain anion vacancies which can exchange oxygen ions with the matrix. Thus, MnS precipiattion ratios for cation vacancy oxides are higher than those for anion vacancy type oxides. This is confirmed by the reported experimental results shown in figure 6.9.

References:

[1] R. N. Wenzel: Ind. Eng. Chem., 28(1936), 988
[2] K. Ogino: Taikabutsu Overseas, 2(1982), 80/84
[3] Slag Atlas, edited by Verein Deutscher Eisenhüttenleute (VDEh), 2nd edition, Verlag Stahleisen GmbH, Düsseldorf, 1995, 513/539
[4] D. Janke, Z. Ma, P. Valentin and A. Heinen: ISIJ International, 40(2000), 31/39
[5] E. Steinmetz, H. -U. Lindenberg, W. Mörsdorf and P. Hammerschmid: Stahl u. Eisen, 97(1977), 1154/1159
[6] C. E. Cicutti, J. Madias and J. C. Gonzalez: Ironmaking and Steelmaking, 24(1997), 155/159
[7] D. Janke and Z. Ma: Veitsch-Radex Rundschau, accepted
[8] H. Goto, K. Miyazawa and T. Tanaka: ISIJ International, 35(1995), 286/291
[9] H. Goto, K. Yamamuchi, S. Ogibayashi, T. Tanaka and S. Nishimori: CAMP-ISIJ, 4(1991), 284
[10] T. Sawai, M. Wakoh, Y. Ueshima and S. Mizoguchi: ISIJ International, 32(1992), 169/173
[11] T. Sawai, M. Wakoh and S. Mizoguchi: Tetsu-to-Hagane, 82(1996), 587/592
[12] M. Wakoh, T. Sawai and S. Mizoguchi: Tetsu-to-Hagane, 82(1996), 593/598
[13] Z. Ma and D. Janke: Technical report “Improvement of nonmetallic inclusions and fine grain structures of continuously cast steel by oxide metallurgy”, European Coal and Steel Community (ECSC) sponsored project under grant No. 7210.CC/115, 1997; 1998.
[14] H. Goto, K. Miyazawa and T. Kadoya: ISIJ International, 35(1995), 1477/82
[15] H. Goto, K. Miyazawa and H. Honma: ISIJ International, 36(1996), 537/42
[16] K. Yamamoto, T. Hasegawa and J. Takamura: ISIJ International, 36(1996), 80/86
[17] M. Wakoh, T. Sawai and S. Mizoguchi: ISIJ International, 36(1996), 1014/21
[18] M. Wakoh, T Sawai, and S. Mizoguchi: Tetsu-to-Hagane, 78(1992), 1697
[19] K. Oikawa, K. Ishida and T. Nishizawa: ISIJ International, 37(1997), 332/38

[20] Z. Ma and D. Janke: "Oxide precipitation and its precipitates acting as nucleation sites for sulfide in steel melts", the 3rd CAST (China Association for Science and Technology) Conference of Young Scientists, Vol. Materials Science and Industrial Technology, China Press of Science and Technology, August 20-23, 1998, 46/50
[21] J. Tamamura and S. Mizoguchi: Proc. 6th Int. Iron and Steel Cong., Vol. 1, ISIJ, Nagoya, (1990), 591/97 and 598/604
[22] T.Sawai, M. Wakoh, Y. Ueshima, and S. Mizoguchi: 6th Int. Iron and Steel Cong., Vol. 1, ISIJ, Nagoya, (1990), 605/11
[23] Y. Ueshima, H. Yuyama, S. Mizoguchi and H. Kajioka: Tetsu-to-Hagane, 75(1989), 501
[24] S. Ogibayashi, K. Yamaguchi, M. Hirai, H. Goto, H. Yamaguchi, K. Tanaka: 6th Int. Iron and Steel Cong., Vol. 1, ISIJ, Nagoya, (1990), 612/17

CHAPTER 7
Effects of Inclusions on Microstructures and Mechanical Properties of Steel

With the concept of oxide metallurgy, nonmetallic inclusions need not necessarily be harmful to steel service properties. These inclusions can effectively serve as nucleation sites for precipitation and phase transformation resulting in an improvement of steel service properties. The generation of finely dispersed oxide inclusions and their function of acting as nucleation sites for precipitation such as MnS were discussed in the preceding chapters. These finely dispersed oxides also serve as nucleation sites for phase transformation such as of fine ferrite causing a refinement of steel microstructures.

Proeutectoid ferrite can nucleate at inclusions within austenite grains. This enables to obtain a fine ferrite-pearlite microstructure despite coarse austenite grains. This method is termed IGF (intragranular ferrite) technology [1-30]. With IGF technology, a fine grain structure is obtained through coarse austenite grains resulting in an improvement of steel service properties such as toughness and strength. It is of great interest to welded structural steels and components of automobiles. It is obvious that the crux of this technology is to generate finely dispersed inclusions within austenite grains which effectively serve as nucleation sites for IGF. Extensive and intensive researches have been undertaken on IGF technology [6-30]. However, most of the researches are focused on weld metals and steels in welding thermal cycles. Only a few studies directly applied IGF technology to steelmaking processes such as solidifica- tion [1-4] and rolling processes [5]. IGF technology in welding processes is quite different from that in casting processes because of different thermal cycles. In the present study it was further found that the ideal of IGF technology can be extended to refine grain structures (not only ferrite, but also other phases) and to modify precipitates through finely dispersed oxide inclusions.

Mechanical properties of the as-cast investigated steels are tested. Generation of finely dispersed oxide inclusions in steel prominently improves notch impact toughness.

7.1 Effect of Inclusions on Microstructures

It is experimentally observed that inclusions in steel such as oxides, sulfides and nitrides can serve as nucleation sites for intragranular ferrite (IGF) in welding thermal cycles [6-30]. The main results are summarized as follows.

Ti oxides and Ti-complex oxides: The formation of IGF in Ti-killed steels is experimentally observed around Ti or complex Ti oxides [6-16]. These oxides are always accompanied by MnS and/or nitrides. Mills et al. [7] reported that Ti oxides are more effective to act as nucleation sites for IGF than Al_2O_3-MnO inclusions. Lee and Pan [8] experimentally showed that Ti oxysulfides possess a better nucleation potential for IGF than Ti oxides and MnS. It is found that the addition of B enhances the ability of IGF nucleation on Ti_2O_3-MnS or Ti_2O_3-MnS-TiN precipitates [6]. A balance of the five elements Ti, B, Al, N and O is rather important to obtain sufficient soluble B and fine dispersed Ti oxides [16]. Several researchers [9-12] found that complex Ti, Al, Mn and Si oxides with a certain amount of dissolved sulfide are effectively utilized as nucleation sites for IGF.

Rare earth metallic oxides/complex oxides containing ZrO_2: Zhu et al. [10] experimentally found that IGF is formed on these fine oxides during the controlled cooling process after welding simulation. These oxides are evenly distributed at higher sulfide contents resulting from deoxidation by rare earth metals and Zr at high oxygen potentials. The investigated steel is X60 of which the composition is: 0.066-0.105% [C], 0.305-0.405% [S]i, 1.30-1.50% [Mn], 0.035-0.045% [Nb], 0.045-0.055% [V].

MnS-VN and MnS-TiN inclusions: The principles of IGF nucleation on fine oxide inclusions have been recently extended to MnS-VN [16,17] and MnS-TiN [18] inclusions in carbon steels. HAZ (heat affected zone) toughness is strongly influenced by the sulfur content in steel plates [8,18-22]. Evans [19] found that S is detrimental to the formation of IGF and Devillers et al. [20] reported that the coating of MnS on oxides reduces the nucleation potential of IGF. On the contrary, St-Laurent and L'Esperance [21] experimentally showed that S is beneficial to the formation of IGF. Yamamoto et al. [6,12] and Ueshima et al. [22] suggested that the precipitation of MnS on Ti oxides causes a depletion of Mn around inclusions leading to

an increase in transformation temperature, thereby promoting the formation of IGF. Lee and Pan [8] reported that there exists an optimal addition of S for Ti-killed carbon steel to promote the formation of IGF. Both strong and small additions of S are detrimental to the formation of IGF. This result was further confirmed by Tomita et al. [18] shown in **Figure 7.1** which quantitatively yields an optimal S content corresponding to a maximum HAZ toughness. It seems that S strongly influences HAZ microstructure and precipitates.

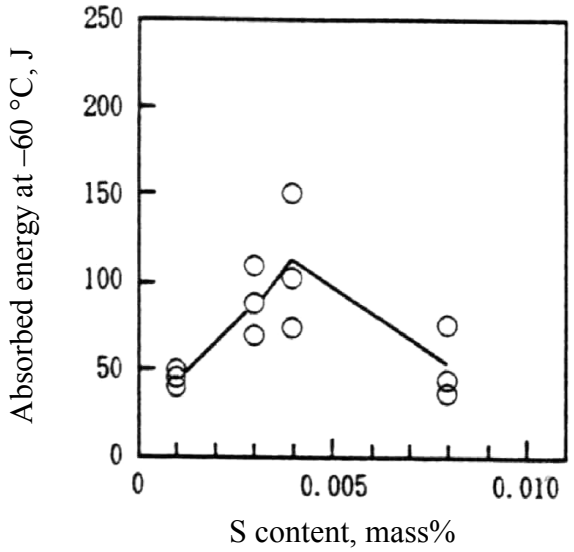

steel composition (mass%):

C	Si	Mn	Cu	Ni	Nb	Ti	Al	N	S
0.05	0.11	1.57	0.30	0.30	0.008	0.009	0.031	0.0037	0.001-0.008

Figure 7.1. Effects of S content on HAZ toughness in one-side single pass submerged arc welded joints with a heat input of 20 kJ/mm [18]

In the present investigation it was found that titanium or complex titanium oxides, sulfides and nitrides serve as nucleation sites for IGF during steel casting and rolling which is clearly demonstrated in **Figures 7.2-7.4**. This fact makes it possible to refine grain structures directly through control of deoxidation and solidification. It suggests the new idea that steel microstructures have a close relation to deoxidation technology.

Conventionally it is thought that steel microstructures are the matter during and after casting. The changes according to the new idea may bring about a great challenge to the current steelmaking practice. We may simplify or abandon some conventional grain refining measures through the adoption of feasible deoxidation techniques and controlled solidification processes. The present study further demonstrates that finely dispersed oxide inclusions generally refine the as-cast steel structure because these inclusions serve as nucleation sites for phase transformation. Therefore, this technology is a promising way to produce future steels which feature not only efficient and cost effective but also environment friendly benefits.

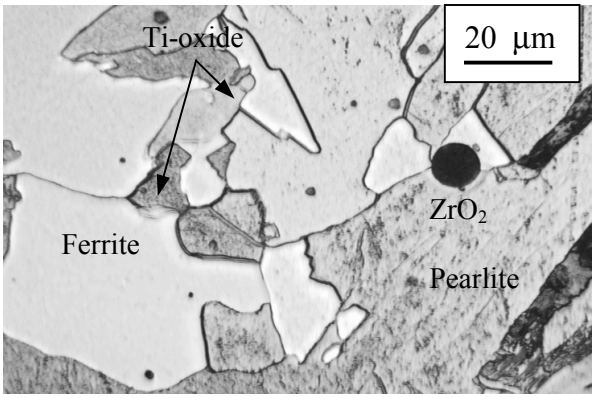

As-cast structures (low carbon steel)

Figure 7.2. Oxides serving as nucleation sites for IGF

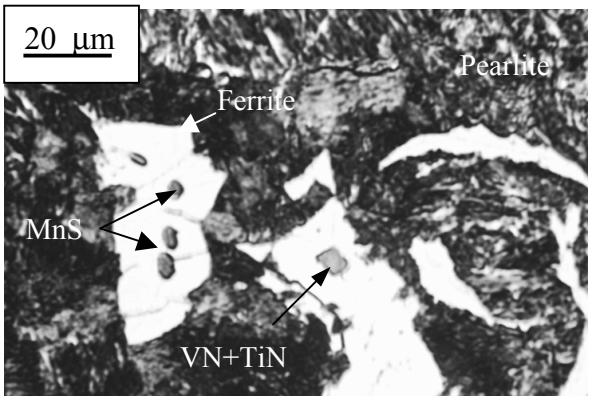

As-cast structures (27MnSiVS steel)

Figure 7.3. Sulfides and nitrides serving as nucleation sites for IGF

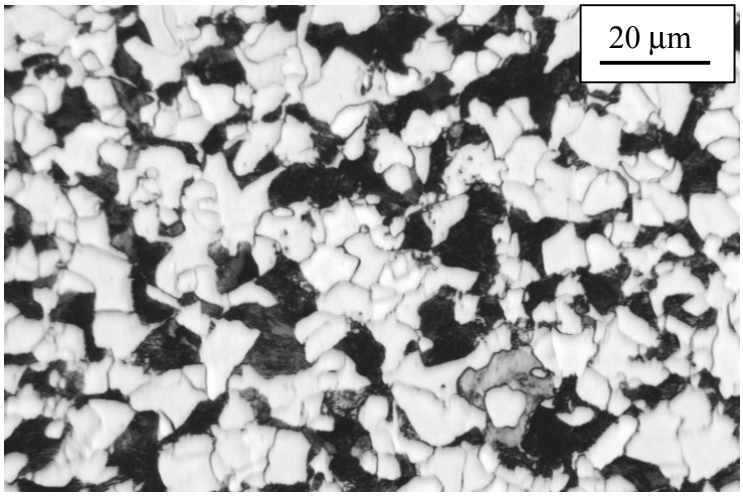

after rolling, 27MnSiVS steel

Figure 7.4. Sulfides and nitrides serving as nucleation sites for IGF

7.2 Mechanism of Inclusions Serving as Nucleation Sites for IGF

Mechanisms of nucleation of IGF at inclusions were discussed and summarized in chapter 2. Here the available mechanisms are listed in **Table 7.1** again in which the references are omitted (details see Table 2.3).

The energy change caused by phase transformation, for example the precipitation of α phase from austenite, can be generally expressed by the following equations according to different conditions:

Nucleation of ferrite inside austenite (generation of IGF):

$$\Delta E = \Delta E_{V,\alpha} + \Delta E_{\alpha-\gamma} + \Delta E_{i-\alpha} + \Delta E_{strain,\alpha} - \Delta E_{V,i} - \Delta E_{strain,i} \quad (7\text{-}1)$$

Nucleation of ferrite at austenite grain boundary (generation of GBF):

$$\Delta E = \Delta E_{V,\alpha} + \Delta E_{\alpha-\gamma} + \Delta E_{i-\alpha} + \Delta E_{strain,\alpha} - \Delta E_{\gamma-\gamma} - \Delta E_{V,i} - \Delta E_{strain,i} \quad (7\text{-}2)$$

$\Delta E_{V,i}$ and $\Delta E_{strain,i}$ become zero if IGF and GBF (grain boundary ferrite) do not nucleate at the surfaces of inclusions.

The meanings of the symbols used in Eqs. (7-1) and (7-2) are as follows

$\Delta E_{V-\alpha}$:	Volume free energy change for the formation of α phase
$\Delta E_{\alpha-\gamma}$:	Surface energy change for the formation of α phase
$\Delta E_{strain,\alpha}$:	Strain energy resulting from the formation of α phase
$\Delta E_{\gamma-\gamma}$:	Surface energy change for the diminution of contacted γ phase
ΔE_{V-i}:	Volume free energy change for the formation of an inclusion
$\Delta E_{strain,i}$:	Strain energy resulting from the formation of an inclusion

Table 7.1. Summary of IGF formation mechanism

Precipitates and/or inclusions	Transformation theory
	Epitaxitial growth theory
	(minimum misfit, δ)
TiO	δ = 3.0%
TiN	δ = 3.8%
VN	δ = 0.7%
FCC galaxite (Al_2O_3·MnO)	δ = 1.8%
γAl_2O_3	δ = 3.2%
CuS	δ = 2.8%
	Thermal expansion theory
$(MnO)_2(Al_2O_3)_2(SiO_2)$	•Thermal strain
Al containing inclusions	• Plastic strain
	Inclusion size theory
Inclusion size	≥ 1 μm: GBF; ≥0.6 μm: IGF
Oxide inclusion	≥ 0.4 μm pining γ grain
Fine inclusions	boundary
	ineffective
	Composition variation
	such as Mn depletion around
	inclusions
(Al·Si-S-Ti-Mn)O, TiN-MnS, TiN	Reduction of interfacial energy

* IGF: intragranular ferrite GBF: grain boundary ferrite

The different energy changes are interpreted by the following equations

$$\Delta E_{V,\alpha} = V_\alpha \cdot \Delta G_V$$
$$\Delta E_{\alpha-\gamma} = A_{\alpha-\gamma} \cdot \sigma_{\alpha-\gamma}$$
$$\Delta E_{i-\alpha} = -A_{i-\alpha}(\sigma_{i-\alpha} - \sigma_{i-\gamma})$$
$$\Delta E_{strain,\alpha} = V_\alpha \cdot \varepsilon_{\alpha-\gamma}$$
$$\Delta E_{\gamma-\gamma} = A_{\gamma-\gamma} \cdot \sigma_\gamma$$
$$\Delta E_{V,i} = V_{i-\alpha}(G_{V,i-\alpha} - G_{V,i-\gamma})$$
$$\Delta E_{strain,i} = V_{i-\alpha}(\varepsilon_{i-\alpha} - \varepsilon_{i-\gamma})$$

Where	V_α:	volume α phase
	$V_{k\text{-}t}$:	volume of k phase in t phase
	σ:	surface or interface tension
	ε:	strain
	$A_{k\text{-}t}$:	surface area of k phase contacting t phase
Subscript:	α:	α phase
	i:	inclusion
	γ:	γ phase
	V:	volume factor

The term $\Delta E_{V,\alpha}$ is negative indicating the driving force of forming α phase. It is reasonable to assume that all factors causing reduction of ΔE favour the formation of α phase both inside austenite and at the austenite grain boundary as shown in Eqs.(7-10) and (7-11). It is obvious that IGF is to precipitate prior to GBF if conditions satisfy the inequality Eq. (7-12).

Maximum of $-\Delta E_{V,\alpha}$ (7-10)

Minimum of $\Delta E_{\alpha-\gamma} + \Delta E_{i-\alpha} + \Delta E_{strain,\alpha} - \Delta E_{V,i} - \Delta E_{strain,i}$ (7-11)

$$(\Delta E_{\alpha-\gamma} + \Delta E_{i-\alpha} + \Delta E_{strain,\alpha} - \Delta E_{\gamma-\gamma} - \Delta E_{V,i} - \Delta E_{strain,i})_{IGF} < (\Delta E_{\alpha-\gamma} + \Delta E_{i-\alpha} + \Delta E_{strain,\alpha} - \Delta E_{\gamma-\gamma} - \Delta E_{V,i} - \Delta E_{strain,i})_{GBF} \quad (7\text{-}12)$$

Unfortunately it is impossible till now to calculate all terms because of the lack of parameters. However, these inequalities give a general criterion for the formation of IGF which can reasonably explain the available mechanisms. The proposed mechanisms are quite different from and even contradictory to different sources. According to the inequality Eqs. (7-10)-(7-11), these mechanisms are no longer different and contradictory but only reflect the contribution of different influencing factors to the inequalities. Here general discussions are given. The favourable conditions for forming IGF are listed and explained in **Table 7.2**. It is obvious that the available mechanisms are only partial contributions to the present unified formulae. These formulae can be treated as a general condition to determine the precipitation of IGF and GBF. **Figure 7.5** demonstrates that GBF and IGF simultaneously precipitate during and after solidification. The favorable conditions for prior IGF are clearly demonstrated in table 7.2.

The above discussions are focused on the thermodynamic point of view. However, the kinetic factors are also important. For example, a high diffusivity of carbon atoms in austenite greatly favours ferrite nucleation. However, the discussion on the kinetics of ferrite nucleation is out side the scope of the present study.

Table 7.2. Favourable conditions for forming IGF

Favorable conditions	Contribution to form IGF	Available mechanism
Minimum misfit between inclusion (inside austenite) and IGF	Increase of $\Delta E_{V,i}$	Epitaxial growth theory
Thermal strain and plastic strain between inclusions and IGF	Increase of $\Delta E_{strain,I}$	Thermal expansion theory
Coarse inclusions and large inclusions	Increase of $\Delta E_{strain,i}$ and $\Delta E_{V,I}$	Inclusion size theory
Reduction of interfacial energy between inclusions and IGF	Decrease of $\Delta E_{I-\alpha}$	Reduction of interfacial energy
Composition of steel	Influencing $\Delta E_{\alpha-\gamma}$ and $\Delta E_{\gamma-\gamma}$	

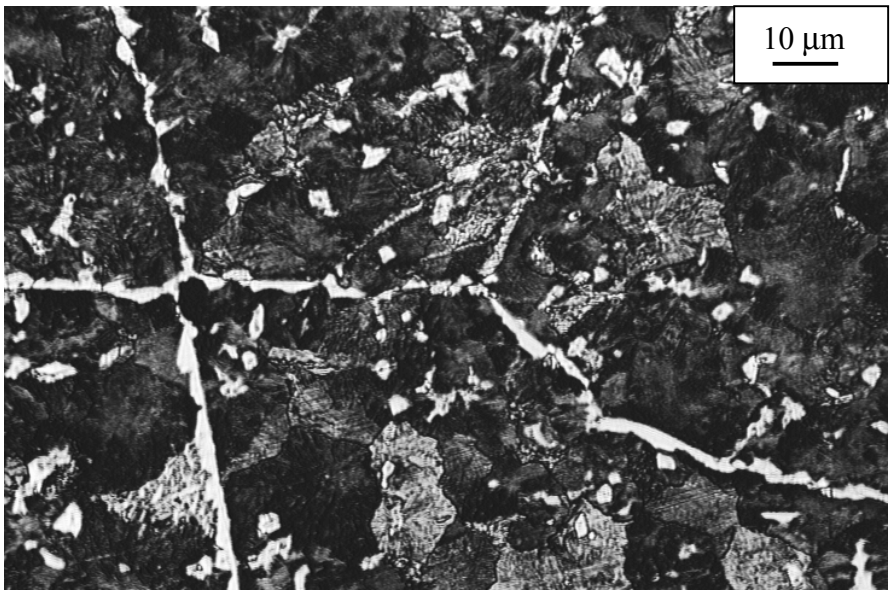

Figure 7.5. Competition of nucleation between GBF and IGF for as-cast 27MnSiVS steel ([V] <100 ppm)

7.3 Relation between Microstructure and Toughness

Figures 7.6-7.8 show the experimental results of charpy-V-notch impact toughness A_V of the investigated steels. It is found that notch impact toughness of the investigated steels is greatly improved by the addition of Ti at S contents below 0.012%. However, it seems that notch impact toughness is influenced by Ti and S contents at high S levels and that an optimal range for Ti and S contents exists to reach high A_V values. High notch impact toughness for Fe-Cr-Ni austenitic stainless steels is also obtained using alternative deoxidation technology. The notch impact toughness of as-cast Fe-Cr-Ni austenite stainless steels meets the standard requirements for the final product. Moreover, the corresponding microstructures for the investigated steels are investigated. It is found that steels with fine grain structure demonstrate a high toughness. For example, **Figures 7.9-7.11** indicate that the steels featuring fine as-cast microstructure and finely dispersed inclusions demonstrate high notch impact toughness. It is concluded that steels produced by oxide metallurgy

afford an improvement of service properties. Further investigations on this subject are needed

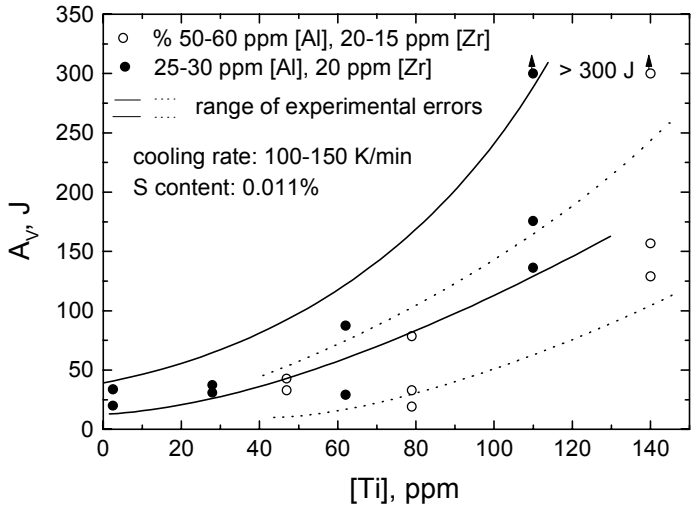

Figure 7.6. Effect of Ti content on charpy-V-notch impact toughness (at room temperature) of as cast low carbon steels

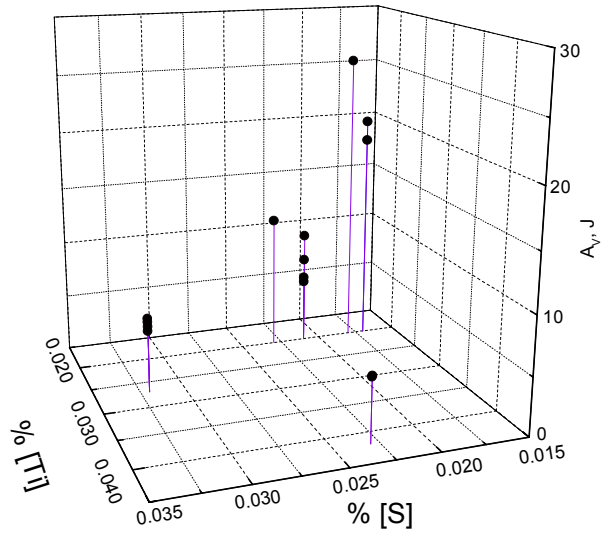

Figure 7.7. Effect of Ti and S contents on charpy-V-notch impact toughness (at room temperature) of as-cast 27 MnSiVS steel (cooling rate: 100-150 K/min)

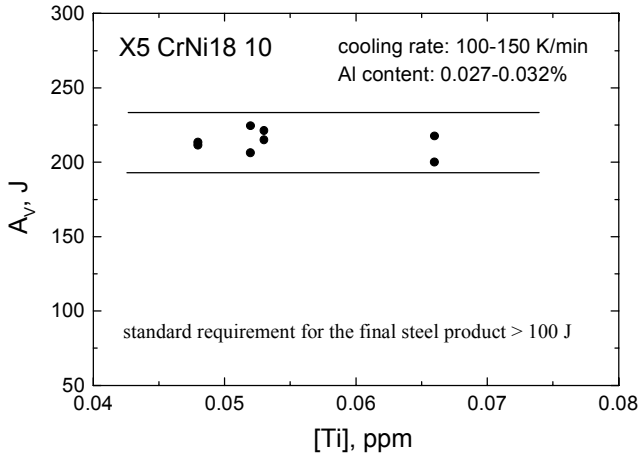

Figure 7.8. Achievement of high Charpy-V-notch impact toughness (at room temperature) of as-cast Cr-Ni based stainless steel through alternative deoxidation technology

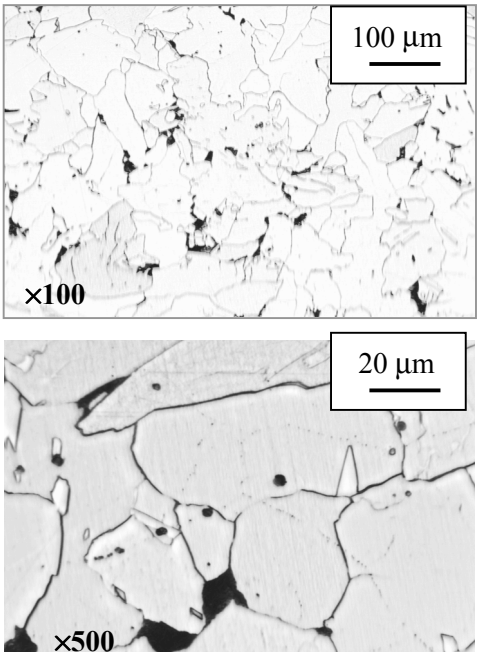

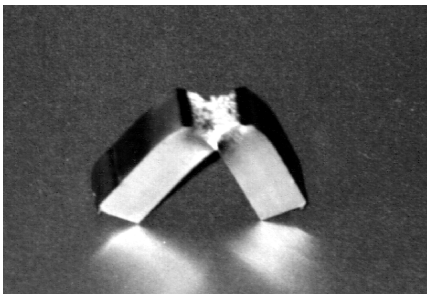

Photo of a sample after the test of Charpy-V-notch impact toughness

Figure 7.9. As-cast structures of low carbon steel (25-30 ppm [Al], 0.011% [Ti])

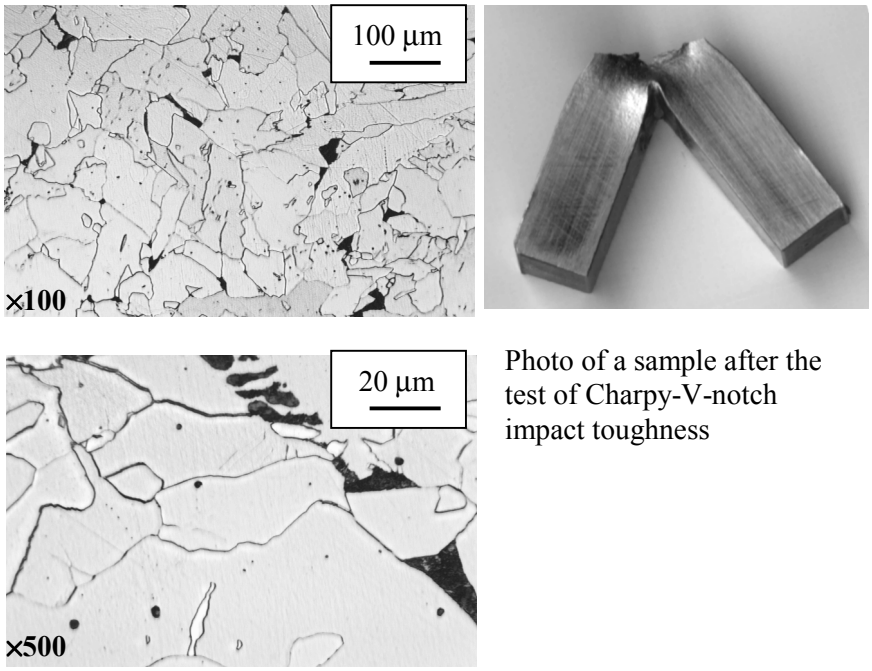

Figure 7.10. As-cast structures of low carbon steel (50-60 ppm [Al], 0.014% [Ti])

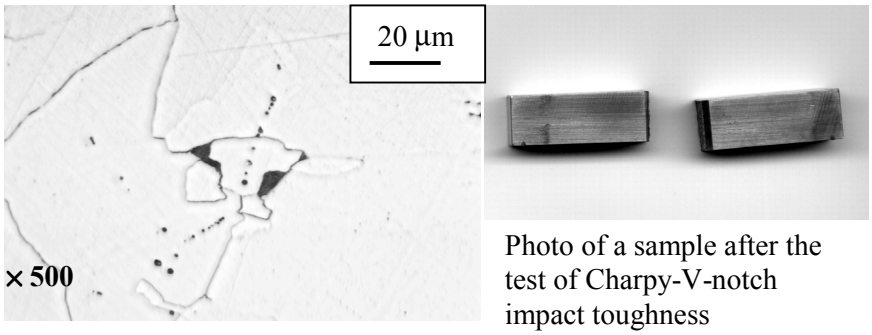

Figure 7.11. As-cast structure of low carbon steel (25-30 ppm [Al], 0.008% [Ti])

References

[1] Z. Ma, D. Peisker and D. Janke: steel research, 70(1999), 178/82

[2] Z. Ma and D. Janke: Technical Report "Improvement of fine grain structures of 27MnSiVS steel", Institute of Iron and Steel Technology, TU Freiberg, November, 1998

[3] S. Mizoguchi: "A study on segregation and oxide inclusions for the control of steel properties" , PhD thesis, The University of Tokyo, 1996

[4] Z. Ma and D. Janke: Annual Technical Report of ECSC Sponsored Project under Grant No. ECSC-95-C2.03c, Institute of Iron and Steel Technology, TU Freiberg, 1998

[5] T. Funakoshi, T. Tanaka, S. Ueda, M. Ishikawa, N. Koshizuka and K. Kobayashi: Trans. ISIJ, 17(1997), 419/24

[6] K. Yamamoto, T. Hasegawa and J. Takamura: ISIJ International, 36(1996), 80/86

[7] R. Mills, G. Thewlis and J. A. Whiteman: Materials Sci. and Tech., 3(1987), 1051/61

[8] J. L. Lee and Y. T. Pan: Mater. Sci. Eng., 136A(1991), 109/19, Metall. Trans. A, 22A(1991), 2818/22, 24A(1993), 1399/1408

[9] D. Yu, F. J. Barbaro, T. Chandra and D. P. Dunne: ISIJ International, 36(1996), 1055/62

[10] Y. Zhu, S. Guo, J. Xu, G. Jiang, D. Yu, L. Pan and Y. Wang: Acta Metallurgica Sinica, 32(1996), 891/6

[11] H. Honma, S. Ohkita, S. Matsuda and K. Yamamoto: 67th AWS Convention, Atlanta, USA, 1986

[12] K. Yamamoto, S. Matsuda, T. Hase, R. Chijiiwa and H. Mimura: "A newly developed Ti-oxide bearing steel having high HAZ toughness", Symp. on Residual & Unspecified Elements in Steel, ASTM-STP, 1989, 264/284

[13] N. Mori, H. Honma, M. Wakabayashi and S. Ohkita: J. Jpn. Weld. Soc., 50(1981), 786

[14] I. Watanada and K. Kojima: J. Jpn. Weld. Soc., 50(1981), 703

[15] T. Yamaguchi, H. Terashima and N. Nishiyama: Proc. of the Symp. on TMCP Steel by Weld. Metall. Comm. of J.W.S., Paper 23, 1990

[16] F. Ishikawa, T. Takahashi and T. Ochi: Metall. Materials Trans., 25A(1994), 929/36

[17] T. Ochi, T. Takahashi and H. Takada: Iron Steelmaker, 16(1989), 21/28
[18] Y. Tomita and N. Saito: ISIJ International, 34(1994), 829/35
[19] G. M. Evans: Met. Constr., 44(1986), 631/36
[20] L. Devillers, D. Kaplan, B. Marandet, A. Ribes and P. V. Riboud: in Conf. on the effects of residual, impurities and micro-alloying elements on the weldability and weld properties, The Welding Institute, Abington, UK, 1983, 1/12
[21] S. St-Laurent and G. L'Esperance: Mater. Sci. Eng., 149A(1992), 203/16
[22] Y. Ueshima, H. Yuyama, S. Mizoguchi and H. Kajioka: Tetsu-to-Hagane, 75(1989), 501/08
[23] R. A. Ricks, P. R. Howell and G. S. Barrotte: J. Mater. Sci., 17(1982), 731/740
[24] D. J. Abson: Weld. World, 27(1989), 76/101
[25] B. L. Bramfitt: Metall. Trans., 1(1970), 1987/1995
[26] F. J. Barbaro, P. Krauklis and K. E. Easterling: Materials Sci. and Tech., 5(1989), 1057/1077
[27] S. Kanazawa, A. Nakashima, K. Okamoto and K. Kanaya: Trans. ISIJ, 1681976), 486/495
[28] J. Jang and J. E. Indacochea: J. Mater. Sci., 22(1987), 689/700
[29] M. Enomoto and H. I. Aaronson: Metall. Trans., 17A(1986), 1381/1384
[30] M. Ferrante, K. Akune and M. Odaina: J. Mater. Sci., 22(1987), 351

CHAPTER 8
Conclusions

It is one of the most important tasks in steelmaking to improve castability and quality of continuously cast steel. Oxide metallurgy offers an effective additional method to alleviate or eliminate nozzle clogging during continuous casting processes and to improve steel service properties through control of inclusions and grain refinement. The fine unagglomerated inclusions in liquid steel give rise to the improvement of castability. The generation of the finely dispersed oxides which easily become nucleation sites for precipitates such as sulfides, nitrides and carbides and for phase transformation with respect to IGF plays a key role in **oxide metallurgy**. Alternative deoxidation techniques with partial or complete substitution of Ti and Zr for Al are presently investigated. The main conclusions and results are summarized as follows:

- **Thermodynamic analysis of metallic solutions (appendices A and B)**
  A modified ε formalism was developed to perform thermodynamic analysis for both dilute and concentrated metallic solutions. This formalism features thermodynamic consistency and higher accuracy in comparison with Wagner's ε formalism. The interaction parameters between solutes in liquid iron at 1873 K were given.

- **Calculation model for size and composition of oxide inclusions (appendix C)**
  A calculation model was proposed to evaluate the size and composition of oxide precipitates in molten steel during solidification. So far, three different models have been developed to describe the precipitation and growth of nonmetallic inclusions during solidification. They were established at IRSID (France), NSC (Japan) and IEST, TU Freiberg (Germany). The present model is the simplest one and accurately predicts the oxide behaviour in molten steel during solidification.

- **The state-of-the-art of research work on oxide metallurgy (chapters 1 and 2)**
  The reported work on oxide metallurgy was summarized and discussed. The present research objectives were outlined.

- **Deoxidation technologies used in steelmaking processes (chapter 3)**
  The available deoxidation technologies are summarized and discussed. Clean deoxidation technology is presently applied in view of the production of clean steel. Alternative deoxidation techniques aiming at the utilization of inclusions in steel are being discussed.

- **Generation of finely dispersed oxide inclusions (chapter 5)**
  Oxide precipitation is important in oxide metallurgy and is affected by many factors. However, deep understanding of the effects of these influencing factors is not available. The present study gives a systematic and profound investigation on this subject. It is experimentally found that the size, distribution and number of oxides in steels are greatly influenced by factors such as the cooling rate and the contents of Ti, Al, Zr, Mn and O. Their influence on size, composition, distribution and shape of oxides is investigated and discussed in the present work. The main results are given in chapter 5.

- **Effect of oxide inclusions on nozzle clogging (chapter 6)**
  Basic principles of nozzle clogging are theoretically discussed. A formula was developed to explain nozzle clogging. This formula successfully interpretes different experimental results from the theoretical point of view. It may help to develop new processes and improve the available processes to avoid nozzle clogging.

- **Effect of oxide inclusions on sulfide precipitation (chapter 6)**
  Oxide inclusions serving as nucleation sites for sulfides are important to guarantee the generation of evenly dispersed sulfides in steel. It is experimentally found that Ti oxides effectively serve as nucleation sites for sulfides in steel. A new mechanism of MnS precipitation on oxides was proposed. This mechanism reasonably explains the available experimental results.

- **Generation of IGF (chapter 7)**
  IGF technology was successfully applied to steel casting and rolling processes. Meanwhile, it has been experimentally confirmed that finely dispersed oxides in steel generally refine grain structures during solidification processes. This technology is most useful for the forthcoming technologies of hot direct rolling, thin slab casting and direct strip casting.

A mechanism of producing IGF was proposed which reasonably unifies the available mechanisms appearing different and even contradictory.

- **Effect of oxide inclusions on mechanical properties of steel (chapter 7)**
  Fine grain structures can be obtained using oxide metallurgy and resulting in an improvement of steel service properties. High charpy-V-notch impact toughness for stainless, low carbon and low alloyed steels is obtained through the control and utilization of inclusions.

Oxide metallurgy is beneficial for various casting and hot working processes, particularly in the case of fast cooling and hot direct rolling. This technology features efficient, cost effective and environment friendly measures. It improves castability and the quality of continuously cast steel without additional metallurgical treatment and without enhancing the effects to increase steel cleanness in conventional refining processes. New steel grades based on fine or ultra fine grain structures can be produced using oxide metallurgy in conventional and new steelmaking processes such as thin slab and direct strip casting.

APPENDIX A
Thermodynamics of Concentrated Metallic Solutions

1. Introduction

The interaction parameter formalism expressed in terms of a MacLaurin series expansion for the partial excess free energy is frequently used to express the thermodynamic properties of dilute solutions, particularly of metals. However, the experimental determination of interaction parameters beyond second-order is almost impossible in practice due to the requirement of an extremely high accuracy. Activity coefficients of solutes at high solute contents have so far been calculated by the first-order interaction parameters, that is, based on the simplest case of a truncated MacLaurin series. Any truncated MacLaurin series expansion weakens the exactness of the expression for the activity coefficient of a solute in a multicomponent system, and at high solute contents the thermodynamic inconsistency can result in significant errors [1-4]. In view of this, many attempts have been made to extend the approach to concentrated solutions.

Darken [1,5] proposed a quadratic formalism which is thermodynamically consistent, but this formalism has never enjoyed much popularity since the published experimental data are mainly presented in terms of the interaction parameter formalism, and the validity of Darken's formalism for ternary and higher order systems with strong interactions needs further proof. The equations based on the quasi-chemical model for dilute ternary and multicomponent systems first solved by Lupis [6] with a formidable mathematical procedure are very similar to Darken's formalism. Bale and Pelton [3,7] have more recently proposed a unified interaction parameter formalism which is thermodynamically consistent by simply adding a term of $\ln \gamma_{solvent}$ in the expression of $\ln \gamma_i$ where i represents the solute. The deduced procedure is based on the integral molar excess Gibbs energy of a multicomponent solution at constant temperature expressed by the general Margules-type polynomial expansion in the mole fractions [7]. Srikanth and Jacob [4] derived the same expression of $\ln \gamma_{solvent}$ by solving the Gibbs-Duhem equation and they also indicated that the expression is valid only for dilute solutions. Furthermore, Srikanth and Jacob [4] have shown that a truncated MacLaurin series being inaccurate at finite contents may be integrated along a constant composition path without significant loss of

accuracy. However, the introduction of this path-depending integral is generally considered to reduce the degree of compositional freedom. The thermodynamic inconsistency retained in this method. Hajra and Frohberg [8,9] proposed suitable expressions involving interaction parameters for presenting thermodynamic properties of the solvent in a ternary system. These expressions were obtained by integration of several series which emerge from the MacLaurin infinite series based on the integral property of the system and subjected to appropriate boundary conditions. But the expression of ln γ_i where i is the solute has not been given by the authors.

A new method is proposed in the present work to describe the thermodynamic properties of multicomponent systems. It is thermodynamically consistent and independent of integration paths.

2. Establishment of the Formalism

For the system 1–2–···–i–···–m with m components, the excess Gibbs free energy of the system can be expressed as an infinite MacLaurin series in terms of the integral function of the system. Eq. (1) gives this approach. Let x_k denote the mole fraction of the k-th component (k=1,2, 3, ···, m). The series is subjected to the following general and boundary conditions:

(a) general condition: $x_1 \to 1$, $x_j \to 0$ (j=2, 3, ···, m) for the system with m components, $\Delta^E G \to 0$,

(b) boundary conditions: $x_i \to 1$, $x_j \to 0$ ($i \neq 1$ and j=2, 3, ···, i-1, i+1, ···, m) for the marginal systems with m-1 components, $\Delta^E G \to 0$.

$$\Delta^E G = (\Delta^E G)_{x_1 \to 1} + \sum_{i=2}^{m} \sum_{n_1=1}^{\infty} \frac{1}{n_1!} \left(\frac{\partial^{n_1} \Delta^E G}{\partial x_i^{n_1}} \right)_{x_1 \to 1} x_i^{n_1}$$

$$+ \sum_{i=2}^{m-1} \sum_{j=i+1}^{m} \sum_{n_1=1}^{\infty} \sum_{n_2=1}^{\infty} \frac{1}{n_1! n_2!} \left(\frac{\partial^{n_1+n_2} \Delta^E G}{\partial x_i^{n_1} \partial x_j^{n_2}} \right)_{x_1 \to 1} x_i^{n_1} x_j^{n_2} + \cdots \qquad (1)$$

When inserting the boundary conditions as mentioned above into the series (1), the following equation is obtained:

$$\sum_{n=1}^{\infty} \frac{1}{n!}\left(\frac{\partial^n \Delta^E G}{\partial x_j^n}\right)_{x_1 \to 1} = 0 \ . \tag{2}$$

Substituting Eq. (2) into Eq. (1) yields

$$\Delta^E G = -\sum_{j=2}^{m}\sum_{n_1=1}^{\infty}(1-x_j^{n_1})\left(\frac{\partial^{n_1}\Delta^E G}{\partial x_j^{n_1}}\right)_{x_1\to 1} + \sum_{i=2}^{m-1}\sum_{j=i+1}^{m}\sum_{n_1=1}^{\infty}\sum_{n_2=1}^{\infty}\frac{1}{n_1!\,n_2!}\left(\frac{\partial^{n_1+n_2}\Delta^E G}{\partial x_i^{n_1}\partial x_j^{n_2}}\right)_{x_1\to 1} x_i^{n_1} x_j^{n_2} + \cdots$$

$$= \sum_{j=2}^{m} x_j(1-x_j)\left[\left(\frac{\partial \Delta^E G}{\partial x_j}\right)_{x_1\to 1} + \sum_{n=1}^{\infty}\left(x_j^n \sum_{k=1}^{n+1}\frac{1}{k!}\left(\frac{\partial^k \Delta^E G}{\partial x_j{}^k}\right)_{x_1\to 1}\right)\right]$$

$$+ \sum_{i=2}^{m-1}\sum_{j=i+1}^{m}\sum_{n_1=1}^{\infty}\sum_{n_2=1}^{\infty}\frac{1}{n_1!\,n_2!}\left(\frac{\partial^{n_1+n_2}\Delta^E G}{\partial x_i^{n_1}\partial x_j^{n_2}}\right)_{x_1\to 1} x_i^{n_1} x_j^{n_2} + \cdots \tag{3}$$

Then the interaction parameters defined in **Table 1** are introduced. The excess Gibbs free energy can be written as Eq. (4) with neglect of the impact terms which are listed in **Table 2**. The neglect takes into account that higher-order interaction parameters are not available and the accuracy of results from high temperature experimental techniques is limited

$$\frac{\Delta^E G}{RT} = \sum_{j=2}^{m}(1-x_j)x_j\left[\ln\gamma_j^o(1+\sum_{n=1}^{\infty}x_j^n) + \sum_{n=1}^{\infty}\varepsilon_j^j\left(1-\frac{1}{n+1}\right)x_j^n\right]$$

$$+ \sum_{j=2}^{m-1}\sum_{k=j+1}^{m} x_j x_k\left(\varepsilon_j^k + \varepsilon_j^k\sum_{n=1}^{\infty}\frac{x_k^n}{n+1} + \varepsilon_j^k\sum_{n=1}^{\infty}\frac{x_j^n}{n+1}\right) + \sum_{j=2}^{m-1}\sum_{k=j+1}^{m}\frac{\varepsilon_j^k}{2}x_j{}^2 x_k{}^2\left[1-\sum_{n=1}^{\infty}(x_j^n + x_k^n)\right] \tag{4}$$

With progression functions the above equation can be rewritten as

$$\frac{\Delta^E G}{RT} = \sum_{j=2}^{m} x_j(1-x_j)\left[\frac{1}{1-x_j}\ln\gamma_j^o + \varepsilon_j^j\left(\frac{1}{1-x_j} + \frac{\ln(1-x_j)}{x_j}\right)\right]$$

$$-\sum_{j=2}^{m-1}\sum_{k=j+1}^{m} x_j x_k \varepsilon_j^k\left[1 + \frac{\ln(1-x_j)}{x_j} + \frac{\ln(1-x_k)}{x_k}\right] + \frac{1}{2}\sum_{j=2}^{m-1}\sum_{k=j+1}^{m}\varepsilon_j^k x_j^2 x_k^2\left[\frac{1}{1-x_j} + \frac{1}{1-x_k} - 1\right] \tag{5}$$

Table 1. Relation between derivatives of the excess Gibbs free energy and the conventional interaction parameters

No.	
1	$\frac{1}{RT}\left(\frac{\partial^3 \Delta G^{xs}}{\partial x_j^3}\right)_{x_1 \to 1} = \varepsilon_j^j + 2\rho_j^j,$
2	$\frac{1}{RT}\left(\frac{\partial^n \Delta G^{xs}}{\partial x_j^n}\right)_{x_1 \to 1} = (n-2)\left(\frac{\partial^{n-1} \Delta G^{xs}}{\partial x_j^{n-1}}\right)_{x_1 \to 1} + J_{j,j}^{(n-1)}, \quad n > 3,$
3	$\frac{1}{RT}\left(\frac{\partial^3 \Delta G^{xs}}{\partial x_k^2 \partial x_j}\right)_{x_1 \to 1} = \varepsilon_k^j + \rho_k^{j,k},$
4	$\frac{1}{RT}\left(\frac{\partial^n \Delta G^{xs}}{\partial x_k^{n-1} \partial x_j}\right)_{x_1 \to 1} = (n-2)\left(\frac{\partial^{n-1} \Delta G^{xs}}{\partial x_k^{n-2} \partial x_j}\right)_{x_1 \to 1} + J_{j,k}^{(n-1)}, \quad n > 3,$
5	$\frac{1}{RT}\left(\frac{\partial^{n_1+n_2} \Delta G^{xs}}{\partial x_j^{n_1} \partial x_k^{n_2}}\right)_{x_1 \to 1} = (n_1+n_2-2)\left(\frac{\partial^{n_1+n_2-1} \Delta G^{xs}}{\partial x_j^{n_1-1} \partial x_k^{n_2}}\right)_{x_1 \to 1} + J_{j,k}^{(n_1+n_2-1)}, \quad n_1, \ n_2 > 3.$

Here ε and ρ are first and second-order activity interaction parameters, respectively, and their subscripts and superscripts are the same as designed by Lupis and Elliott [6]. The J denotes higher-order interaction parameters.

Table 2. With neglect of the impact terms in Eq. (3)

No.	Terms
1	Higher than second-order interaction parameters
2	$\left(\frac{\partial^{n_1+n_2+n_3}\Delta^E G}{\partial x_i^{n_1}\partial x_j^{n_2}\partial x_k^{n_3}}\right)_{x_1\to 1}$ and analogous derivations wit more components
3	$\left(\frac{\partial^{n_1+n_2}\Delta^E G}{\partial x_i^{n_1}\partial x_j^{n_2}}\right)_{x_1\to 1}$ for $n_1\geq 3$ and $n_2\geq 3$

The partial excess Gibbs free energy can be written as

$$\frac{\Delta^E G_i}{RT} = \frac{\Delta^E G}{RT} + \frac{1}{RT}\sum_{j=2}^{m}(\delta_{ij} - x_j)\frac{\partial \Delta^E G}{\partial x_j} \tag{6}$$

where δ_{ij} is the Kronecker delta, i.e. $\delta_{ij} = \begin{cases} 1 & i = j \\ 0 & i \neq j \end{cases}$

According to Eq. (6) and $\ln \gamma_i = \Delta^E G_i/RT$, the expression for $\ln \gamma_1$ of the solvent can be derived from Eq. (4) as

$$\begin{aligned}
\ln\gamma_1 &= \frac{\Delta^E G}{RT} - \frac{1}{RT}\sum_{i=2}^{m} x_i \frac{\partial \Delta^E G}{\partial x_i} \\
&= \sum_{i=2}^{m}\varepsilon_i^i[x_i + \ln(1-x_i)] - \sum_{j=2}^{m-1}\sum_{k=j+1}^{m}\varepsilon_j^k x_j x_k\left(1 + \frac{\ln(1-x_j)}{x_j} + \frac{\ln(1-x_k)}{x_k}\right) \\
&+ \sum_{i=2}^{m}\sum_{\substack{k=2 \\ (k\neq i)}}^{m}\varepsilon_i^k x_i x_k\left(1 + \frac{\ln(1-x_k)}{x_k} - \frac{1}{1-x_i}\right) + \frac{1}{2}\sum_{j=2}^{m-1}\sum_{k=j+1}^{m}\varepsilon_j^k x_j^2 x_k^2\left(\frac{1}{1-x_j} + \frac{1}{1-x_k} - 1\right) \\
&- \sum_{i=2}^{m}\sum_{\substack{k=2 \\ (k\neq i)}}^{m}\varepsilon_i^k x_i^2 x_k^2\left(\frac{1}{1-x_i} + \frac{1}{1-x_k} + \frac{x_i}{2(1-x_i)^2} - 1\right)
\end{aligned} \tag{7}$$

If the component i is a solute then

$$\ln\gamma_i = \ln\gamma_1 + \frac{1}{RT}\frac{\partial\Delta^E G}{\partial x_i}$$

$$= \ln\gamma_1 + \ln\gamma_i^o - \varepsilon_i^i \ln(1-x_i) - \sum_{\substack{k=2\\(k\neq i)}}^{m} \varepsilon_i^k x_k \left[1 + \frac{\ln(1-x_k)}{x_k} - \frac{1}{1-x_i}\right]$$

$$+ \sum_{\substack{k=2\\(k\neq i)}}^{m} \varepsilon_i^k x_k^2 x_i \left(\frac{1}{1-x_i} + \frac{1}{1-x_k} + \frac{x_i}{2(1-x_i)^2} - 1\right) \qquad (8)$$

Eqs. (7) and (8) express the activity coefficients of solvent and solutes, respectively, in multicomponent systems in terms of first-order interaction parameters and mole fractions of solutes. These expressions are thermodynamically consistent with the Gibbs-Duhem equation and they give more accurate results in comparison with the classical Wagner approach. The expressions are complex, but they can simply be handled in computer calculation. The application of the formulae (7) and (8) is demonstrated in the special case of ternary systems

$$\ln\gamma_1 = \varepsilon_2^2[x_2 + \ln(1-x_2)] + \varepsilon_3^3[x_3 + \ln(1-x_3)] + \varepsilon_2^3 x_2 x_3 \left(1 - \frac{1}{1-x_2} - \frac{1}{1-x_3}\right)$$

$$- \frac{\varepsilon_2^3}{2} x_2^2 x_3^2 \left(\frac{3}{1-x_2} + \frac{3}{1-x_3} + \frac{x_2}{(1-x_2)^2} + \frac{x_3}{(1-x_3)^2} - 3\right) \qquad (9)$$

$$\ln\gamma_i = \ln\gamma_1 + \frac{1}{RT}\frac{\partial\Delta^E G}{\partial x_i}$$

$$= \ln\gamma_1 + \ln\gamma_i^o - \varepsilon_i^i \ln(1-x_i) - \varepsilon_i^k x_k \left(1 + \frac{\ln(1-x_k)}{x_k} - \frac{1}{1-x_i}\right)$$

$$+ \varepsilon_i^k x_k^2 x_i \left(\frac{1}{1-x_i} + \frac{1}{1-x_k} + \frac{x_i}{2(1-x_i)^2} - 1\right) \qquad (10)$$

for i, k=2, 3 and k≠i. In this case the index k of the right-hand side of Eq. (10) is determined by the index i, i.e. k=3 for i=2, and k=2 otherwise.

References

[1] L. S. Darken: TMS-AIME, 239(1967), 80-89
[2] R. Schuhmann, Jr.: Metall. Trans., 16B(1985), 807-13
[3] A. D. Pelton and C. W. Bale: Metall. Trans. A, 17A(1986), 1211-15
[4] S. Srikanth and K. T. Jacob: Metall. Trans. B, 19B(1988), 269-75
[5] L. S. Darken: TMS-AIME, 239(1967), 90-96
[6] C. H. P. Lupis and J. F. Elliott: Acta Metall., 14(1966), 529-38; 1019-32
[7] C. W. Bale and A. D. Pelton: Metall. Trans. A, 21A(1990), 1997-2002
[8] J. P. Hajra and M. G. Frohberg: Metall. Trans. B, 23B(1992), 23-28
[9] J. P. Hajra and M. G. Frohberg: steel research, 60(1989), 479-84

APPENDIX B

Table 1. Interaction parameters in liquid iron at 1873 K [1-9]

(1-A)

j	C	Si	Mn	P	S	Cr	Ni	Cu	Co
e_C^j	0.19	0.08	-0.012	0.051	0.044	-0.023	0.01	0.016	0.0075
e_{Si}^j		0.103	-0.0146	0.09	0.066	-0.0003	0.005	0.0144	0.006
e_{Mn}^j			-0.0026	0.06	-0.048	0.0039	-0.0072	*-0.012*	-0.0036
e_P^j				0.054	0.034	-0.018	0.003	-0.035	0.004
e_S^j					-0.046	-0.0105	0	-0.0084	0.0026
e_{Cr}^j						-0.00067	0.0002	0.016	-0.019
e_{Ni}^j							0.0007	0.009	0.012
e_{Cu}^j								-0.02	*-0.0060*
e_{Co}^j									0.0051
γ_j^0	0.599	0.0013	1.44			1.18	0.66	9.11	1.05

continued on the next page

(1-b) continued from the above page

j	Mo	Ti	V	Al	Nb	N	O
e_C^j	-0.0137	-0.07	-0.03	0.043	-0.059	0.11	-0.32
e_{Si}^j	2.36	1.23	0.025	0.058	0	0.092	-0.119
e_{Mn}^j	0.0046	-0.05	0.0057	0.027	0.0073	-0.091	-0.083
e_P^j	0.001	-0.04	-0.024	0.037	-0.012	0.13	0.13
e_S^j	0.0027	-0.18	-0.019	0.041	-6.013	0.01	-0.27
e_{Cr}^j	0.0018	0.059	0.012	0.019	*0.0091*	-0.182	-0.12
e_{Ni}^j	-0.011	-0.60	-0.12	0.0097	-0.066	0.015	0.01
e_{Cu}^j	*0.0059*	*-0.0058*	*0*	*-0.025*	*0.0067*	0.025	-0.065
e_{Co}^j	*0*	*-0.017*	*-0.0085*	*-0.023*	*-0.0048*	0.037	0.018
e_{Mo}^j	0.0121	*0.021*	*0.011*	*0.016*	*0.011*	-0.1	0.0083
e_{Ti}^j		0.042	*0.029*	*-0.0029*	*0.027*	-2.06	-3.40
e_V^j			0.031	*-0.0001*	*0.018*	-0.4	-0.46
e_{Al}^j				0.043	*0.0093*	0.015	-1.98
e_{Nb}^j					0	-0.475	-0.72
e_N^j						0	-0.12
e_O^j							-0.17
γ_j^0	1.0	0.017	0.08	0.058	0.2		

$$e_j^i = \frac{1}{230}\left[(230e_i^j - 1)\frac{M_j}{M_1} + 1\right], \quad \varepsilon_i^j = \frac{M_j}{M_1}(230e_i^j - 1) + 1$$

$$\varepsilon_N^{Cr} = -9.84 + 0.10989[\%Cr] \quad [4]$$

The values in italics were estimated based on the calculated results [9]

References:

[1] Steelmaking data sourcebook, revised by the Japan Society for the Promotion of Science, The 19th committee on steelmaking, Gordon and Breach Science Publ., New York, 1988, 278/293
[2] E. T. Turkdogan: Fundamentals of steelmaking, The University Press, Cambridge, 1996, 92/94
[3] Z. Ma, J. Ohser and D. Janke: Acta Metallurgica Sinica, 10(1997), 375/385
[4] Z. Ma and D. Janke: Acta Metallurgica Sinica, 11(1998), 235/240
[5] Z. Ma and D. Janke: Acta Metallurgica Sinica, 12(1999), 127/138
[6] Z. Ma and D. Janke: ISIJ International, 38(1998), 46/52
[7] C. Bodsworth: Physical Chemistry of Iron and Steel Manufacture, Langmans, Gree and Co. Ltd., 1963, 462/475
[8] Selected equilibrium values for steelmaking reactions, The 19th Committee on steelmaking, The Japan Society for the Promotion of science, Rep. No. 19-10588 (Nov. 1984)
[9] Q. Han: Rare earth, alkaline earth and other elements in metallurgy, JATIS, Ohmsha Ltd. And IOS Press, Tokyo, 1998, 254/260

APPENDIX C
Calculation of Precipitates in Molten Steel during Solidification

Oxide precipitation and growth in molten steel during solidification are important to control steel quality. The present study is an attempt to theoretically predict composition and size of oxide precipitates during solidification with the help of a thermodynamic analysis and a microsegregation model.

1. Calculation Model

The present calculation model is based on the following assumptions
(1) the equilibrium at the interfaces between oxides and the molten steel is attained,
(2) growth of oxides is controlled by the diffusion of oxygen in the molten steel,
(3) secondary precipitates are all retained in steel,
(4) the molten steel is always completely mixed and of constant density during solidification.

For the purpose of mass balance, oxygen in a volume element at any time is equal to the initial total oxygen in the molten steel on the basis of the above third assumption. It is assumed that the oxides are uniformly dispersed in steel. Then the following equation is obtained to calculate the change of radii and composition of the oxides during solidification based on the fourth assumption. If the oxides are not assumed as uniformly dispersed in steel, the terms concerning the number of oxides in the solid and liquid steel will be replaced by the corresponding new terms that take the distribution of oxides into account

$$\begin{aligned}
&\frac{4}{3}\pi r_o^3 N\rho_s^o W_O^o + (1-\frac{4}{3}\pi r_o^3 N)[wt\%O]_o \rho_m \\
&= \sum_{t=0}^{t=t} (f_s(t+\Delta t) - f_s(t))\frac{4}{3}\pi (r(t))^3 N\rho_s(t) W_O(t) \\
&\quad + \left(1 - f_s(t+\Delta t) - \frac{4}{3}\pi (r(t))^3 N\left(1 - f_s(t+\Delta t)\right)\right)[wt\%O](t+\Delta t)\rho_m \\
&\quad + \frac{4}{3}\pi \left(r(t+\Delta t)\right)^3 N(1 - f_s(t+\Delta t))\rho_s(t+\Delta t) W_O(t+\Delta t) \qquad (1)
\end{aligned}$$

where

r_o	:	initial radius of oxide equals to r(0) (cm)
ρ_s^o	:	initial density of oxides equals to $\rho_s(0)$ ($g \cdot cm^{-3}$)
W_O^o	:	initial mass percentage of oxygen in oxides equals to $W_O(0)$
N	:	number of the oxides per unit volume (cm^{-3})
ρ_m	:	density of molten steel ($g \cdot cm^{-3}$)
r(t)	:	radius of oxide during solidification (cm)
$W_O(t)$	:	mass percentage of oxygen in oxides during solidification
$\rho_s(t)$	:	density of oxides during solidification ($g \cdot cm^{-3}$)

The left hand side of the above equation represents the initial total oxygen content in molten steel and the first term of the right hand side in Eq. (1) is the sum of oxygen content in oxides which exist in solid steel. The second term represents the remaining amount of oxygen in molten steel at the time $t+\Delta t$ and the third term is the amount of oxygen contained in the oxides presented in molten steel.

Microsegregation of solutes in molten steel can be calculated using Ohnaka's equation [1,2]:

$$[wt\%i](t) = [wt\%i]_o \left[1 - \left(1 - \frac{\beta k_i}{1+\beta} \right) f_s(t) \right]^{(k_i - 1)/(1 - \beta k_i/(1+\beta))} \tag{2}$$

where $\beta = \dfrac{4 D_i \bullet \tau}{\lambda^2}$

[wt%i](t): content of solute i at time t during solidification (mass%)

$[wt\%i]_o$: initial concentration of solute i (mass%)

k_i: equilibrium distribution coefficient of solute i between liquid and δ phase

f_s: solid fraction

D_i: diffusion coefficient of solute i in solid ($cm^2 \cdot s^{-1}$)

λ: secondary dendrite arm spacing (cm)

τ: local solidification time (s)

The secondary dendrite arm spacing (μm) can be empirically expressed by regression as Eq. (3)

$$\lambda = a \cdot R_C^b \quad (3)$$

a, b: constant

R_C: cooling rate ($K \cdot min^{-1}$)

For low carbon steel a and b are determined as 688 and -0.36, respectively [3].

It is considered that the solidification or δ/l transformation in a given area is completed when the actual temperature of steel reaches the δ/γ transformation temperature and the liquidus and solidus temperature can be calculated using the following relationships [4]

$$T_L=1809-78[wt\%C]-7.6[wt\%Si]-4.9[wt\%Mn]-34.4[wt\%P]-38[wt\%S] \quad (4)$$

$$T_s=T_{\delta/\gamma} =1665+1122[wt\%C]-60[wt\%Si]+12[wt\%Mn]-140[wt\%P]-160[wt\%] \quad (5)$$

In a region where solid and liquid coexist in a dendrite cell, the temperature at the solid-liquid interface, T, is given by Eq. (6) [5]. This estimated temperature is assumed to be the temperature of liquid steel during solidification according to the assumption of local equilibrium at the interface between oxide and molten steel attained

$$T = T_o - \frac{T_o - T_L}{1 - f_S \frac{T_L - T_S}{T_o - T_S}} \quad (6)$$

where T_o, T_L and T_S represent the melting point of pure iron (1809 K), liquidus and solidus temperature of alloy steel studied, respectively.

The local solidification time is simply equal to $(T_L-T_S)/R_c$ (min) and the equilibrium distribution coefficients of solutes and diffusion coefficients of solutes in the solid are given in **Table 1**. Then the segregation of solutes in molten steel during solidification can be calculated by the above mentioned method.

Table 1. Equilibrium distribution coefficients and diffusion coefficients of solutes in iron [4]

Element	$k^{\delta/L}$	D_i^{δ} ($cm^2 \cdot s^{-1}$)
Ti	0.4 [6]	68exp(-62400/RT) [9]
C	0.19	0.0127exp(-19450/RT)
Si	0.77	8.0exp(-59500/RT)
Mn	0.76	0.76exp(-53640/RT)
P	0.23	2.9exp(-55000/RT)
S	0.05	4.56exp(-51300/RT)
Al	0.60 [7]	n.d.
O	0.022 [8]	0.0371exp(-23050/RT) [9] $D_O^L=1.2\times10^{-4}$ [10]
N	0.32 [6]	$10^{-2405/T-2.97}$ [11]

The number of the oxides per unit volume is an important parameter for the calculation of oxide precipitation and growth during solidification. It is assumed that the relation between the number of oxides per unit volume and cooling rates can be expressed as following equation:

$$N = m \cdot R_C^b \quad \text{i.e.} \quad \ln N = a + b \ln R_C \tag{7}$$

where m, b and a are constants and $a = \ln m$.

This empirical formula was confirmed by many experimental results. For example, Goto et al's experimental results [3] for Ti-killed low carbon steel are replotted in **Figure 1**. It is obvious that the relation between N and R_C satisfies the empirical formula. However, further investigations on the relationship between N and R_C are needed. More considerations such as temperature, energy and structure should be involved in this relation.

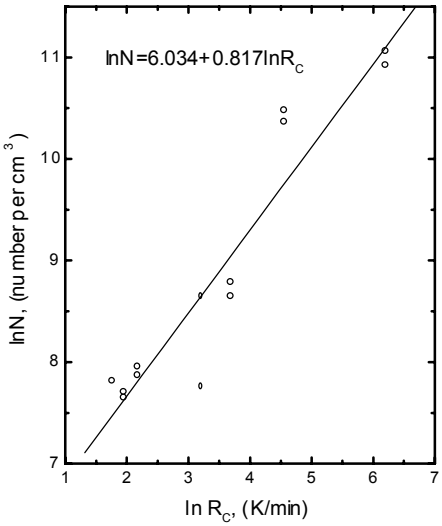

Figure 1. Relationship of the number of oxides per unit volume as a function of the cooling rate for low carbon steel [3] (cooling from about 1580°C; specimens were cut from continuous cast slabs in the thickness direction)

2. Examples

The steel studied by Goto et al. [3] was taken as an example having a composition of 0.06% [C], 0.05% [Si], 1.20% [Mn], 0.001% [Al], 0.014% [Ti], 0.0027% [O] where the main deoxidizers are Ti, Si and Mn. The contents of P, S and N are not given and are assumed to be 0.025% [P], 0.025% [S] and 0.006% [N].

2.1 Results of Calculation and Discussion

The equilibrium at the interface between oxide and molten steel is assumed to be attained, that is, the following oxidation reactions reach equilibrium

$2\underline{Ti} + 3\,\underline{O} = (Ti_2O_3)$	$\log K_{2Ti\text{-}3O} = 56{,}060/T - 18.08$	[12]	(8)
$2\underline{Al} + 3\,\underline{O} = (Al_2O_3)$	$\log K_{2Al\text{-}3O} = 64{,}000/T - 20.57$	[13]	(9)
$\underline{Si} + 2\,\underline{O} = (SiO_2)$	$\log K_{Si\text{-}2O} = 30{,}110/T - 11.40$	[13]	(10)
$\underline{Mn} + \underline{O} = (MnO)$	$\log K_{Mn\text{-}O} = 11{,}749/T - 4.666$	[14]	(11)

Figure 2 illustrates the change of the oxide radius during solidification. It is obvious that the radius of secondary oxides is greatly affected by the cooling rate. On the other hand, the radii of primary oxides are hardly influenced by the cooling rate during solidification, particularly in the case of larger primary oxides and at higher cooling rates. At a low cooling rate of 6K/min, the oxide radius will reach 3 to 3.5 μm at the end of solidification as shown in figure 2 whereas the initial radius r_o amounts to several Angstrom units (the critical radius for an oxide nucleus is normally in the order of 1 to 10 Å). At 100K/min and 500K/min, secondary oxide radii reach less than 2μm and 1μm, respectively. This result may lead to a useful method of distinguishing the secondary oxides from primary oxides according to their size. For instance, in the presently studied Ti-deoxidized low carbon steel, the oxides with radii below approximately 1μm are considered as secondary oxides which precipitate and grow during solidification, and those above 1μm are considered as primary deoxidation products which exist before solidification at a cooling rate of 500K/min.

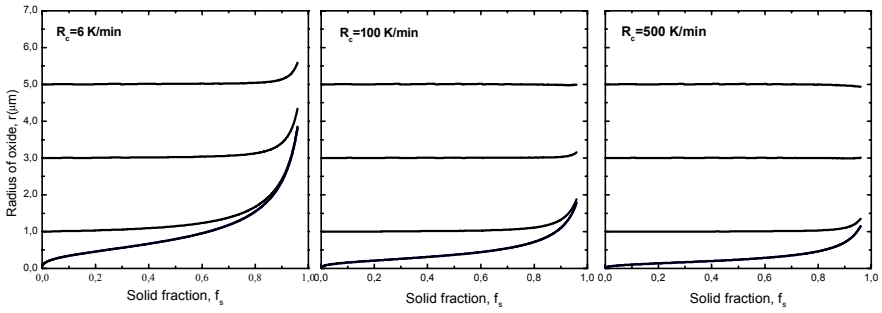

Figure 2. Calculated radii of oxides during solidification of Ti-deoxidized low carbon steel at three different cooling rates (cooling from liquidus to solidus temperature)

Figure 3 reflects the change of oxide composition during solidification. The content of Al_2O_3 tends to increase and Ti_2O_3 has the tendency for decrease during solidification. Comparisons of calculated with experimental results were made in chapter 5. A good agreement between calculated and experimental results is reached.

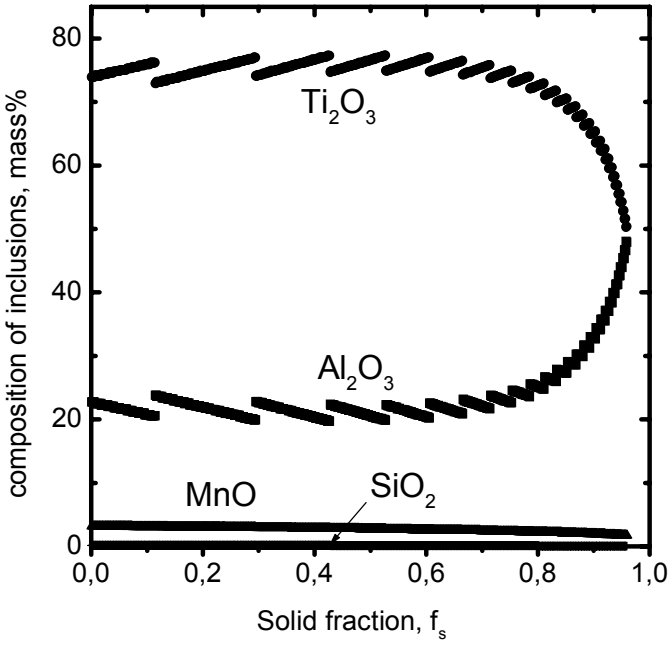

Figure 3. Change of composition of oxides during solidification of Ti deoxidized steel (temperature range from liquidus to solidus)

According to the calculated results for the above mentioned Ti-deoxidized steel, TiN and MnS are apart from oxides possible nonmetallic inclusions to precipitate during solidification. **Figures 4** and **5** show the precipitation behaviour of TiN and MnS, respectively. The calculated results indicate that Ti reacts with N in molten steel to form TiN which possibly precipitates at the surface of oxides for suppression of AlN precipitation. This was verified by Ouchi et al [15], Coleman et al [16] and Suzuki et al's [17] experimental results. The precipitation of MnS occurs possibly at the end of solidification, but MnS is not precipitated as pure MnS, but only in complex sulfides (supersaturation of MnS, S<0.5 shown in figure 5) and it is highly probable to precipitate at the surface of the oxides.

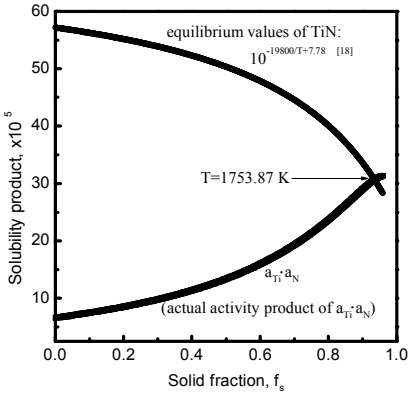

Figure 4. Precipitation of TiN in molten low carbon steel during solidification (Temperature range from liquidus to solidus)

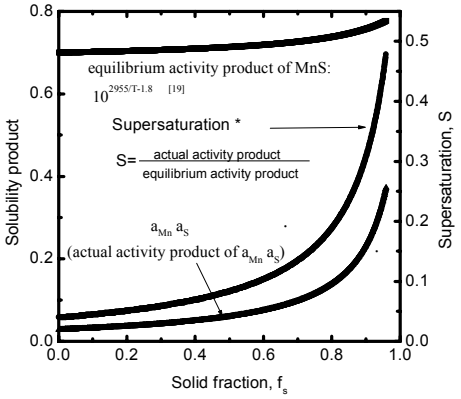

Figure 5. Precipitation of MnS in low carbon molten steel during solidification (Temperature range from liquidus to solidus)

*supersaturation of MnS:
S = actual activity product of MnS/equilibrium activity product of MnS

REFERENCES

[1] Ohnaka: Tetsu-to-Hagane, 70(1984), S913
[2] Ohnaka: Trans. Iron Steel Inst. Jpn., 26(1986), 1045/1051
[3] H. Goto, K. Miyazawa, K. Yamaguchi, S. Ogibayashi and K. Tanaka: ISIJ Intern., 34(1994), 414/419
[4] Y. Ueshima, S. Mizoguchi, T. Matsumiya and H. Kajioka: Metall. Trans. B, 17B(1986), 845/859
[5] J. Matsuno: Proc. Symp. Solidification Phenomena, Solidification Comm., ISIJ, Tokyo, (1976), 2
[6] E. T. Turkdogan: Proc. 70th AIME Steelmaking Conf., (1987) cited from K. Suzuki, S. Miyagawa, Y. Saito and K. Shiotani: ISIJ Intern., 35(1995), 34/41
[7] Y. Kawashita and H. Suito: ISIJ Intern., 35(1995), 1468/1476
[8] W. A. Fischer, H. Spitzer and M. Nishinuma: Arch. Eisen., 31(1960), 365

[9] H. Besteand K. W. Lange: Arch. Eisenhuttenwes., 43(1972), 20
[10] Solidification of Steel, Suppl., Solidification Committe, ISIJ, Tokyo, (1977), 1
[11] G. S. Ershov and A. M. Kovalenko: Metallurgy, (1972), 60

[12] Iron and Steel Handbook, 3rd ed., Vol. 1, ed. by ISIJ, Maruzen Co. Ltd., Tokyo, (1981), 15
[13] Steelmaking data sourcebook, Revised edition by The Japan Society for the Promotion of Science The 19th Committee on Steelmaking, Gordon and Breach Science Publishers, (1988), 235/242, 45/53
[14] S. Dimitov, A. Weyl and D. Janke: steel research, 66(1995), 87/92
[15] C Ouchi, T. Sanpei and K. Matsumoto: Tetsu-to-Hagane, 69(1979), A293
[16] T. H. Coleman and J. R. Wilcox: Mat. Sci. Tec., 1(1985), 80
[17] K. Suzuki, S. Miyagawa, Y. Saito and K. Shiotani: ISIJ Intern., 35(1995), 34/41
[18] E. T. Turkdogan: Physical Chemistry of High Temperature Technology, Academic Press, (1980), 8
[19] Y. Ito, N. Yonezawa and K. Matsubara: Trans. Iron Steel Inst. Jpn., 20(1980), 19

Acknowledgements

Sincere appreciation is due to Professor Dr.-Ing. habil. Dieter Janke, Head of the IIST, for his general supervision. I am also grateful for his interest and active role in my doctoral work as well as his valuable suggestions and discussions.

The author acknowledges with gratitude the helps received from many persons during my doctoral work. Particular thanks are due to Prof. Dr.-Ing. habil. Gerd Neuhof for his kind help and useful discussions; Dr.-Ing. Hans-Peter Heller for his help and cooperation in my experimental work; Dr.-Ing. B. Luft, Dr.-Ing. A. Franke, Dr.-Ing. A. Weiß, Dr.-Ing. H. Baum (Institut für Metallkunde), Mr. P. Neuhold, Mr. M. Uhlmann, Mr. D. Reinhardt, Mr. E. Fischer and Ms. I. Grahl for their helps on preparing samples and doing chemical and physical analyses; Dr. K. S. Oh (POSCO, South Korea) and Dr. P. Valentin (Saarstahl AG) for their discussions; Ms. K. Brock, secretary of the Institute of Iron and Steel Technology, for her kind help in different aspects with respect to daily life. Many others inside and outside the Institute of Iron and Steel Technology have directly and indirectly given me different helps. They are unfortunately too numerous for me to mention them all here.

Sincere thanks are due to Prof. Dr.-Ing. habil. Heinz-Joachim Speis (Institut für Werkstofftechnik, TU Bergakademie Freiberg) and Prof. Dr.-Ing. habil. Eberhard Steinmetz (Haus der Technik e.v., Essen) for reviewing my dissertation as appraisers.

Finally, it is a pleasure for me to express my gratitude to the Institute of Iron and Steel Technology, TU Freiberg, for assistance of this study. Financial support from ECSC (European Coal and Steel Community) under grant No. 7210.cc/115 is also gratefully acknowledged.

This dissertation is dedicated to my wife Lixin Ma and my daughter Xiyu Ma. Their strong support and encouragement during the extended period of research are gratefully recognized. The dedication of this work to them is indeed a small compensation for their many sacrifices.

October 2000

Zhongting Ma Freiberg, Germany